

N° : 41536

## THESE DE DOCTORAT

Présentée et soutenue publiquement à  
L'UNIVERSITE DES SCIENCES ET TECHNOLOGIES DE LILLE

---

***Fundamental approach for fouling growth mechanisms  
comprehension at a stainless steel surface:  
Development of antifouling coating for stainless steel***

---

Pour obtenir le grade de DOCTEUR

Spécialité : Molécules et Matière Condensée

Par : Ghassan Saadon Dawood AL-OGAILI

Maître de conférences à l'université de Tikrit (Irak)

Thèse dirigée par

Pr. Michel TRAISNEL et Dr. Maude JIMENEZ

Soutenue le 07 Novembre 2014 devant la commission d'Examen composée de:

**Jury :**

Pr. Romain JEANTET	Président
Dr. Fouad BENTISS	Rapporteur
CR. Luc FILLAUDEAU	Rapporteur
DR. Guillaume DELAPLACE	Examineur
Dr. Séverine BELLAYER	Invitée
Pr. Michel TRAISNEL	Directeur de Thèse
Dr. Maude JIMENEZ	Co-directeur de Thèse

## *Acknowledgments*

This manuscript concerns my PhD work that was carried out in the laboratory UMET headed by Prof. Alexandre Legris in the team (Ingénierie des Systèmes Polymères) managed by DR. Jean-Marc Lefebvre, as well as Prof. Serge Bourbigot and Prof. Michel Traisnel for welcoming and giving me the opportunity to work on this interesting project.

I would like to thank Prof. Michel Traisnel and Dr. Maude Jimenez for the supervision of my work. They bring me a lot of advices in order to guide my work, I also want to thank them for their patience and their time spent to correct my work.

I would like to thank DR Luc Fillaudeau and Dr. Fouad Bentiss HDR, for having accepted to take of their time and to bring their expertise as examiners to assess this manuscript and DR. Guillaume Delaplace and Prof. Romain Jeantet for having accepted to be examiner during the PhD defense.

As the most part of my study included the fouling test, I would like to thank Mr. Gilles Ronse and DR. Guillaume Delaplace from INRA for them helpful support, collaboration and results discussion. Also I would like to acknowledge Dr Audrey Allion from Aperam to support this study by stainless steel coupons.

I would like to acknowledge the support of University of Tikrit (Irak) for funding this work and Nord-Pas-de-Calais Region for supply this project.

I really would like to thank Dr. Séverine Bellayer for here participate in this thesis and for the EPMA, SEM analyses, many thanks are addressed to Dr. Nicolas Nuns for ToF-SIMS analysis and his explanations, to Arnaud Beaurain for XPS analysis, to Dominique Deresmes for AFM analysis, and to Ahmed Addad for SEM analysis.

I really would like to thank my brother Dr. Ihssan Dawood for the advice and for the moral support in some difficult periods.

I also would like to acknowledge all the persons working in the laboratory during my PhD for their welcome and discussion: Andréa, Antoine, Brigitte, Carmen, Clémence, Charaf, Fabienne, Fouad, Gaëlle, Gwenaëlle, Hassan, Jérémie, Marianne, Marion, Maryska, Matilde, Nicolas, Pauline, Pierre, Sophie and Trang.

Finally, many thanks to my family and my friend for their patience, affection and their immeasurable support.

## ***ABSTRACT***

Fouling caused by milk during heat treatment is a crucial issue in the dairy industry and is the main subject of the work presented. The aim of this thesis was in first place to design a surface in such a way that the effects of dairy fouling are reduced to some degree, i.e. to design an “antifouling” surface. But in order to develop these surfaces, a preliminary study on the interactions at a nanoscale between a usual stainless steel surface and the milk solution will be carried out.

To do that, the behaviour of two different model dairy fouling solutions on an austenitic stainless steel surface were investigated after various times of exposure to dairy solutions in a heat exchanger using different techniques, such as Electron-Probe Micro Analysis (EPMA), Time-of-Flight Secondary Ion Mass Spectroscopy (ToF-SIMS) and Atomic Force Microscopy (AFM). Deposits were formed using two model fouling solutions which were made from a whey protein dissolved in Total Hardness zero (TH0) water or in tap water at 90°C, respectively containing 30 ppm and 120 ppm Calcium. The fouling layers obtained after 2 hours fouling are completely different depending on the fouling solution. When TH0 water is used, the fouling layer is thin, smooth and homogeneous. When tap water is used, the fouling layer, which covers the surface and fills in the grain boundaries, is at the contrary very thick, rough, and shows a growth mechanism in arborescence. X-Ray mappings show that calcium and proteins are detected at the same places. To better understand the fouling growth of the first layers at the interface, samples were submitted to only one minute fouling in both solutions. When TH0 water is used, AFM analyses show a smooth homogeneous surface constituted of small clusters of size 60 nm and fitting the steel surface roughness. Three dimension ToF-SIMS reconstructions

evidence that calcium is in low amount and appears at the same places than the protein. It also confirms that the protein is present both on the steel surface and in the steel defects such as grain boundaries.

When tap water is used, both protein layer and grapes of round particles, corresponding to amorphous calcium carbonate particles (150-300 nm) are clearly visible. These particles seem to be preferentially dispatched inside the steel surface defects. 2D and 3D ToF-SIMS reconstructions show that the protein appears at the interface with the steel plate earlier than calcium carbonate. In our experimental conditions, the fouling was thus proven to be initiated by the unfolded protein (size of 60 nm) in the first seconds of exposition to a fouling solution. The unstable amorphous calcium carbonate nuclei (size 150-400 nm) formed in the tap water at 90°C are stabilized by the protein and precipitate preferentially in the steel roughnesses, in which they are trapped. The unfolded protein covers again these calcium particles, etc. This explains the growth structure in arborescence observed by EPMA. This phenomenon is not observed when THO water is used, as this solution is not supersaturated in calcium: calcium ( $\text{Ca}^{2+}$ ) is chelated or trapped in the protein layer, without creating the same roughness effect.

In order to try to reduce the fouling caused by milk components during heat treatment, the studies were then focused on the modification of stainless steel surfaces by the association of different surface treatment techniques. To get a better adhesion between the surface and the coating layers, two pre-treatments were used, i.e. polishing and activation of the surface by atmospheric pressure plasma treatments.

Two techniques were used to coat the pre-treated stainless steel surfaces: atmospheric pressure plasma treatments and sol-gel treatments. Concerning

the atmospheric pressure plasma treatment, a hexamethyldisiloxane (HMDSO)-based plasma coating was found to show the best adhesion on the stainless steel surface and gave repeatable interesting results against fouling. There is no appreciable difference between the fouling deposited mass of modified (using sol-gel) and unmodified stainless steel surfaces, but the initial fouling layer did not adhere to the coated stainless steel as strongly as on classical steel.

Mechanical profilometry, Atomic Force Microscopy (AFM), Electron Probe Micro Analysis (EPMA), Flight-Secondary Ion Mass Spectroscopy (ToF-SIMS), X-Ray Photoelectron Spectrometry (XPS) and goniometry were used to evaluate the coating roughness, morphology, surface energy and chemical composition.

The surface energy was obtained by the contact angle method and calculated following the Lewis acid-base theory. The fouling quantities were not clearly correlated with the measured surface properties. The peeling phenomenon of fouling deposits on the modified surface indicated that there was a weak adhesion of the fouling on the modified surface in comparison to the stainless steel surface. The surface morphology results show that the fouling percentage obtained on the modified surfaces was correlated with its surface roughness. Indeed, the roughness increase of the surface tends to increase the growth mechanism of the fouling. The growth behaviour of fouling on a modified surface needs a better and full understanding of the interfacial behavior to further develop anti fouling coatings.

## **RÉSUMÉ**

Le présent travail porte principalement sur un problème crucial de l'industrie laitière : l'encrassement causé par le lait pendant un traitement thermique (stérilisation, pasteurisation). L'objectif de ce travail de thèse est de comprendre le mécanisme de dépôt et de croissance de l'encrassement afin de pouvoir ensuite élaborer une surface qui permette d'empêcher l'encrassement ou au moins de le limiter.

Le comportement de l'encrassement laitier à l'interface d'une surface d'acier inoxydable austénitique a été examiné en fonction de différentes durées d'exposition à des solutions laitières (contenant différents taux de calcium) dans un échangeur de chaleur. Les dépôts ont été formés en utilisant deux solutions d'encrassement composées de protéines de lactosérum dissoutes dans une eau à dureté nulle ou dans de l'eau de robinet à 90°C (Pasteurisation haute). Ces solutions contenaient respectivement 30 et 120 ppm de calcium. Les couches obtenues après deux heures sont complètement différentes en fonction de la solution d'encrassement. Quand de l'eau, avec un titre hydrotimétrique nul (TH0), est utilisée la couche d'encrassement est fine, lisse et homogène. Inversement, avec l'eau fortement concentrée en calcium du réseau de la métropole Lilloise (TH50), la couche d'encrassement couvrant la surface est très épaisse, rugueuse et montre un mécanisme de croissance en arborescence. Afin de mieux comprendre le mécanisme d'encrassement sur les premières couches (à l'interface acier/encrassement), les échantillons ont été soumis à un processus d'encrassement limité à une minute pour les deux solutions. De nombreuses techniques innovantes et très performantes ont été utilisées dans ce travail pour la caractérisation autant chimique que morphologique de la surface encrassée ou non de l'acier utilisé : la profilométrie mécanique,

la microscopie à force atomique (AFM), la microanalyse par sonde électronique (EPMA), la spectroscopie de masse d'ions secondaires (ToF-SIMS), la goniométrie et la spectroscopie des rayons X (XPS).

Quand l'eau de dureté nulle est utilisée, les analyses AFM montrent des surfaces homogènes et lisses constituées de particules de 60 nm de diamètre correspondant probablement à une protéine (la beta-lactoglobuline) déployée. Des reconstructions 3D d'analyses ToF-SIMS montrent que le calcium est présent sur l'acier et dans les joints de grain de l'acier, en faible proportion et aux mêmes endroits que la protéine. Lorsque l'eau du robinet (TH 50) est utilisée, les couches de protéines ainsi que des particules qui ont été identifiées d'après la littérature comme des particules de carbonate de calcium amorphes (150-300 nm) sont clairement visibles. Ces particules semblent être préférentiellement présentes à l'intérieur des défauts de surface, ce qui expliquerait l'ancrage de l'encrassement et les difficultés de nettoyage. Les reconstructions ToF-SIMS 2D et 3D montrent que la protéine est présente à la surface de l'acier avant le carbonate de calcium. Il a été également démontré que l'encrassement est initié par la protéine dépliée (taille de 60 nm) dans les premières secondes d'exposition à une solution encrassante. Les particules de carbonate de calcium (taille 150-400 nm) formées dans l'eau du robinet à 90°C sont entourées et stabilisées par la protéine déployée et se déposent dans les rugosités de l'acier où elles sont piégées. La protéine dépliée couvre de nouveau ces particules de calcium, qui s'empilent etc. Ceci explique la croissance en arborescence observée par microsonde électronique. Ce phénomène est absent dans le cas de l'eau à dureté nulle, puisque cette solution n'est pas saturée en calcium : le  $\text{Ca}^{++}$  intrinsèque à la protéine est seulement présent à très faible concentration

dans la couche de protéine et n'a pas la possibilité de créer un effet de rugosité similaire.

Une surface d'acier lisse devrait donc limiter l'encrassement, la faible rugosité et l'absence de joints de grain permettant d'éviter au carbonate de calcium amorphe d'être piégé et de s'accumuler. Des surfaces polies ont donc été soumises au test d'encrassement et les résultats obtenus par reconstruction 3D ToF-SIMS corroborent cette hypothèse : l'encrassement est nettement moindre sur la surface lisse. Il est cependant très long et onéreux d'effectuer ce polissage dit « miroir » sur de grandes conduites industrielles.

Notre étude s'est donc ensuite portée sur la mise au point de dépôts permettant la réduction de l'encrassement, dépôts dits « antifouling ». Le but est, d'après la littérature, d'obtenir soit des revêtements très peu rugueux superhydrophiles ou superhydrophobes, soit des revêtements possédant une nano-rugosité permettant d'imiter « l'effet lotus ». Notre étude s'est essentiellement focalisée sur la modification de la surface de l'acier inoxydable par des revêtements déposés soit par plasma atmosphérique soit par voie sol-gel. Le plasma atmosphérique a également été envisagé pour améliorer l'adhésion des revêtements à la surface de l'acier inoxydable. Parmi les différents revêtements réalisés, les dépôts par voie plasma atmosphérique du précurseur Hexaméthylidisiloxane (HMDSO) semble être prometteurs pour limiter l'encrassement. Leur tenue aux tests très sévères de nettoyage doit cependant encore être optimisée.

# Table of Contents

INTRODUCTION	1
CHAPTER ONE: LITERATURE REVIEW	
1. Introduction	6
2. Organic and Mineral Fouling	7
2.1. Organic fouling	8
2.2. Mineral fouling	12
3. Interfacial Behavior of Dairy Fouling at Stainless Steel	14
3.1. Fouling process	14
3.1.1. Initiation	14
3.1.2. Transport	14
3.1.3. Attachment	15
3.1.4. Removal	15
3.1.5. Aging of the deposit	16
3.2. Milk fouling mechanisms	16
4. Factors Affecting on Milk Fouling	18
4.1. Influence of pH	18
4.2. Influence of temperature	19
4.3. Influence of dissolved gases	20
4.4. Influence of flow velocity	21
4.5. Influence of surface properties	21
5. Dairy Heat treatment	22
6. Fouling Cleaning	25
6.1. Cleaning Agents	26
6.2. Cleaning Duration	27
6.3. Cleaning Procedures	27
7. Stainless Steel	28
8. Surface Modification Techniques	29
8.1. Atmospheric Pressure Plasma treatment	31
8.2. Sol gel coatings	33
Conclusion	35
References	37

## CHAPTER TWO: SURFACE CHARACTERIZATION TECHNIQUES, MATERIAL AND EXPERIMENTAL METHODS

1. Surface Characterization Techniques	58
1.1. Introduction	58
1.2. Time-of-Flight Secondary Ion Mass Spectroscopy (ToF-SIMS)	58
1.3. X-Ray Photoelectron Microscopy (XPS)	62
1.4. Atomic Force Microscopy (AFM)	65
1.5. Scanning Electron Microscopy (SEM)	67
1.6. Electron Probe Micro Analysis (EPMA)	68
1.7. Optical Microscopy	70
1.8. Contact Angle Measurement	74
1.9. Roughness Measurements	77
2. Material and Experimental Methods	79
2.1. Materials	79
2.2. Experimental Fouling Equipment	81
2.3. Polishing Process	84
2.3.1. Mechanical polishing	84
2.3.2. Electropolishing	85
2.4. Small Scale Fouling Test Development	85
2.5 Plasma Coating	86
2.6. Sol-Gel Preparation	89
2.6.1. Dip Coating	90
2.6.2. Effect of immersion time:	91
Conclusion	92
References	93

## CHAPTER THREE: FUNDAMENTAL COMPREHENSION OF THE FOULING BEHAVIOR AT THE STAINLESS STEEL SURFACE

1. Introduction	101
2. Fouling Characterization	103
2.1. Stainless Steel Analysis	103
2.2. Analysis of the fouling layer after 2 hours fouling	106
3.2.1. Study of the fouling layer after fouling in a solution containing whey protein and TH0 water	107
3.2.2. Study of the fouling layer after fouling in a solution containing	111

whey protein and tapwater	
3.3. Analysis of the fouling layer after 1 minute	116
2.3.1 Solution containing whey protein and TH0 water	116
2.3.2. Analysis of the fouling layer after 1 minute fouling in the solution using tapwater	121
4. Growth Mechanism	128
4.1. Fouling growth mechanism in presence of whey protein and TH0 water	128
4.2. Mechanism in presence of whey protein and tapwater	130
4.3. Chemical form of calcium particles	131
4.4. Fouling mechanism during the first minutes of experiment	136
5. Influence of Roughness on Fouling Process	137
5.1. Mechanical Polishing	137
5.1.1. Surface morphology and roughness of unpolished stainless steel	137
5.1.2. Surface morphology and roughness of polished stainless steel	139
5.2. Electropolishing	142
6. Water Contact Angle and Surface Energy	143
7. Fouling Test	144
7.1. Initial deposition behavior	146
Conclusion	154
References	157
<b>CHAPTER FOUR: DEVELOPMENT OF ANTI-FOULING COATINGS</b>	
1. Introduction	163
Physical method by atmospheric pressure plasma	165
2. Effect of Stainless Steel Pre-treatment on Its Surface Energy	165
2.1. Effect of the distance between plasma source and substrate	165
2.2. Effect of Aging time	166
2.3. Effect of the number of passes	167
3. Antifouling Efficiency of the Different Coating	168
3.1. Plasma Coating	168
3.1.1. Fluorosilane based precursor	168
3.1.2. Silicon based precursor	169
3.1.3. HMDSO Coatings	170
3.1.3.1 Surface characterization of HMDSO coatings	173

3.1.3.2 Small Scale Fouling Test	176
3.1.3.3. Pilot-Plant Test with Fouling Model Fluid	177
4. Roughness Effect	180
5. Surface Energy Effect	181
Chemical method by Sol-Gel	184
6. Sol-Gel Based Coating	184
7. Sol-Gel Results	185
7.1. Effect of the Deposition Time	185
7.2. Water Contact Angle	186
7.4. Antifouling Effect of Sol-Gel Coatings	187
Conclusion	189
General Conclusion	191
Recommendation for Future Research	195
References	196
APPENDIX 1	201
APPENDIX 2	204
APPENDIX 3	205
APPENDIX 4	206

### ***List of Publications:***

Paper I: Jimenez M., Delaplace G., Nuns N., Bellayer S., Deresmes D., Ronse G., Alogaili G., Collinet-Fressancourt M., Traisnel M., Toward the understanding of the interfacial dairy fouling deposition and growth mechanisms at a stainless steel surface: A multiscale approach. *Journal of Colloid and Interface Science* 404 (2013) 192–200  
[doi: 10.1016/j.jcis.2013.04.021]

Paper II: Collier N., Callens D., Campistron P., Nongaillard B., Jimenez M., Alogaili G., Debreyne P., Ronse G., Delaplace G., Ultrasonic adhesion measurement of whey protein fouling. In proceeding of International Conference on Heat Exchanger Fouling and Cleaning, (2013), Budapest, Hungary 36, (2015), 771-779 [DOI: 10.1080/01457632.2015.954963]

Paper III: Al-ogaili G., Jimenez M., Bellayer S., Nuns N., Allion A., Beaurain A., Ronse G., Delaplace G., Traisnel M., Development Anti-dairy fouling Surface of 316L 2B Stainless steel by Atmospheric Pressure Plasma Treatment. In Process.

### ***Conferences:***

Al-ogaili G., Jimenez M., Bellayer S., Nuns N., Allion A., Beaurain A., Ronse G., Delaplace G., Traisnel M., Development Anti-dairy fouling Surface of 316L 2B Stainless steel by Atmospheric Pressure Plasma Treatment. 41 International Conference On Plasma Science (ICOPS 2014) and 20<sup>th</sup> International Conference on High-Power Particle Beams (Beams 2014), Washington DC, USA.

Collier N, Callens D, Campistron P, Carlier J, Nongaillard B, Jimenez M, Alogaili G, Debreyne P, Ronse G, Delaplace G (2013) Ultrasonic adhesion measurement of whey protein fouling. Proceeding of International conference on Heat Exchanger Fouling and cleaning, Budapest, Hongrie, 9-14 juin, p446-452 Editors: M.R. Malayeri, H. Muller-Steinhagen, A.P. Watkinson

Jimenez M., Delaplace G., Nuns N., Bellayer S., Deresmes D., Ronse G., Alogaili G., Traisnel M., Toward a better understanding of the first stages of dairy fouling growth at a stainless steel surface, IVC19 congress, Paris, France, Septembre 2013

Jimenez M., Delaplace G., Nuns N., Bellayer S., Deresmes D., Ronse G., Alogaili G., Traisnel M., Multiscale characterization of dairy fouling growth at a stainless steel surface, 15th European Conference on Applications of Surface and Interface Analysis 2013, ECASIA'13, Sardaigne, Italie, Octobre 2013

## ***Preamble***

This short part aims at presenting my personal data, background and career, I will then detail my teaching and research activities and the articles published before my PhD thesis.

### **PERSONAL DATA**

Name: Ghassan Saadoon Dawood AL-OGAILI  
Address: Resid. ARSENAL DES POSTES, Log. 112,  
47 Bd de Strasbourg,  
Lille 59000,  
France  
Telephone : +33.60.50.99.86.1  
E-mail : [g.dawood@yahoo.com](mailto:g.dawood@yahoo.com)

### **EDUCATION**

Dates (from – to)	2010 up to now Ph.D. chemistry USTL.
Dates (from – to)	1/11/2003 to 21/6/2006
College/ University	College of Sciences / University of Baghdad
Principal subjects	Chemistry
Skills covered	“Adsorption Study of lead ions on the surfaces of ion-exchange resin and some Iraqi clays”
Title	M.Sc

### **Professional Experiences**

Date (from – to)	16/10/2006 to 18/10/2010
Job title	Lecturer
Hours worked per week	35 Hours
Major tasks performed as my part of duties:	For the programs of the second and third years, I taught thermodynamics, kinetics chemistry and electrical chemistry. For the fourth year of the program, I taught the philosophy of science
Teaching of laboratory practical:	I taught organic chemistry practical works for first year students

## ARTICLES

1. AL-SAADI K. and DAWOOD G., (2006), "Thermodynamics and kinetics study of lead ions adsorption on Iraq bentonite" Tikrit journal of pure science Vol. 11 No. 2. pp 150-153
2. AL-SAADI K. and DAWOOD G., (2007), "Adsorption of Pb ions by using some of natural clays" Nahrain University journal for science, Vol. 16 No. 3.
3. AL-TAKRITY E.T.B., DAWOOD G. (2009)."Study of Adsorption of methyl Orange and methyl Violet Dyes on the surface of Teriethyl amine glyceryl maleate polymer". The first scientific conference, college of science, Tikrit University.
4. AL-Taie A. K., Yako D. M. and DAWOOD G. (2009). "Study the stability of some Schiff bases from 3-methoxy-4-hydroxy benzaldehyde with some ions" Nahrain University journal of science 12.
5. DAWOOD G. (2010)" Removal Orange (G) Dye from aqueous solution by adsorption on Bentonite". Tikrit journal of science Vol.2 No.12.

## List of Figures

Figure 1.1:	Milk fouling on heat exchanger plates and in a stainless steel pipe	6
Figure 1.2:	Denaturation of $\beta$ -Lg	9
Figure 1.3:	The milk proteins	10
Figure 1.4:	Schematic illustration of adsorption process of $\beta$ -Lg	11
Figure 2.1:	Diagram of ToF-SIMS	60
Figure 2.2:	Diagram of an X-ray photoelectron spectrometer	65
Figure 2.3:	Diagram of an AFM	67
Figure 2.4:	Diagram of scanning electron spectrometer	68
Figure 2.5:	Diagram of an EPMA	70
Figure 2.6:	Principles of imaging with an optical microscope: (a) ray diagram of the simplest two-lens microscope; (b) definition of parameters of an objective lens; (c) point spread function with the first minimum at $r=W/2$ ; (d) Airy patterns in the image plane. “F” marks the foci of lenses. “R” shows the separation distance between the centers of Airy discs.	71
Figure 2.7:	The optical column	73
Figure 2.8:	Optical Microscopy	74
Figure 2.9:	Schematic of a sessile-drop contact angle system	75
Figure 2.10:	Scheme representing a measurement of contact angle	77
Figure 2.11:	Profilometer (Tencor Alpha- Step IQ, Science)	79
Figure 2.12:	Pilot plant test ring for the fouling test.	81
Figure 2.13:	Heat exchanger pilot (INRA)	83
Figure 2.14:	Kinetic of the heating process	83
Figure 2.15:	Mechanical polishing instrument.	85
Figure 2.16:	Small scale fouling test	86
Figure 2.17:	(a) Structure of plasma source, and (b) schematic diagram of the experimental setup.	88
Figure 2.18:	Apparatus for dip coating.	90
Figure 2.19:	Infrared instrument	91
Figure 3.1:	Depth profiles (ToF-SIMS) in $\text{Cr}^+$ , $\text{CsFe}^+$ , $\text{Cs}_2\text{O}^+$ and $\text{CNCs}_2^+$ of the stainless steel	103
Figure 3.2 :	AFM image of virgin stainless steel surface on a $4\ \mu\text{m} \times 4\ \mu\text{m}$ surface: 3D representation (a) with a zoom	104

	around the steel fissure (b) and profile analysis of the failure (c)	
Figure3.3:	Optical picture of the steel plate surface	105
Figure3.4:	AFM picture of the steel plate on a 200nm*200nm surface	105
Figure 3.5:	Comparison of the numerical pictures of the samples before fouling (a) and after two hours fouling in solutions containing whey protein in TH0 water (b) or in tapwater (c)	106
Figure 3.6:	Optical picture taken after 2 hours fouling in the fouling solution containing whey protein and TH0 water	107
Figure 3.7:	SEM images of the surface fouling layer at different magnifications (a)X3000, (b)X10000, (c)X70000	108
Figure 3.8:	AFM image of the 2 $\mu$ m*2 $\mu$ m surface after two hours fouling with TH0 water: 3D representation(a) and picture obtained using phase imaging (b)	109
Figure 3.9:	AFM pictures taken on the plane part of the 2 $\mu$ m*2 $\mu$ m surface: 3D picture (a), picture obtained using phase imaging (b) and particle profile(c)	110
Figure 3.10:	Primary sequence of $\beta$ -lactoglobulin	111
Figure 3.11:	SEM image of the fouling layer obtained after 2 hours fouling in tapwater	112
Figure 3.12:	SEM analysis of the steel surface when the main fouling layer has been removed	113
Figure 3.13:	BSE cross-section image of the fouling layer obtained after 2 hours fouling	114
Figure 3.14:	Fe, Cr, Ca and S X-Ray mappings of the cross section of the fouling layer	115
Figure 3.15:	AFM 3D pictures of the fouling layer obtained after 1 min in a fouling solution using TH0 water on 4 $\mu$ m*4 $\mu$ m (a) and 2 $\mu$ m*2 $\mu$ m (b) surfaces	117
Figure3.16:	AFM images of the fouling layer obtained after 1 min in a fouling solution using TH0 water on a 500nm*500nm surface (a) 3D representation, (b) picture obtained using phase imaging (c) zoom on some particles	118
Figure 3.17:	ToF-SIMS depth profiles of the fouling layer obtained after	119

	1 minute fouling in TH0 water	
Figure 3.18:	3D ToF-SIMS reconstructed pictures of the fouling layer after 1 minute fouling in the solution using TH0 water	120
Figure 3.19:	AFM images of the fouling layer obtained after 1 min in a fouling solution containing protein and using tapwater on a $4\mu\text{m} \times 4\mu\text{m}$ surface: 3D representation (a), picture obtained using phase imaging (b) and profile of the fissure (c)	122
Figure 3.20:	AFM images of the fouling layer obtained after 1 min in a fouling solution containing protein and using tapwater on a $2\mu\text{m} \times 2\mu\text{m}$ surface : 3D representation (a), imaging mode (b), picture obtained using phase imaging (c), particle profile (d)	123
Figure 3.21:	AFM images of the fouling layer obtained after 1 min in a fouling solution containing protein and using tapwater on a $500\text{nm} \times 500\text{nm}$ surface: on the smooth part (a), on the particules containing part (b), with a zoom on one particule using phase mode (c) and imaging mode (d) including a profile on the particule roughness (e)	124
Figure 3.22:	(a) imaging mode on a $20\mu\text{m} \times 20\mu\text{m}$ surface, (b) $\text{CsFe}^+$ 2D reconstruction, (c) $\text{Ca}^+$ 2D reconstruction, (d) $\text{CNCS}^{2+}$ 2D reconstruction, (e) Overlay of the three reconstructions	126
Figure 3.23:	3D ToF-SIMS reconstructed pictures of the fouling layer after 1 minute fouling in the solution using tapwater	127
Figure 3.24:	Schematic representation of the fouling growth mechanism in presence of whey protein and TH0 water	129
Figure 3.25:	Schematic representation of the fouling growth mechanism in presence of whey protein and tapwater	130
Figure 3.26:	XPS spectra of $\text{Ca}2p$ for both fouling solutions	132
Figure 3.27:	Fouling solution “appearance” when put in contact with steel	135
Figure 3.28:	Deposition mechanism of the first fouling layers when whey protein and tapwater are present in the fouling solution	137
Figure 3.29:	The optical microscopic photograph of stainless steel	138

	surface	
Figure 3.30:	The SEM images of stainless steel surface, A) 5 $\mu\text{m}$ ; B) 10 $\mu\text{m}$ and C) 50 $\mu\text{m}$	138
Figure 3.31:	The AFM morphological image of the stainless steel surface, (a) 3D image, (b) Profile chart	139
Figure 3.32:	The optical microscopic photograph of stainless steel 1000 grade polished	139
Figure 3.33:	The AFM image of the stainless steel 1000 grade polished, (a) 3D image, (b) Profile chart	140
Figure 3.34:	The optical microscopic photograph of mirror like stainless steel	140
Figure 3.35:	The SEM images of mirror like stainless steel, A) 5 $\mu\text{m}$ ; B) 10 $\mu\text{m}$ and C) 50 $\mu\text{m}$	141
Figure 3.36:	The AFM image of mirror like stainless steel, (a) 3D image, (b) Profile chart	141
Figure 3.37:	The optical microscopic photograph of electropolished stainless steel	143
Figure 3.38:	The AFM image of electropolished stainless steel, (a) 3D image, (b) Profile chart	143
Figure 3.39:	deposition masses on different plate surfaces	145
Figure 3.40:	The relationship between the surface energy ( $\gamma$ ) and the fouling mass deposit on the plate surfaces	146
Figure 3.41:	3D images of ToF-SIMS (A) mirror polished, (B) Electropolished, (C) paper 1000, (D) Ref	149
Figure 3.42:	2D images of ToF-SIMS (A) Mirror like, (B) Electromirror like, (C) 1000, (D) Ref	152
Figure 4.1:	Effect of distance on water contact angle	166
Figure 4.2:	Aging time effect on water contact angle	166
Figure 4.3:	Effect of the number of passes on the water contact angle	167
Figure 4.4:	Pilot-plant fouling tests results for fluorosilane based precursor	169
Figure 4.5:	Pilot-plant fouling tests results for silicon based precursor	170
Figure 4.6:	The structure of hexamethyldisiloxane HMDSO	171
Figure 4.7:	The water contact angle versus plasma coating experiment	172
Figure 4.8:	AFM image of HMDSO coating	173

Figure 4.9:	ToF-SIMS sputtering depths profiles of the HMDSO coating	174
Figure 4.10:	XPS (a). C1s, (b). Si 2p and (c) O1s spectra from HMDSO plasma coating	176
Figure 4.11:	Laboratory fouling test	177
Figure 4.12:	The HMDSO coating substrates after Laboratory fouling test	177
Figure 4.13:	Pilot-plant fouling test for MHDSO coatings	178
Figure 4.14:	EPMA image and chart analyses of fouling on the uncoated stainless steel	178
Figure 4.15:	EPMA image and chart analyses of fouling on the HMDSO coated stainless steel	179
Figure 4.16:	EPMA image and chart analyses of HMDSO coated stainless steel after cleaning with NaOH solution	179
Figure 4.17:	Effect of the dipping time on the contact angle	185
Figure 4.18:	The water contact angle of different substrates	186
Figure 4.20:	Sol-gel (S2) coated on stainless steel with chemical analysis chart	187
Figure 4.21:	Pilot-plant test with fouling model fluid	187
Figure 4.22:	The sol-gel coating substrates after cleaning with NaOH	188

## Abbreviations

ACC	Amorphous Calcium Carbonate
AFM	Atomic Force Microscopy
$\beta$ -Lg	Beta Lactoglobulin
BSE	Back Scattering electron
CIP	Cleaning in place
DCPD	Di-Calcium Phosphate Di-hydrate
DMP	Dimethylphosphate
EDS	Energy Dispersive Spectroscopy
EMP	Electron Microprobe
EP	Electropolishing
EPMA	Electron Probe Micro Analysis
FEG	Field Electron Gun
FM1	Fouling medium with whey protein and TH0 Water
FM2	Fouling medium with whey protein and tap water
HAP	Hidroxyapatite
HEP	Heat Exchangeur Plates
HET	Heat Exchangeur Tube
HM	Hexamethyldisiloxane
HMDS	Hexamethyldisilazane
HMDSO	Hexamethyldisiloxane
HMDZ	Hexamethyldisilazane
HTST	Hight Temperature Short Time
LMIG	Liquid Metal Ion Gun
LiF	Crystal of Lithium Fluoride
MTES	Methyltrimethoxysilane
MRS	Micro Raman Spectroscopy
OCP	Octacalcium Phosphate
PECVD	Plasma Enhanced Chemical Deposition
PDMS	Polydimethyl siloxane
PEG	PolyEthylene Glycol
PET	Crystal of pentaerythritol
PHE	Plate Heat Exchanger
PS	Perfluorooctyltriethoxysilane
PTFE	Poly(tetrafluoroethylene)
RF	Radiofrequency
RMS	Root Mean Square
SE	Secondary Electron
SEM	Scanning Electron Microscopy

SS304L	Stainless Steel 304 Low carbon
SS316L	Stainless Steel 316 Low carbon
TC	Tetramethylcyclotetrasiloxane
TE	Tetraethoxysilane
TEOS	Tetraethoxysilane
TH	Total Hardness
TH0	Total Hardness Zero
TMES	Trimethylethoxysilane
TMDSO	Tetramethyldisiloxane
TMOS	Tetramethoxysilane
Tof SIMS	Time-of-Flight Secondary Ion Mass Spectroscopy
TTMSP:	Tris(trimethylsilyl)phosphine
WCA	Water Contact Angle
WDS	Wavelength Dispersive X-Ray Spectroscopy
WPC	Whey Protein Concentrate
XPS	X-Ray Photoelectron Spectroscopy
XRD	X-Ray Diffraction

## ***INTRODUCTION***

Fouling is the colonization of surfaces by a biotic and organisms ([Rittschaf, 2001](#)). Fouling results from the accumulation on surfaces of unwanted material which is formed through the contact between the surfaces with liquids or gases. This accumulation involves molecular bonding between the substances and surfaces. Fouling is a severe problem in the food industry, leading to the functional decline of equipment and decreased quality. In many processing industries, fouling of heat transfer surfaces is the major factor responsible for the reduction of process efficiency and performance with time ([Lund 1981](#)). Fouling in food industries is more severe in comparison to other industries ([Changani et al., 1997](#)), and thus requires more frequent and expensive cleaning steps ([Hasting 1994](#)). Fouling caused by milk in pasteurization/ sterilization operations, is one of the major issues. The processes (pasteurization/ sterilization) occur simultaneously and depend on the operating conditions. Usually removal rates increase with increasing amounts of deposit whereas deposition rates are independent of the amount of deposit but do depend on the changes caused by deposits such as increase in flow velocity and surface roughness.

In the dairy industry, fouling and the resulting cleaning of the process equipment account for about 80% of the total production costs ([Bansal and Chen, 2006](#)). Total fouling costs equate to 0.25% of the gross national product (GNP) for developed countries such as the USA, and 0.15% of the GNP for less industrialized countries such as New Zealand ([Müller-Steinhagen et al., 2000](#)). Costs due to over-sizing of heat exchangers, extra fuel consumption, maintenance and loss of production all contribute to the total costs of fouling. In the USA and New Zealand, total fouling costs have been estimated as US 7billion \$ ([Müller-Steinhagen et al., 2000](#)) and NZ

97.3 million \$ respectively (Müller-Steinhagen et al., 1990). This includes the costs of additional energy consumption and over-sizing of the heat exchanger unit due to blockage of channel and reduction in overall heat transfer coefficient, cleaning of the equipment, and loss of production during cleaning cycle (Gillham et al., 2000).

The direct costs of fouling and cleaning have been categorized by (Gillham, 1997):

- Loss of production: reduced process efficiency and need to shut down to clean.
- Maintenance costs: due to the necessity to install complex cleaning processes.
- Fuel costs: increased heating and pumping power to maintain process conditions.
- Capital expenditure: overestimating heat exchanger area and installation of extra pump capacity to allow for fouling.
- Environmental effect: are of increasing importance. They are increasing global concerns to reduce the amount of waste from food production and less CO<sub>2</sub> emissions.

Table 1 shows the annual costs of fouling in some different countries based on 1992 estimation.

Country	Fouling Costs (million \$)	Fouling Cost /GNP %
US	14175	0.25
UK	2500	0.25
Germany	4875	0.25
France	2400	0.25
Japan	10000	0.25
Australia	463	0.15
New Zealand	64.5	0.15

Table 1: Annual costs of fouling in some countries (Tay and Yang, 2006).

From this table, it is clear that fouling costs are substantial and any reduction in these costs would be a welcome contribution to profitability and competitiveness.

The goal of this doctoral study is (i) to understand the interactions at micro and nanoscales between the heat exchangers surface and the milk components to understand the adhesion mechanism in order to (ii) modify the stainless steel surface in such a way that the effects of dairy fouling are reduced to some degree and finally to (iii) propose antifouling solutions.

The outline of this PhD thesis is the following on: the general aspects of fouling and anti-fouling technologies will be presented in Chapter I, the literature review. Chapter II will describe briefly the materials and experimental methods, and in particular the surface characterization techniques used in this study to understand the fouling phenomena (Chapter III) and to characterize functional coatings (Chapter IV). Chapter III will detail the steps of comprehension of the fouling mechanism at the 316L stainless steel surface, by two dairy fouling deposits at a stainless steel surface after different processing times in a pilot plate heat exchanger at different scales, and impact roughness by polishing processes. The thesis involves developing anti-fouling surface by physical and chemical methods. The physical method used the plasma atmospheric pressure and chemical

method used the Sol-gel technique on 316L 2B Stainless steel substrate, the details of which are discussed in Chapters IV.

***CHAPTER ONE***  
***LITERATURE REVIEW***

## 1. Introduction

Fouling of food components (e.g. minerals, proteins, etc.) onto the surface of food contact materials during food processing is a major concern for the food industry as it adversely impacts heat transfer rate and efficiency during processing, resulting in an overall increase of operating costs (De Jong, 1997).

In dairy industry, fouling by milk proteins and minerals during the thermal processing of milk (Figure 1.1) is considered to be a major problem.

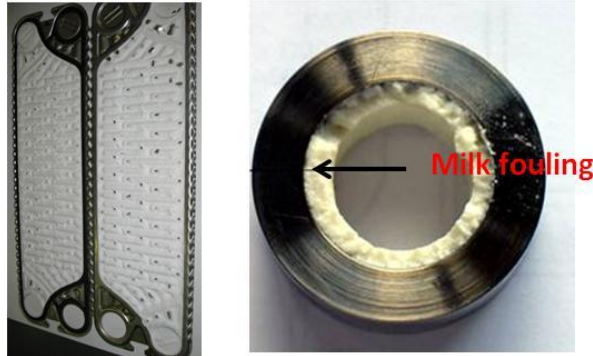


Figure 1.1: Examples of dairy fouling on heat exchanger plates (ECP) and in a heat exchanger tube (ECT).

Fouling is considered to have a major impact on the performance of the thermal equipment as it not only reduces heat transfer, it also increases pressure drop, both phenomena leading to increased processing costs. Fouling indeed leads to increased production costs due to reduced run time and to increased energy, maintenance and cleaning in plate (CIP) expenses, including costs associated with product losses (Bennett, 2007).

In the dairy industry, every product is heated at least once, and so heat treatment is by far the major unit operation. Furthermore, the formation of

biofilms –i.e. increased number of bacteria- can lead to the early shutdown of the plant for cleaning (Bansal et al., 2009).

Enhancing cleaning processes is therefore an important challenge to optimize production cycles, increasing the profitability plus the quality of the final product and reducing environmental impacts. One approach to reduce fouling and to increase the removal of formed deposits is the defined modification of the energetic and topographic surface properties.

As such, reducing the accumulation of fouling material during food (and milk in particular) processing by material surface modification has been widely studied and reviewed (Kananeh et al., 2010; Al-Janabi et al., 2010; Rungraeng et al., 2012; Barish and Goddard, 2013; Keshani et al., 2013; Patel et al., 2013) and it is of first importance to thoroughly study the substrate properties and milk fouling deposits to get a better comprehension of the general subject

## ***2. Organic and Mineral Fouling***

Milk is a complex biological fluid composed of several components including whey proteins, calcium and lipids. The composition of milk depends on its source and hence may not be possible to change. A seasonal variation in milk fouling depends on differences in milk composition (Burton 1968, Belmar-Beiny et al. 1993, de Jong 1997). These last twenty years, many research teams (Fryer et al., 2006; Rosmaniho and Melo, 2006; Saikhuran et al., 2010; Zhai et al., 2011; Rosmaniho et al., 2007; Huppertz et al., 2004) have tried to understand the mechanisms leading to dairy fouling of plate heat exchangers. The chemical composition of fouled layers has

been characterized in various process conditions, and the main role of temperature was evidenced (Burton, 1968; Lyster, 1965). Indeed, two main chemical compositions of dairy fouling can be distinguished. Type A fouling, or “protein fouling” is found under 100°C: it forms a rough and white deposit, composed of 50-60% proteins, as well as 30-35% minerals (essentially calcium and phosphate), and about 5% lipids (Belmar-Beiny et al., 1993). Temperatures over 100°C lead to the formation of type B fouling, or “mineral fouling”, that is a grey and brittle deposit containing 70% minerals, 15-20% proteins, and around 5% lipids (Fryer et al., 2006; Prakash et al., 2006). A classification can also be made depending on the nature of the milk products. At low temperatures, mineral fouling can predominate in liquids with a high ratio of minerals to protein. In industrial heat treatments of pasteurization (Belmar-Beiny et al., 1993), type A fouling is favored.

### ***2.1. Organic fouling***

The adsorption of proteins plays one of the most important roles in the overall process of fouling of the metallic surfaces, due to their heat sensitivity and high concentration in foodstuff.

Protein adsorption occurs when any protein-containing fluid comes into contact with a foreign surface.

Adsorption of proteins onto a solid surface can be considered a complex phenomenon. This complexity comes from the structural features of protein molecules themselves as they contain hydrophobic and hydrophilic amino acid residues and carry negative and/or positive electric charges (Ngadi, 2009). The adsorption of the proteins to the surface was driven by hydrophobic, electrostatic, hydrogen bonding and Van Der Waals interactions. Hydrophobic and electrostatic interactions appeared to be the

main driving forces for the adsorption of proteins (Pasche et al., 2005, Lamotte et al., 2008). Electrostatic interaction is important when surfaces are charged in aqueous solution.

$\beta$ -lactoglobulin ( $\beta$ -Lg), accounting for half of the whey milk proteins, is predominant in fouling ability of milk derivatives: indeed, under 100°C, thermal treatments in heat exchangers induce the denaturation of whey proteins. The mechanism, by which  $\beta$ -Lg fouling follows from its denaturation, is the following one: under heat treatment,  $\beta$ -Lg denatures according to a two steps reaction. In the first step,  $\beta$ -Lg loses its tertiary structure and becomes reactive by exposing a free thiol. This phenomenon, called unfolding, enables on one hand the aggregation reaction, in which unfolded  $\beta$ -Lg associates with other whey proteins (Labouré et al., 2004; Perez and Pilosof, 2004). Figure 1.3 presents an overview of the milk proteins.

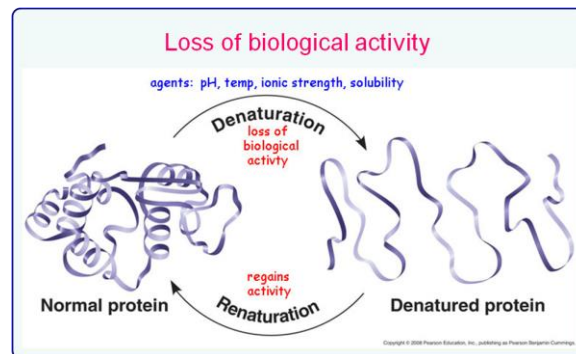


Figure 1.2: Denaturation of  $\beta$ -Lg.

Protein	mmol/m <sup>3</sup> Milk	g/kg Milk	g/100 g Protein	Molar Mass	g Protein/g N	Remarks
Casein	1120	26	78.3		6.36	IEP = 4.6
$\alpha_{S1}$ -Casein	450	10.7	32	-23600	—	Phosphoprotein
$\alpha_{S2}$ -Casein	110	2.8	8.4	-25200	—	Same, contains -S-S-
$\beta$ -Casein	360	8.6	26	23983	—	Phosphoprotein
$\kappa$ -Casein	160	3.1	9.3	-19550	—	"Glycoprotein"
$\gamma$ -Casein	40	0.8	2.4	-20500	—	Part of $\beta$ -casein
Serum proteins	-320	6.3	19	—	-6.3	Soluble at IEP
$\beta$ -Lactoglobulin	180	3.2	9.8	18283	6.29	Contains cysteine
$\alpha$ -Lactalbumin	90	1.2	3.7	14176	6.25	Part of lactose synthase
Serum albumin	6	0.4	1.2	66267	6.07	Blood protein
Proteose peptone	-40	0.8	2.4	4000-40000	-6.54	Heterogeneous
Immunoglobulins	-4	0.8	2.4	—	-6.20	Glycoproteins
IgG1, IgG2	—	0.65	1.8	-150000	—	Several types
IgA	—	0.14	0.4	-385000	—	
IgM	—	0.05	0.2	-900000	—	Part is cryoglobulin
Miscellaneous	—	0.9	2.7	—	—	
Lactoferrin	-1	0.1	—	86000	6.14	Glycoprotein, binds Fe
Transferrin	-1	0.01	—	76000	6.21	Glycoprotein, binds Fe
Membrane proteins	—	0.7	2	—	-7.1	Glycoproteins, etc.
Enzymes	—	—	—	—	—	

Note: Approximate composition. IEP = isoelectric pH.

Figure 1.3: The milk proteins (Walstra et al., 2006).

Unfolding and aggregation reactions were reviewed in detail in some previous works (Petit et al., 2011; Petit et al., 2012). On the other hand,  $\beta$ -Lg thiol activation by unfolding causes fouling reactions on the heat exchanger hot surfaces. The adsorption behavior of  $\beta$ -Lg has been studied for stainless steel (Itoh et al., 1995; Santos et al., 2006; Kim and Lund, 1997, 1998; Sakiyama et al., 1999). Most of these studies were concerned with the adsorption at room temperature.

The binding of  $\beta$ -Lg onto stainless steel seemed to be irreversible since less than 10% of the adsorbed  $\beta$ -Lg was redissolved into the buffer solution.

Arnebrant et al. (1987) reported a small fraction of adsorbed  $\beta$ -Lg was rinsed out at a temperature below denaturation and suggested that  $\beta$ -Lg adsorption onto a hydrophilic chromium surface might be partly reversible.

Luey et al. (1991) studied the effect of pH and NaCl concentration on the equilibrium adsorption behavior of  $\beta$ -Lg at hydrophilic and hydrophobic silicon surfaces by ellipsometry. They showed that the amount saturated  $\beta$ -Lg adsorbed onto hydrophobic surface was greater than that adsorbed onto hydrophilic surfaces. They also suggested that electrostatic interactions played a major role in the adsorption onto hydrophilic surfaces, while a greater importance of non-electrostatic interactions was suggested for the case of hydrophobic surface.

It was also suggested that  $\beta$ -Lg multilayer formation occurs via the attachment of aggregates with an activated free sulphhydryl group through an interchange reaction with a disulphide bond in the adsorbed protein monolayer (Santos et al., 2006)

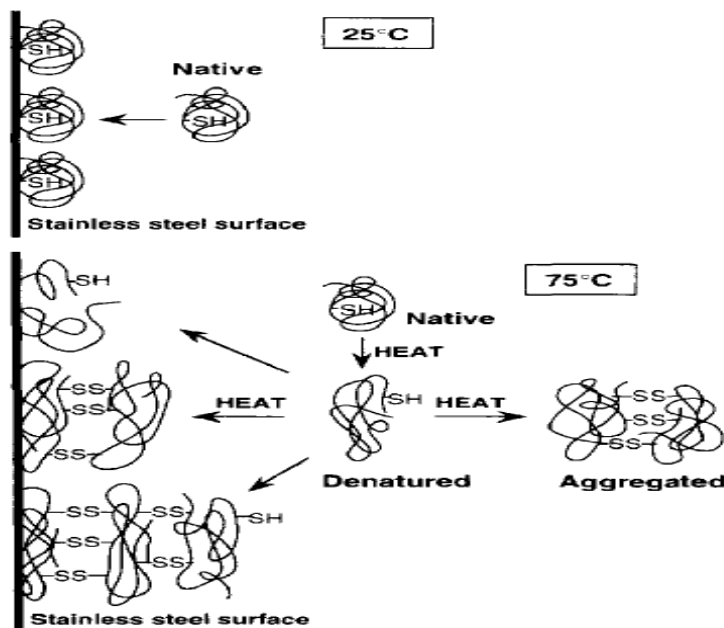


Figure 1.4: Schematic illustration of adsorption process of  $\beta$ -Lg. (Itoh et al. 1995).

## ***2.2. Mineral fouling***

Most of the milk fouling studies until now were primarily focused on the protein fouling mechanisms, hardly including fouling caused by mineral precipitation. But even when a significant part of the milk deposit is composed of proteins, a mineral layer usually predominates next to the deposition surface (Changani et al., 1997). This emphasizes the importance of the interactions between mineral deposits and metal surfaces in milk processing.

The enrichment of milk with calcium salts, and particularly calcium phosphates, is gaining interest to achieve higher calcium intake per serving; however, its impact on the heat stability of milk depends on the source and level of calcium fortification (Vyas and Tong 2004). Much work has been carried out into the effect of calcium and calcium phosphate on milk fouling; Pappas and Rothwell (Pappas and Rothwell, 1991) carried out experiments where  $\beta$ -lg solutions were heated to different temperatures with and without calcium. The  $\beta$ -lg was completely aggregated when heated with calcium for 30 min at 80 and 90° C and for 10 min at 110° C. However, when heated under identical conditions, but without calcium, the aggregation was considerably less compared with samples heated with calcium. Treatment of  $\beta$ -lg at 25° C with calcium does not bring about any aggregation; it is suggested that calcium binding groups become exposed due to heat-induced unfolding of the protein molecule. Xiong (1992) notes that calcium can cause bridging between adjacent carboxyl groups of the  $\beta$  -lg molecules and that it stabilizes aggregates.

The calcium and the phosphate ions present in milk indeed influence the denaturation temperature of  $\beta$ -Lg, promote aggregation by attaching to  $\beta$ -Lg, and enhance the deposition by forming bridges between the proteins adsorbed on the heat transfer surface and aggregates formed in the bulk (Xiong 1992; Changani et al., 1997; Christian et al., 2002). In addition, the solubility of calcium phosphate, which is an inverse solubility salt, decreases with heating. (Delsing and Hiddink 1983 ; Daufin et al., 1987 ; Grandison 1988 ; de Jong 1997 ; de Jong et al., 1998). When in solution, calcium phosphate precipitates in several Ca–P phases, including mainly dicalcium phosphate ( $\text{CaHPO}_4 \cdot 2\text{H}_2\text{O}$ , DCPD), octacalcium phosphate ( $\text{Ca}_8(\text{HPO}_4)_2(\text{PO}_4)_4 \cdot 5\text{H}_2\text{O}$ , OCP) and hydroxyapatite ( $\text{Ca}_5(\text{PO}_4)_3\text{OH}$ , HAP). HAP is considered more thermodynamically stable in physiological environments than OCP and DCPD. Because the Ca–P system equilibrium in milk is quite complex, a mixture of the various calcium phosphate phases is normally encountered in the deposits formed during its heat treatment, depending on the bulk temperature, level of supersaturation, pH or overall ionic environment (Andritsos et al., 2002). For milk with a pH around 6.7 and a heating temperature which is sufficiently high, the prevailing phase is the thermodynamically stable microcrystalline HAP, preceded by the formation by OCP, which is spherulitic in nature (Visser and Jeurnink, 1997).

### ***3. Interfacial Behavior of Dairy Fouling at Stainless***

#### ***3.1. Fouling process***

Epstein's (1983) classified fouling mechanisms with five major categories and five sequences of events in each category. These sequences are: initiation, transport, attachment, removal and aging.

##### ***3.1.1. Initiation***

The induction period is influenced by the materials surface temperature, the material itself, the surface finish and roughness. During the induction period, nuclei for crystallization of deposit will be formed. This period can take various times, depending on conditions: it can take several weeks or a few minutes or even seconds. The induction period decreases with increasing temperature. If the initial period decreases with increasing surface temperature, crystallization fouling would be changed (Epstein, 1983). With the increase of surface roughness the induction period tends to decrease (Epstein, 1981). Additional sites are developed by the roughness projections, which promotes crystallization while grooves provide regions for particulate deposition.

##### ***3.1.2. Transport***

Transport refers to the movement of particles or ions from the bulk fluid to the surface by mass transfer processes. Fouling substances from the bulk fluid are transported to the heated surface across the boundary layer. This phenomenon is dependent on the physical properties of the system and concentration difference between the bulk and the surface fluid interface. Transport is accomplished by a number of phenomena including diffusion,

sedimentation and thermophoresis (Somerscales and Knudsen, 1981; Melo et al., 1988).

### ***3.1.3. Attachment***

Attachment refers to the adherence of deposit components to the surface, which is governed by Van der Waals and attractive double layer forces or by surface integration in the case of crystallization. At this stage, the deposits are adherent to the surface and among the deposits layers itself. Salt ions approaching to the surface are attracted to it due to electromagnetic forces and adhere to the surface to form nucleation and gradually it grows with time to form a fouling layer. Thus forces acting on the particles as they approach the surface are not sufficient in determining attachment properties. Properties of the materials, such as size, density and surface conditions are indeed dominating the attachment phenomenon. The properties of the particles (density, elasticity, surface and state) and the nature of the surface (roughness and type of material) both play important roles in sticking of various particles to the surface.

### ***3.1.4. Removal***

Removal encompasses dislodgment of deposits from the surface to the bulk fluid. The removal process may or may not occur immediately after the deposition process has started. There is competition between removal and deposition of the foulants, up to the steady growth of the deposition on the surface. Shear forces at the interface between the fluid and deposited fouling are responsible for removal. The velocity gradients at the surface, the viscosity of the fluid and surface roughness are guiding the shear forces.

Removal from the surface is performed through the mechanism of dissolution, erosion and spalling.

Velocity of the fluid and the roughness of the surface can also play an important role in the removal mechanism. Erosion by particulate matter or by liquid impingement can remove material from the fouling layer.

### ***3.1.5. Aging of the deposit***

Aging is the alteration of a chemical or crystal structure (e.g. polymerization or dehydration) that begins immediately after the deposition process has started. Aging usually strengthens the deposit. During ageing, there may be transformation of the fouling deposit to improve or decrease the deposition strength with time. The mechanical properties (i.e. mechanical strength) of the deposit can change due to changes in the surface state or chemical structure.

## ***3.2. Milk fouling mechanisms***

Since milk is a complex mixture of various biological fluid components, the mechanism of deposition onto the heat exchanger surface (fouling) during thermal processing has not yet been unraveled, although an intensive discussion is still going around this subject. While ( $\beta$ -Lg) is the main protein in milk (around half of total whey proteins) therefore, it has been generally accepted that  $\beta$ -Lg plays a dominant role in fouling heat exchangers (de Jong, 1997). As detailed earlier, milk fouling research has established clearly that calcium phosphate and whey protein are the main components of milk deposits (Jeurnink et al., 1996), the former predominating at lower temperatures. It is believed that fouling starts with whey protein adhesion at

room temperature and a monolayer of protein is immediately adsorbed on the stainless steel when they are in contact. Upon heating, more layers of proteins deposit on this first layer formed when the whey protein start to unfold and expose a free S-OH group (Visser and Jeurink, 1997). This protein unfolding happens when the proteins are exposed to heating and it is generally accepted that a direct link exists between fouling and heat denaturation of these proteins in dairy fluids processing (Visser and Jeurink, 1997). The thermal unfolding of whey protein involves two stages (Aymard et al., 1996). The first one occurs at a temperature around 50° C, leading to the dissociation of native  $\beta$ -Lg dimer into monomers. Further heating up to a temperature of 60 to 80°C leads to a partial unfolding of the  $\beta$ -Lg monomer, exposing the free sulphhydryl group and thus allowing the hydrophobic residues to become available for further reactions in the surrounding solvent. Upon heating of milk, part of the calcium phosphate ions will tend to precipitate as a calcium phosphate salt which ultimately will form a mineral deposit on the stainless steel surface in a typical crystallization fouling process (Bott, 1995; Krause, 1993; Amjed, 1998) which starts with the formation of stable clusters of ions or molecules in the liquid, in a process called nucleation that occurs either in the bulk liquid (homogeneous nucleation) or at the surface of a foreign material (heterogeneous nucleation) (Mullin, 1993). The crystallization process of calcium phosphate is a very complex issue since several forms can be formed at the same time depending on ambient conditions like pH of solution, the temperature and the presence of other milk components.

#### ***4. Factors Affecting on Milk Fouling***

Fouling in a heat exchanger depends on various parameters like heat transfer method, hydraulic and thermal conditions, heat transfer surface characteristics, type and quality of milk along with its processing history etc. The factors affecting on milk fouling in heat exchangers can be broadly classified into two major categories: milk composition and operating conditions in heat exchangers (Bansal and Chen, 2006). The factors affecting on the milk fouling are:

##### ***4.1. Influence of pH***

It has been recognized that milk of high acidity is likely to coagulate in heat exchanger, so reduction in the pH of milk (e.g. from 6.8 to 6.4) would give a large amount of deposit, and mainly factors can explain that (Burton, 1965; Burton, 1968; Gordon et al., 1968; Foster et al., 1989). First all the heat stability of milk proteins decreases with a reduction in pH (Foster et al., 1989; Xiong 1992; Corredig and Dalgleish 1996; de Jong et al., 1998). A decrease in pH can also result in an increase in concentration of ionic calcium, possibly due to the dissolution of calcium phosphate from casein micelle and its increased solubility (Lewis and Heppell 2000). A slight increase in pH has been observed to increase processing time (Skudder et al., 1986).

A third factor can be the additional deposition of caseins (Skudder *et al.*, 1986; Patil and Reuter, 1988). Generally, it appears that the increased deposit formation of pH-reduced milk is mainly due to the reduced stability of protein to heat (Skudder *et al.*, 1986).

The fat present in milk has little effect on fouling (Foster et al., 1989; Visser and Jeurnink, 1997). However, decreasing the pH is found to increase the

amount of fat within the deposits (Lewis and Heppell 2000). The pH thus not only effects on the amount of deposit but is also responsible for its overall composition, shifting from mainly protein to mineral (Visser et al., 1997).

#### ***4.2. Influence of temperature***

Temperature of milk in a heat exchanger is probably the single most important factor controlling fouling (Burton 1968; Kessler and Beyer 1991; Belmar-Beiny et al., 1993; Toyoda et al., 1994; Corredig and Dalgleish 1996; Elofsson et al., 1996; Jeurnink et al., 1996; Santos et al 2003). Increasing the temperature results in higher fouling. Beyond 110 °C, as mentioned earlier, the nature of fouling changes from type A to type B (Burton 1968). It is worth mentioning that both the absolute temperature and temperature difference are important for fouling. This means that it is feasible to have fouling in coolers where the wall temperature is lower than the bulk temperature. Chen and Bala (1998) investigated the effect of surface and bulk temperatures on fouling of whole milk, skim milk, and whey protein and found that the surface temperature was the most important factor in initiating fouling. When the surface temperature was less than 68°C, no fouling was observed, even though the bulk temperature was up to 84°C.

At pasteurization and sterilization temperatures (85–110° C), milk produces a highly proteinaceous deposit whilst at UHT temperatures (110–140° C) the deposit is mostly composed of Calcium, Ca, and Phosphorous, P, because of the inverse solubility of these salts with temperature. Preheating of milk (often termed for warming) causes denaturation and aggregation of proteins

before the heating section, which then leads to lower fouling in heat exchangers. The effect of milk preheating on protein deposit has been investigated extensively using various combinations of preheating temperatures and holding times (Bell and Sanders 1944; Iyler, 1965; Burton, 1966, Burton 1968; Lalande et al., 1984; Mottar and Moermans 1988; Foster et al., 1989; Jeurnink et al., 1989, Yoon and Lund, 1989; Kessler and Beyer, 1991; de Jong et al., 1992). The main effect of forewarming is the denaturation of  $\beta$ -Lg and its association with casein micelle and hence reduction in the amount of type A deposits also, there is a reduction in the availability of ionic calcium with preheating as calcium phosphate gets attached to casein micelle (Lewis and Heppell 2000).

#### ***4.3. Influence of dissolved gases***

The solubility of air in milk decreases on heating. If the local pressure is too low (below the saturation pressure), air bubbles can arise (Burton, 1988). The formation of air bubbles may also be enhanced by mechanical forces that are induced by valves, expansion vessels or free-falling streams. It has been suggested that air in milk encourages fouling only if it forms bubbles on the heating surface, which then act as nuclei for deposit formation (Thom, 1975; Jeurnink, 1995). In addition, the composition of the deposit is influenced by the evaporation in the boundary layer of the air bubbles, which are mainly associated with caseins, resulting in the fouling layer having higher casein content. At the beginning of the fouling process air bubbles generated by heating have been held responsible for inducing turbulence. This results in an increased heat transfer rate (Delsing and Hiddink, 1983). Walstra et al. suggested that at a hot surface in contact with a liquid, air bubbles of about 1mm may readily form if the liquid contains

sufficient air for it to become supersaturated at the high temperature. The air in the bubbles is saturated with water vapor. If a bubble remains at the surface, it can considerably enhance fouling.

#### ***4.4. Influence of flow velocity***

Velocity influences fouling at a significant level. In most cases, fouling decreases at higher fluid velocities (Muller-Steinhagen and Middis, 1989; Cooper et al., 1980; Wlaker, 1982). Increasing flow velocity increases the fluid shear stress which causes more removal. For weak deposits (particulate fouling), increasing the flow velocity may completely eliminate fouling. For stronger deposits, increasing the flow velocity beyond a particular point may not decrease fouling significantly (Wlaker, 1982). For very strong deposits, increasing the flow velocity may not have any effect at all (Ritter, 1983). Burton (1988) suggested a possible explanation for the effect of flow velocity which is that at low velocities the thickness of laminar sub-layer adjacent to the heating surface is greater, so that the volume of material subject to higher temperatures, relatively long periods near to the surface, are greater. Fouling decreases with increasing turbulence (Belmar-Beiny et al., 1993; Santos et al., 2003). According to Paterson and Fryer (1988) and Changani et al. (1997), the thickness and subsequently the volume of laminar sublayer decrease with increasing velocity and as a result, the amount of foulant depositing on the heat-transfer surface decreases.

#### ***4.5. Influence of surface properties***

The heat-transfer surface to which the deposits stick affects fouling (Wahlgren and Arnebrant 1990, 1991). It influences the adhesion of

microorganisms as well (Flint et al., 2000). The surface characteristics are generally important at the beginning of the process, i.e. until the surface gets covered with the deposits. The surface treatment can be of great benefit in case fouling occurs after a time delay and the strength of the adhesion of the deposits onto the metal surfaces is weaker, giving way to an easier cleaning in place (CIP) process. Stainless steel is the standard material used for surfaces that are in contact with milk. Factors that may affect fouling of a stainless-steel surface are presence of a chromium oxide or passive layer, surface charge, surface energy, surface microstructure (roughness and other irregularities), presence of active sites, residual materials from previous processing conditions, and type of stainless steel used (Jeurnink et al., 1996a; Visser and Jeurnink 1997). Modifications of the heat-transfer surface characteristics through electro-polishing and surface coatings can reduce fouling by altering the surface roughness, charge, and wettability (Yoon and Lund 1994; Pie-linger-Schweiger 2001; Santos et al., 2001, 2004; Beuf et al., 2003; Rosmaninho et al., 2003, 2005; Ramachandra et al., 2005, Rosmaninho and Melo 2006). It is generally reported that hydrophobic surfaces adsorb more protein than hydrophilic surfaces (Wahlgren and Arnebrant 1991). Increasing the surface roughness provides a larger effective surface area and results in a higher effective surface energy than a smooth surface (Yoon and Lund 1994). As a result, the adhesion of deposits with a rough surface would be comparatively stronger.

## ***5. Dairy heat treatment***

The manufacture of virtually all milk and dairy products involves heat treatment. Such treatment is mainly aimed at killing microorganisms and inactivating enzymes, or at achieving some other, mainly chemical, changes.

Liquids can be heated and cooled in a batch process, in a heat exchanger, or in a packaged form. Moreover, direct mixing with steam can be combined with heat exchange. Highly viscous liquids can be heat-treated in a scraped-surface heat exchanger.

Originally, batch processing was in general use for pasteurizing beverage milk. It is the so-called holder pasteurization, e.g., 30 min at 63°C. The method is still in use in the manufacture of starters, whipping cream, and other small scale products. Usually, the vats involved are fitted with an agitator; steam or hot water circulates through a double jacket, followed by cold water. Among the advantages of holder pasteurization are the simplicity, flexibility, and satisfactory temperature control (little fluctuation in temperature occurs unless highly viscous liquids are treated). A drawback is that the warming and cooling times are long (excessive for large containers). Furthermore, regeneration of heat is not well possible and connection to continuous processes is awkward.

Currently, flow-through heaters or heat exchangers are commonly used. Hot water or condensing steam constitutes the heating medium. Sometimes, vacuum steam heating is applied to minimize the difference in temperature with the liquid to be heated.

In *plate heat exchangers*, a large heating surface is assembled in a confined space and on a small floor area. The heating agent and the incoming liquid are present in thin layers and are separated by a thin wall, i.e., a plate. Because of the large heating surface per unit volume of liquid that is to be heated, the difference between the temperature of the heating agent and the temperature of the liquid to be heated can be small, e.g., 2°C when milk is heated from 65°C to 75°C. This may be an advantage for some heat-sensitive products, where fouling of the heat exchanger is greater for

a higher wall temperature. Furthermore, warming and cooling proceed rapidly in plate heat exchangers.

A plate heat exchanger is made up of various sections connected in series, including a regeneration section, a heating section, a holding section (may also be a tube), and cooling sections. Each section consists of a great number of plates, being partly connected in parallel and partly in series. In this way, the liquid is properly distributed among the plates and arrives at a speed that is high enough to reduce fouling.

***Tubular heat exchangers*** generally have a smaller heating surface per unit volume of liquid to be heated than plate heat exchangers. Accordingly, the difference in temperature between the heating agent and the incoming liquid will generally be greater. To restrict fouling and enhance heat transfer, high flow rates are used, which necessitates high pressures. But this causes no problems because tubes are much stronger than plates; some tubular heat exchangers even have no sealing gaskets but have (spirally bent) concentric tubes. Tubular heat exchangers can readily be applied to obtain very high temperatures (e.g., 150°C). Accordingly, they are excellently fit for indirect Ultra-high temperature (UHT) treatment. Like a plate heat exchanger, a tubular heat exchanger can be built of regeneration, heating, holding, and cooling sections.

In modern heat exchangers, the milk may be in counter flow with water throughout the apparatus. The water is kept circulating and is heated by means of indirect steam heating immediately before it heats the milk to the maximum temperature desired. In such cases, the flow rates on either side of a separating wall need not be the same, implying that the temperature difference is not constant. This method of working has advantages with

respect to temperature control, rapid and even heat transfer, and saving of energy (Walstra et al., 2006).

### ***6. Fouling Cleaning***

Cleaning can be described as the removal of unwanted deposit (fouling) to return to a system at its original state after fouling occurs. If not controlled carefully, deposits can cause deterioration in the product quality because milk cannot be heated up to the required pasteurization temperature. When the deposits attach to the walls of the heat exchanger in stainless steel, flow passage is blocked and overall heat transfer coefficient decreases which then results in operational losses (Toyoda et al., 1994; Müller-Steinhagen, 1993). These deposits decrease the heat transfers and increase the pressure drop, and hence affect the production rate of the plant. The deposit on the walls is also very favorable for microbial growth as the formation of deposits promotes the adhesion of microorganisms to the heat transfer surface. For all these reasons, cleaning in place processes (CIP) in the dairy industry are carried out every 5–10 h depending on fouling severity (Murray and Deshares, 2000). The deposits must be removed by regular and intensive cleaning procedures in order to comply with hygiene and quality regulations for the dairy industry (Augustin et al., 2007). Cleaning is a complex process involving interaction between the cleaning components and the deposit. Cleaning begins with the deformation of the fouling by the reaction of cleaning detergent (Grasso, 1997). This is agreed by (Karlsson et al. 1998) who concluded that cleaning is strongly influenced by deposit and surface characteristics together with the choice of cleaning agent. When the proteins are the main component, an alkali based is the best detergent to apply. For milk fouling, cleaning of processing equipment starts

with a hot water rinse to melt the fats and thus enhance the contact between the deposit and the chemical solution. For these reasons, the researchers were starting to search for a way to get an anti-fouling surfaces or “self-cleaning” surfaces by modified the surface of stainless steel.

### ***6.1. Cleaning Agents***

Alkaline solutions (e.g., 1% NaOH, i.e., 0.25 M) can, in principle, dissolve proteinaceous materials and hence type-A deposit and most membrane fouling. Too weak a solution causes insufficient dissolution, but too high a concentration of NaOH tends to change the deposit into a rubbery layer that is hard to remove. Acid solutions (generally phosphoric or nitric acid of about 0.2 molar) serve to dissolve type-B deposit (scale). Alkali tends to enhance scale deposition.

If the water used has considerable hardness, a water conditioner, e.g., a polyphosphate that keeps calcium in solution, can be added to minimize such deposition.

Usually, alkali treatment is followed by a separate acid rinse. If fouling is not excessive and involves little scale, a combined detergent often is used, containing an alkaline substance and a calcium chelating agent, such as ethylene diamine tetra-acetic acid (EDTA).

Surfactants, i.e., soap-like materials, are added in some cases. A soap solution can loosen a fatty deposit from a surface and keep oil molecules dispersed inside the soap micelles. Hence, a surfactant is certainly needed when a fatty layer is present. It is not necessary to remove fat globules, which are readily dispersed in water (because of their surface layers). In the cleaning of ultrafiltration membranes, etc., proteolytic enzymes are occasionally used.

## **6.2. Cleaning Duration**

Dissolution of the deposit may take a long time if the detergent has to diffuse into the layer, as is often the case. Timescales are several minutes to half an hour. For very thick layers, the diffusion time may be hours and then other mechanisms come into play.

## **6.3. Cleaning Procedures**

Cleaning operations can be performed in various ways, but ‘cleaning in place’ (CIP) is generally preferred because of its convenience (the equipment need not be dismantled and control is relatively simple), efficiency, and low cost. Two variants of CIP may be distinguished. For heat exchangers and similar equipment of relatively small internal volume, the apparatus is more or less used as when making a product, but now with cleaning liquid; it is thus completely filled. Often, the cleaning liquid is recirculated for a while. It may take a long time before the desired temperature is reached, and a separate heat exchanger for bringing the liquid to the desired temperature, say, 80°C, is sometimes used. For equipment containing relatively large vessels such as tanks, spraying of cleaning liquids is applied. Care must be taken that every spot at the inner surface is reached and with sufficient intensity. Similar conditions hold for apparatuses such as bottle washers. CIP often occurs in the following steps.

1. **Prerinsing:** Vigorous prerinsing with water can remove some 80% to 90% of the residual (i.e., not-deposited) material in the equipment. Especially for viscous products (stirred yogurt and evaporated milk), it may take a long time before all of the product is washed away. To limit loss of

milk and production of wastewater, most milk residues should be removed before pre-rinsing.

2. **Cleaning steps:** A much-applied method is first cleaning with an alkali and then with an acid solution. The alkali removes most of the deposit, leaving a certain amount of scale. After rinsing with water to remove most of the alkali, nitric or phosphoric acid is introduced to remove the scale. Instead of this two-step cleaning, one-step cleaning by using compound detergents can be applied. Cleaning with alkali and acid is always done after serious fouling of equipment (e.g., heat exchangers for sterilizing milk, and evaporators), whereas compound detergents are generally used for less tenacious fouling, as occurs for low pasteurization of plain milk.

3. **Final rinsing:** Rinsing with water is meant to remove cleaning agents. After acid cleaning, the acid should exhaustively be washed away, particularly when disinfection with sodium hypochlorite is subsequently applied ([Walstra et al., 2006](#)).

## 7. *Stainless Steel*

Stainless steel (Fe based alloy with a minimum of 10.5% Cr by mass for an atmospheric corrosion resistance) is utilized in many fields of technology due to its excellent corrosion resistance, physical and mechanical properties. The traditional and well established applications of stainless steel include construction, transportation and process industries, whereas the upcoming developments would include among others medical application and energy industries (power plants and solar thermal collectors) ([Bautista et al., 2003](#), [Taneike et al., 2003](#)).

Stainless steel (SS) based materials are employed in a wide range of modern applications due to their ability to withstand corrosive environments while

maintaining good mechanical properties. Corrosion resistance of stainless steel depends, among other parameters, on its surface state. As a matter of fact, the corrosion resistance of SS arises from a passive chromium rich oxide-hydroxide film that forms spontaneously on its surface when SS is exposed to air, and acts as a barrier against ion diffusion between the steel and the environment ([Jin and Atrens, 1987](#); [Jin and Atrens, 1990](#); [Mishler et al., 1988](#)).

It is the complex interaction of oxygen with the alloy surface which results in a protective oxide film which makes stainless steel so useful.

Stainless steel 316L (SS316L) is the most common food contact material used in the manufacture of food processing equipment, including heat exchangers for high temperature short time (HTST) processing. Unfortunately, SS316L is prone to fouling due to its high surface energy and hydrophilic nature, and fouling is exacerbated in heat exchangers due to wall heating and the resulting localized precipitation of minerals ([Baek et al., 2010](#); [Bansal and Chen, 2006](#); [De Jong, 1997](#)).

## ***8. Surface Modification Techniques***

Surface preparation is the essential first stage treatment of a substrate before the application of any coating. The performance of a coating is significantly influenced by its ability to adhere properly to the substrate material. It is generally well established that correct surface preparation is the most important factor affecting the total success of surface treatment.

To insure proper primer adhesion to the substrate, all contaminants must be removed. Depending on the type of substrate to be prepared, various methods should be used.

For effective bonding, the adhesive must completely wet the surface of each substrate being joined together. In addition, strong attractive interactions must form between the adhesive and the substrates. The presence of even small amounts of surface contaminants, such as oil, grease, oxides etc. can physically impair and reduce coating adhesion to the substrate. It is difficult to achieve good adhesion on substrates without specialized processing. Surface treatment is the process whereby the adherent surface is cleaned and/or chemically treated to promote better adhesion.

The method used to prepare such surfaces for adequate wetting will depend on the type of contaminant and the nature of the adherent. Some mechanical, physical and chemical methods were used for this purpose.

Various techniques have been used to deposit superhydrophobic thin films. Superhydrophobic surfaces have drawn a lot of interest both in academia and in industry because it reduces the amount of surface contamination and also the self-cleaning properties. They include chemical vapor deposition of poly(tetrafluoroethylene) (PTFE) ([Chen et al. 1999](#); [Li et al., 2002](#)), carbon nanotubes and walls ([Fang et al. 2003](#)), modulated Radio Frequency glow discharge ([Fivia et al., 2003](#)), microwave Plasma Enhanced Chemical Vapor Deposition (PECVD) ([Hozumi and Takai, 1997](#)), self-organization of fluorinated polymers ([Yabu et al., 2005](#)), etc. In general, fluorocarbon compounds are found to be water and oil repellent, due to their lower surface energies. Teflon is a fluorocarbon compound and Teflon-like coatings are deposited by different methods.

These methods include polymerization of fluorocarbon precursors in radio frequency plasma ([d'Agostino, 1990](#)), ion beam sputtering ([Wang et al., 1997](#)), and RF sputtering ([Chonkourov et al., 2002](#); [Bodas et al., 2005](#)).

### ***8.1. Atmospheric Pressure Plasma treatment***

In the early 1990s, the studies and applications of atmospheric plasma treatments have gradually increased due to its low cost and to its flexibility (inline process). In this field a surface modification is used to improve the adhesion properties between different kinds of materials for water base adhesives and paints (Kim et al., 2003). Many materials, including organic materials, inorganic materials, and metals could be readily surface-modified by plasma treatments (Park and kim, 2004; Chen et al., 2001; Kwon et al., 2005; Tang et al., 2005; Boudou et al., 2003; chai et al., 2004; Seo et al., 2005; Zhang et al., 2000; Dabhad et al., 2004; Kim et al., 2004; Lynach et al., 1999). Especially atmospheric pressure plasma has shown many advantages (Lynach et al., 1999) compared to other plasma systems, such as corona (no electric field uniformity) and low-pressure plasmas. Generally, low-pressure plasma has a wide range of applications in materials processing, but the vacuum system is expensive and requires heavy maintenance. Besides, the size of the object that could be treated is limited by the size of the vacuum chamber.

The advantage of atmospheric pressure plasma is firstly the relative speed of coating deposition. Amongst the precursors used to be deposited by atmospheric plasma, hexamethyldisilazane and hexamethyldisiloxane (HMDSO) (O'Neill et al., 2010; Yang et al., 2009; Ji et al., 2009; kim et al., 2005; Chen et al., 2008) are commonly used.

In order to improve the adhesion of these coatings on the substrate, and since adhesion largely depends on the surface properties of the materials, it is necessary to modify this near-surface region without affecting the bulk properties of the material (Tang et al., 2005). Recently, considerable research has been performed to improve the surface properties of different

materials, and in the field of surface modification, plasma processing has been proved to be a useful method in modifying the wettability, permeability, conductivity, adhesion or biocompatibility (Tang et al., 2005). In a review, Lin and Chang (2011) investigated surface behavior before and after surface modification by Ar/N<sub>2</sub>/O<sub>2</sub> plasma under atmospheric pressure condition. They found that the plasma treatment of a stainless steel plate has a significant effect on the wettability, contact angle, and free energy of the SS 304L stainless steel surface. Tang et al. (2005) used a poly(pyromelitic dianhydride-co-4,4-oxydianiline) to treat a stainless steel surface.

They proved that the surface energy was improved after plasma treatment and that it mainly influenced the polar components of stainless steel. Kim et al. (2003) discussed the effect of a N<sub>2</sub> and O<sub>2</sub> plasma jet on the surface of stainless steel, and it was proved that the surface of stainless steel became more hydrophilic because new functional groups appeared after the N<sub>2</sub> and O<sub>2</sub> plasma jet treatment. Yoon and Lund (1994) found higher milk fouling rates for the PTFE-coated plates in plate heat exchangers than for the SS 304L stainless steel plates with a higher surface energy. Zhao and Müller-Steinhagen (2001) report that the properties like surface roughness, charge and charge density play an important role for protein adsorption. Bornhorst et al. (1999) reported that deposit layers of fouling formed on SiF<sup>+3</sup>-implanted and DLC surface were thinner and easier to remove compared to uncoated stainless steel. They reported that surface modifications have a stronger effect on cleaning than on fouling deposition.

## ***8.2. Sol gel coatings***

The sol-gel process, as its name implies, involves the evolution of inorganic nanoscale networks through the formation of a colloidal suspension (sol) and the gelation of the sol to form a network in a continuous liquid phase (gel). Through controlled hydrolysis and condensation reactions different end products can be obtained.

Sol-gel technologies have developed greatly during the last twenty years. In the sol-gel reaction, homogenous inorganic materials with desirable properties of hardness, optical transparency, chemical durability, tailored porosity and thermal resistance can be formed. At the beginning, sol-gel was mainly used for producing purely ceramic coatings, foams, fibers and powders. The discovery that the sol-gel processing readily yields both inorganic and hybrid organic-inorganic materials, has greatly widened the scope of applications ([Arkles, 2001](#)).

The basic principle of the sol-gel process is to form a solution of the elements of the desired compound in an organic solvent, polymerize the solution to form a gel, and dry/ heat this gel to displace the organic components and form a final inorganic oxide ([Yi and Sayer, 1991](#)).

The raw materials in sol-gel processing are usually silicon or metal alkoxide precursors. The most widely used metal alkoxides are the alkoxy silanes, such as tetramethoxysilane (TMOS) and tetraethoxysilane (TEOS). Water is needed for hydrolysis reactions, where alkoxide (OR) groups are replaced by hydroxyl groups (OH). Alcohol is used as a solvent, because water and alkoxides are immiscible. It also facilitates the hydrolysis by homogenizing the system. In the condensation reactions the silanol (Si-OH) groups are condensing to form siloxane bonds (Si-O-Si). As by-products of the reaction, water and alcohol are usually formed. The raw materials and

by products of the reactions can be selected so that the process is environmentally friendly.

Various forms of applying such coatings exist, among which dip coating, spray coating ([Patial, 1999](#)) and spin coating ([Scriven, 1988](#)) are the most well-known ones.

Amongst these methods, the dip coating technique is the simplest for technical developments at the laboratory scale, since it does not require any sophisticated instrumentation but provides excellent reliability and reproducibility.

In the recent years, synthesis of water repellent surfaces has received a great attention because of their wide spectrum of applications such as frictionless flow through water pipes and micro channels ([Watanabe and Udagawa, 2001](#)), corrosion resistance coatings on metals ([Thim et al., 2000](#)), transparent and hydrophobic coatings on vehicle windshields ([Shang et al., 2005](#)), and efficient transportation of small quantities of liquids without mass loss using super hydrophobic surfaces ([Rao et al., 2005](#)).

The antifouling and easy-to-clean-properties of metal surfaces can also be improved by sol-gel hybrid coatings.

## ***Conclusion***

Dairy fouling results from the accumulation of unwanted material on heated surfaces. In general terms, fouling of milk products can mainly be divided into two groups: Protein fouling and Mineral fouling. The calcium phosphate and whey proteins are the main components of milk deposits, and the  $\beta$ -lg plays a dominant role in the fouling heat exchangers. The factors affecting on milk fouling in heat exchangers can be classified into three major categories: milk composition, operating conditions in heat exchanger and surface state of heat exchanger.

Cleaning in the dairy industry is done every 5-10 h depending on fouling severity and this operation is expensive and causes great losses in time and energy, for this reason the phenomena occurring at the interface steel-milk must be understood and surface modifications of stainless steel to reduce fouling must be extensively investigated.

Fouling deposits thus form as a result of adhesion of species to the surface and cohesion between elements of material. The physical properties of both fouling deposits and surface as well as process conditions (which influence adsorption of organic and/or mineral components onto food contact surfaces and subsequently built up of additional layers) will affect adhesive/cohesive strengths (Fryer et al., 2005). Cleaning can result from either or both adhesive and cohesive failure depending on the part of the respective strengths. In removing a deposit during cleaning, both cohesive (deposit-deposit) and interfacial adhesive (surface-deposits) forces must be overcome. In this context, surface modification for reduction of fouling, either by inhibiting attachment of depositing species or by increasing

the ease of the removal during cleaning has received more and more attention in the food sector.

To understand the reaction interface between the milk components and this substrate surface and to understand the mechanism of the adhesion, the surface must be characterized by surface characterization techniques, which will be displayed in the next chapter of this thesis.

**References:**

- Agle, M.E., 2007. Biofilms in the food industry. Biofilms in the food environment. Blackwell Publishing Ltd, 3–18.
- Al-Janabi A., Malayeri M. R., Müller-Steinhagen H. (2010). Experimental fouling investigation with electroless Ni-P coatings. *International Journal of Thermal Sciences*, 49, 1063-1071
- Al-Roubaie, S. M. and Burton, H. (1979). Effect of free fatty acids on the amount of deposit formed from milk on heated surfaces. *Journal of Dairy Research*, 46(3), 463-471.
- Amjad, Z. (1998). Calcium Phosphate in Biological and Industrial Systems, The BF Goodrich Company (Eds.), Boston/Dordrecht/ London: Kluwer Academic Publishers.
- Andritsos, N., Yiantsios, S. G., & Karabelas, A. J. (2002). Calcium phosphate scale formation from simulated milk ultrafiltrate solutions. *Food and Bioproducts Processing*, 80(C4), 223–230.
- Arkles B., (2001). “Commercial Applications of Sol-Gel-Derived Hybrid Materials”, *MRS Bulletin*, p. 402
- Arnebrant, T., Barton, K. and Nylander, T. (1987). Adsorption of  $\alpha$ -lactalbumin and  $\beta$ -lactoglobulin on metal surfaces versus temperature. *J. Colloid Interface Sci.* 119(2), 383-396.
- Augustin, W., Geddert, T., Scholl, S. (2007). Surface treatment for the mitigation of whey protein fouling. In: *Proceedings of 7<sup>th</sup> International Conference on Heat Exchanger Fouling and Cleaning*, Tomar, Portugal, ECI Symposium Series, Volume RP5, pp. 206–214.
- Aymard, P., Gimel J. C., Nicolai T., and Durand D. (1996). Experimental evidence for a two-step process in the aggregation of b-lactoglobulin at

pH 7: Journal de chimie physique et de Physico-Chimie Biologique, V. 33, P. 987-997.

Baek, S.M., Seol, W.S., Lee, H.S., Yoon, J.I. (2010). Decreasing the fouling of heat exchanger plates using air bubbles. Defect Diffus. Forum 297, 1199–1204.

Bansal, B., Chen, X.D., 2006. A critical review of milk fouling in heat exchangers. Compr. Rev. Food Sci. Food Saf. 5, 27–33.

Bansal, B., Habib, B., Rebmann, H., and Chen, X. D. (2009). Effect of Seasonal Variation in Milk Composition on Dairy Fouling. In Processing of International Conference on Heat Exchanger Fouling and Cleaning VIII.

Barish J. A. and Goddard J. M. (2013). Anti-fouling surface modified stainless steel for foodprocessing. Food and bioproducts processing, 91, 352–361.

Bautista, A., Velasco, F., Campos, M., Rabanal, M., and Torralba, J. Oxidation behavior at 900° C of austenitic, ferritic, and duplex stainless steels manufactured by powder metallurgy, Oxidation of metals, Volume 59, 2003, pp. 373-393.

Bell RW, Sanders CF. (1944). Prevention of milkstone formation in a high-temperature short-time heater by preheating milk, skim milk and whey. J Dairy Sci 27:499–504

Belmar-Beiny MT, Gotham SM, Paterson WR, Fryer PJ, Pritchard AM. (1993). The effect of Reynolds number and fluid temperature in whey protein fouling. J Food Eng 19:119–39.

Bennett, H. A. E. (2007). Aspects of Fouling in Dairy Processing. Ph. D. thesis, Massey University, Palmerston North, New Zealand.

- Beuf M, Rizzo G, Leuliet JC, Müller-Steinhagen H, Yiantsios S, Karabelas A, Benezech T. (2003). Potency of stainless steel modifications in reducing fouling and in improving cleaning of plate heat exchangers processing dairy products. In: Proceedings of heat exchanger fouling and cleaning—fundamentals and applications. Santa Fe, N.M, U.S.A. May 18-22: Engineering Conferences International, New York, U.S.A.
- Bodas D.S., Mandale A.B. and Gangal S.A., (2005). Deposition of PTFE thin films by RF plasma sputtering on silicon substrates Appl. Surf. Sci. 245, 202.
- Bornhorst A., Zhao Q., Müller-steinhagen H. (1999). Reduction of Scale Formation by Ion Implantation and Magnetron Sputtering on Heat Transfer Surfaces. Heat Transfer Engineering, Vol.20, No. 2, 6-14.
- Bott, T.R. (1995). Fouling of Heat Exchangers. Elsevier Science & Technology Books. 529.
- Boudou J. P., Paredes J. I., Cuesta A., Martinez-Alonso A., Tascon J. M. D. (2003). Oxygen plasma modification of pitch-based isotropic carbon fibres. Carbon. 41, 41.
- Brusilovsky, M., Borden, J. and Hasson, D., (1992). Flux Decline due to Gypsum Precipitation on RO Membranes. Desalination, 86: p. 187-222
- Burton, H. (1965). A method for studying the factors in milk which influence the deposition of milk solids on a heated surface. Journal of Dairy Research, 34,65-78.
- Burton, H. (1966). A comparison between a hot-wire laboratory and a pleat heat exchanger for determining the sensitivity of milk to deposit formation. Journal Dairy Research, 33, 317-324.

- Burton, H. (1968). Reviews of the progress of dairy science. *Journal of Dairy Research*, 35,317-330.
- Burton H. (1968) Deposits from whole milk in heat treatment plant – a review and discussion. *Journal of Dairy Research* 35 317-330.
- Burton, H. (1988) *Ultra-High-Temperature Processing of Milk and Milk Products*. Elsevier Applied Science, London.
- Burton H. (1968) Deposits from whole milk in heat treatment plant – a review and discussion. *Journal of Dairy Research* 35 317-330.
- Chai J. N., Lu F. Z., Li B. M., Kwok D. Y. (2004). Wettability interpretation of oxygen plasma modified poly(methyl methacrylate). *Langmuir*. 20, 10919.
- Changani, S. D., Belmar-Beiny, M. T. and Fryer, P. J. (1997). Engineering and chemical factors associated with fouling and cleaning in milk processing, *Experimental Thermal and Fluid Science*, 14, 392-406.
- Chen W., Fadeev A.F., Hsieh M.C., Oner D., Youngblood J. and McCarthy T.J., (1999). Ultrahydrophobic and Ultralyophobic Surfaces: Some Comments and Examples, *Langmuir* 15 (10), 3395.
- Chen Q. D., Dai L. M., Gao M., Huang S. M., Mau A. (2001). Plasma modification of carbon nanotubes for chemical modification. *J. of Phys. Chem. B* 105, 618.
- Chen G., Chen S., Feng W., Chen W., Yang S. Z. (2008). Surface modification of the nanoparticles by an atmospheric room-temperature plasma fluidized bed. *Appl. Surf. Sci.* 254, 3915.
- Choukourov A., Pihosh Y., Stelmashuk V., Biederman H., Slavinska D., Kormunda M. and Zajickova L., (2002). Rf sputtering of composite SiOx / plasma polymer films and their basic properties *Surf. Coat. Technol.* 151/152, 214.

- Christian G. K., Changani S. D. & Fryer P. J. (2002) The effect of adding minerals on fouling from whey protein concentrate – development of a model fouling fluid for a plate heat exchanger. *Transactions of IChemE (part C)* 80 231-239.
- Cooper, A., Sutor, J. W. and Usher, J. D. (1980). Cooling Water Fouling in Plate Heat Exchangers. *Heat Transfer Engineering*, 1(3): p. 50-55.
- Corredig M, Dalgleish DG. (1996). Effect of temperature and pH on the interactions of whey proteins with casein micelles in skim milk. *Food Res Int* 29(1):49–55.
- D’Agostino R., (1990). *Plasma Deposition, Treatment and Etching*, Academic Press, New York.
- Dabhade R. V., Bodas D. S., Gangel S. A. (2004). Plasma-treated polymer as humidity sensing material—a feasibility study. *Sens. Actuators, B, Chem.* 98, 37.
- Daufin G, Labbé JP, Quemerais A, Brulé G, Michel F, Roignant M, Priol M. (1987). Fouling of a heat exchanger surface by whey, milk and model fluids: an analytical study. *Lait* 67:339–64
- de Jong, P., Waalewijn, R. and Van der Linden, H.J.L.J. (1993) Validity of a kinetic fouling model for heat treatment of whole milk. *Lait* **73**, 293–302.
- De Jong, P. (1996) *Modelling and Optimization of Thermal Treatments in the Dairy Industry*. Delft University.
- De Jong, P., 1997. Impact and control of fouling in milk processing. *Trends Food Sci. Technol.* 8, 401–405.
- De Jong P, van der Horst HC, Waalewijn R. (1998). Reduction of protein and mineral fouling. *Fouling and Cleaning in Food Processing*; Jesus

- College, Cambridge, England; April 6-8, p 39–46: Office for Official Publications of the European Communities, Luxembourg.
- Delsing BMA, Hiddink J. (1983). Fouling of heat transfer surfaces by dairy fluids. *Netherlands Milk Dairy J* 37:139–48.
- deWit, J. N. and Klarenbeek, G., 1984, Effects of Various Heat Treatments on Structure and Solubility of Whey Proteins . *J Dairy Sci*, 67 : 2701–2710.
- Elofsson UM, Paulsson MA, Sellers P, Arnebrant T. (1996). Adsorption during heat treatment related to the thermal unfolding/aggregation of  $\beta$ -lactoglobulin A and B. *J Coll Interf Sci* 183:408–15.
- Epstein, N. (1981). Fouling in heat exchangers. In *Low Reynolds Number Flow Heat Exchangers*, S. Kakac, R. K. Shah, and A. E. Bergles (eds.). Hemisphere, New York.
- Epstein, N., *Heat Exchanger Theory and Practice*, in: J. Taborek, G. Hewitt (1983). *Heat exchangers in Heat Exchanger Theory and Practice*, McGraw-Hill.
- Favia P., Cicala G., Milella F., Palumbo F., Rossini P. and d'Agostino R., (2003). Deposition of super-hydrophobic fluorocarbon coatings in modulated RF glow discharges, *Surf. Coat. Technol.* 169/170, 609.
- Fehlner F. and Graham M. (2002). Thin oxide film formation on metals, P Marcus (Ed.), *Corrosion Mechanisms in Theory and Practice*, Marcel Dekker Inc., New York, 171-187.
- Feng L., Song S., Zhai J., Liu B., Xu J., Jiang L., Zhu D., (2003). Creation of a Superhydrophobic Surface from an Amphiphilic Polymer *Angew. Chem. Int. Ed.* 42, 800.

- Flint S.H., Brooks J.D., Bremer P.J. (2000). Properties of the stainless steel substrate influencing the adhesion of thermo-resistant streptococci. *J Food Eng* 43(4):235–42.
- Foster C.L., Britten M, Green M.L. (1989). A model heat-exchanger apparatus for the investigation of fouling of stainless steel surfaces by milk I. deposit formation at 100°C. *J Dairy Res* 56:201–9.
- Fryer PJ, Robbins PT. (2005). Heat transfer in food processing: ensuring product quality and safety. *Applied Thermal Engineering.*, 25, 2499-510.
- Fryer PJ, Christian GK, Liu W. (2006) How hygiene happens: physics and chemistry of cleaning. *International Journal of Dairy Technology.* 59, 76-84.
- Fung L., McCarthy O. J. & Tuoc T. K. (1998) The effect of fat globule membrane damage on fouling of whole milk. *Fouling and Cleaning in Food Processing '98*, Jesus College, Cambridge, UK 33-38.
- Gillham C.R. (1997) Enhanced cleaning of surfaces fouled by whey proteins. University of Cambridge, Cambridge, UK. 46, 3, 199-209.
- Gillham, C.R., Fryer, P.J., Hasting, A.P.M., Wilson, D.I. (2000). Enhanced cleaning of whey protein soils using pulsed flows. *J. Food Eng.* 46, 199–209.
- Gordon, K.P., Hankison, D. J. and Carver, C. E. (1968). Deposition of milk solids on heated surface. *Journal of Dairy Science*, 51(4), 520-526.
- Grandison A.S. (1988). Effects of natural (or seasonal) variation in concentration of components of milk and addition of divalent cations on ultra-high temperature processing characteristics. *J Soc Dairy Technol* 41:117–9.

- Grasshoff, A. (1997) Cleaning of heat treatment equipment. For: IDF monograph, Fouling and cleaning in Heat Exchangers. 90, 4, 433-440.
- Gillham, C.R., Fryer, P.J., Hasting, A.P.M., Wilson, D.I. (2000). Enhanced cleaning of whey protein soils using pulsed flows. *J. Food Eng.* 46, 199–209.
- Hasting, A. P. M., (1994), The importance of fouling and cleaning to the food industry, *Proc. Fouling and Cleaning in Food Processing*, Jesus College, Cambridge, V – VI
- Hillier R. M., Lyster R. L. J. and Cheeseman G. C. (1979). Thermal denaturation of  $\alpha$ -lactalbumin and  $\beta$ -lactoglobulin in cheese whey: effect of total solids concentration and pH. *Journal of Dairy Research*, 46(1), 103-11.
- Hozumi A., Takai O., (1997). Preparation of ultra water-repellent films by microwave plasma-enhanced CVD, *Thin Solid Films* 303, 222.
- Huppertz T, Fox PF, Kelly AL. (2004). High pressure-induced denaturation of alpha-lactalbumin and beta-lactoglobulin in bovine milk and whey: a possible mechanism. *Journal of Dairy Research.*, 71, 489-95.
- Itoh, H., Nagata, A., Toyomasu, T., Sakiyama, T., Nagai, T., Saeki, T., Nakanishi, K. (1995). Adsorption of  $\beta$ -lactoglobulin onto the surface of stainless steel particles. *Biosci. Biotech. Biochem.*, 59(9), 1648-1651
- Jeurnink TJM, de Kruif KG. (1995). Calcium concentration in milk in relation to heat stability and fouling. *Netherlands Milk Dairy J* 49:151–65.
- Jeurnink T., Verheul M., Stuart M.C., de Kruif K.G. (1996). Deposition of heated whey proteins on a chromium oxide surface. *Colloids Surf B Biointerf* 6:291–307.

- Jeurnink, T. J. M., Walstra, P., & de Kruif, C. G. (1996). Mechanisms of fouling in dairy processing. *Netherlands Milk and Dairy Journal*, 50, 407–426.
- Ji Y. Y., Kim S. S., Kwon O. P., Lee S. H. (2009). Easy Fabrication of Large-Size Superhydrophobic Surfaces by Atmospheric Pressure Plasma Polymerization with Non-Polar Aromatic Hydrocarbon in an In-Line Process. *Appl. Surf. Sci.* 255, 4575.
- Jin S. and Atrens A., (1987). ESCA-studies of the structure and composition of the passive film formed on stainless steels by various immersion times in 0.1 M NaCl solution. *Appl. Phys., A* 42, 149.
- Jin S. and Atrens A. (1990). Passive films on stainless steels in aqueous media. *Appl. Phys., A* 50, 287.
- Jun, S., & Puri, V. M. (2005). Fouling models for heat exchangers in dairy processing: A review. *Journal of Food Process Engineering*, 28(1), 1–34.
- Kananeh A. B., Scharbeck E., Kück U.D., (2010). Rübiger N.. Reduction of milk fouling inside gasketed plate heat exchanger using nano-coatings. *Food and bioproducts processing*, 88, 349–356
- Karlsson, A-C. (1999). Fouling and Cleaning of Solid Surface: The influence of surface characteristics and operating conditions. Lund University, Sweden, 5, 28-33.
- Keshani S., Daud W., Woo M., Nourouzi M. M., Talib M., Chuah A., Russly A.R. (2013). Reducing the deposition of fat and protein covered particles with low energy surfaces. *Journal of Food Engineering*, 116, 737–748.
- Kessler H.G., Beyer H.J. (1991). Thermal denaturation of whey proteins and its effect in dairy technology. *Int J Biological Macromolec* 13:165–73.

- Kim, J. C. and Lund, D. B. (1997). Adsorption behavior of  $\beta$ -lactoglobuline onto stainless steel surfaces. *J. of Food Proc. And Pres.*, 21, 303-317.
- Kim, J. C. and Lund, D. B. (1998). Kinetics of  $\beta$ -lactoglobuline adsorption onto stainless steel surfaces. *Boitech. Prog.*, 14, 951-985.
- Kim M. C., Song D. K., Shin H. S., Baeg S. H., Kim G. S., Boo J. H., Han J. G., Yang S. H. (2003). *Surface and Coating Technol.* 171, 312.
- Kim J. S., Kim Y. E., Lee K. H. (2004). Effects of atmospheric plasma treatment on the interfacial characteristics of ethylene–vinyl acetate/polyurethane composites. *J. of Colloid Interface Sci.* 271, 187.
- Kim S. H., Kim J. H., Kang B. K., Uhm H. S. (2005). Superhydrophobic CFx Coating via In-Line Atmospheric RF Plasma of He-CF<sub>4</sub>-H<sub>2</sub>. *Langmuir.* 21, 12213.
- Krause, S. (1993). Fouling of heat-transfer surfaces by crystallization and sedimentation. *International Chemical Engineering*, 33(3), 355–401.
- Kwon O. J., Tang S., Myung S. W., Lu N., Choi H. S. (2005). Surface Free Energy Change of Polypropylene Film Treated by Atmospheric Pressure plasma. *Surface Coating Technol.* 192, 1.
- Labouré H, Cases E, Cayot P. (2004). Heat induced [ $\beta$ ]-lactoglobulin polymerization: role of the change in medium permittivity. *Food Chemistry.*, 85, 399-406.
- Lalande, M., Tissier, J. P. and Corrieu, G. (1984). Fouling of a plate heat-exchanger used in ultra-high-temperature sterilization of milk. *Journal Dairy Research*, 51(4), 557-568.
- Lamotte, L.B., Nonville, S., Goubard, F., Marque, P. and Pauthe, E. (2008). Kinetics of conformational changes of fibrinogen adsorbed onto model surfaces. *Colloids and Surfaces B: Biointerfaces.* 63. 129-137.

- Lewis M, Heppell N. (2000). Fouling, cleaning, and disinfecting. In: Continuous thermal processing of foods. Gaithersburg, Md.: Aspen Publishers.
- Li S., Li H., Wang X., Song Y., Liu Y., Jiang L. and Zhu D., (2002). Super-Hydrophobicity of Large-Area Honeycomb-Like Aligned Carbon Nanotubes, *J. Phys. Chem. B* 106, 9274.
- Lin J. W., Chang H. C. (2011). Surface modification of SUS304 stainless steel by atmospheric pressure Ar/N<sub>2</sub>/O<sub>2</sub> plasma. *Nuclear Instruments and Methods in Physics Research. B* 269, 1801.
- Luey, J. K., McGuire, J., Sproull, R. D. (1991). The effect of pH and NaCl concentration on adsorption of  $\beta$ -lactoglobulin at hydrophilic and hydrophobic silicon surface. *J. Colloid Interface Sci.*, 143, 489-500.
- Lund, D., (1981), State of the art of fouling: Heat transfer surfaces, *Proc. Fundamentals and Applications of Surface Phenomena Associated with Fouling/Cleaning Processing*, Sweden, 27-56
- Lynach J. B., Spence P. D., Postlethwaite T. A. (1999). Atmospheric pressure plasma treatment of polyethylene via a pulse dielectric barrier discharge: Comparison using various gas compositions versus corona discharge in air. *J. Appl. Polym. Sci.* 71, 319.
- Lyster, R. L. J. (1970). Denaturation of  $\alpha$ -lactalbumin and  $\beta$ -lactoglobulin in heated milk. *Journal of Dairy Research*, 37(2), 233-43.
- Lyster, R. L. J. (1965). The composition of milk deposits in an ultra-high-temperature plant. *Journal Dairy Research*, 32, 203-208.
- Melo, L. F., Bott, T. R., and Bernardo, C. A. (1988). *Fouling Science and Technology*. Kluwer, Dordrecht.

- Mishler S., Mathieu H.J., Landolt D. (1988). Investigation of a passive film on an iron—chromium alloy by AES and XPS. *Surf. Interface Anal.*, 11, 182.
- Mottar J. and Moermans R. (1988). Optimization of the forewarming process with respect to deposit formation in indirect ultra high temperature plants and the quality of milk. *J Dairy Res* 55:563–8.
- Muller-Steinhagen, H. M. and Middis, J. (1989). Particulate Fouling in Plate Heat Exchangers. *Heat Transfer Engineering*, 10(4): p. 30-36.
- Muller-Steinhagen, H. (1993). Fouling: the ultimate challenge for heat exchanger design. In: 6<sup>th</sup> Int. Symposium on Transport Phenomena in Thermal Engineering. Seoul, Korea, May 9–13, Begell House, New York, USA.
- Müller-Steinhagen, H. M. (2000), Handbook of heat exchanger fouling : Mitigation and cleaning technologies Publications ;Institution of Chemical Engineers, Essen Rugby.
- Murray, B.S., Deshares, C., (2000). Monitoring protein fouling of metal surfaces via a quartz crystal microbalance. *J. Colloid Interface Sci.* 227 (1), 32–41.
- Mullin, J. W. (1993). *Crystallization* (3<sup>rd</sup> ed). London: Butterworths.
- Nancollas, G. H., Amjad, Z. and Koutsoukos, P., 1979, Calcium phosphates—speciation, solubility, and kinetic considerations, in Jenne, E. (ed). *Chemical Modelling in Aqueous Systems*, ACS Symposium Series, 93: 475–497.
- Newstead D. F., Groube G. F., Smith A. F. and Eiger R. N. (1998). Fouling of UHT plants by recombined and fresh milk: some effects of preheat treatment. *Fouling and Cleaning in Food Processing '98*, Jesus College, Cambridge, UK 17-24.

- Ngadi N. (2009). Mechanisms of Molecular Brush Inhibition of Protein Adsorption onto Stainless Steel Surface. Ph.D. thesis, Department of Chemical and Process Engineering, University of Canterbury.
- O'Neill L., Herbert A. P. F., Stallard C., Dowling D. P. (2010). Investigation of the Effects of Gas versus Liquid Deposition in an Aerosol-Assisted Corona Deposition Process. *Plasma process Polym.* 7, 43.
- Oudar J. (2002). Introduction to surface reactions: Adsorption from gas phase, P Marcus (Ed.), *Corrosion Mechanisms in Theory and Practice*, Marcel Dekker Inc., New York, 19-51.
- Pasche, S., Voros, J., Griesser, H. J., Spencer, N. D. and Textor, M. (2005). Effects of ionic strength and surface charge on protein adsorption at PEGylated surfaces. *Journal Physic Chemistry B.* 109. 17545-17552.
- Pappas, C. P. and Rothwell, J., 1991, The effects of heating, alone or in the presence of calcium or lactose, on calcium binding to milk protein. *Food Chem*, 42: 183–201.
- Parkar, S.G., Flint, S.H., Brooks, J.D., (2004). Evaluation of the effect of cleaning regimes on biofilms of thermophilic bacilli on stainless steel. *Journal of Applied Microbiology*, 96 (1), 110–116.
- Patel J. S., Bansal B., Jones M. I., Hyland M. (2013). Fouling behaviour of milk and whey protein isolate solution on doped diamond-like carbon modified surfaces. *Journal of Food Engineering*, 116, 413–421.
- Paterson W.R., Fryer P.J. (1988). A reaction engineering approach to the analysis of fouling. *Chem Eng Sci* 43(7):1714–7.
- Patil, G.R. and Reuter, H. (1988) Deposit formation in UHT plants. III. Effect of pH of milk in directly and indirectly heated plants. *Milchwissenschaft* **43**, 360–362.

- Patil P.S. (1999). Versatility of chemical spray pyrolysis technique. *Materials Chemistry and Physics* 59, 185.
- Pielinger-Schweiger S. (2001). Electrochemical and chemical polishing of heat exchangers. In: Proceedings of heat exchanger fouling—fundamental approaches & technical solutions. Davos, Switzerland; July 8-13. New York, U.S.A.: United Engineering Foundation, Inc.
- Prakash S. DH, Grandison A., Lewis M. (2006). Role of ionic calcium in fouling of heat treated milk. *Fouling, cleaning & disinfection in food processing*. Cambridge, UK.
- Petit J, Herbig AL, Moreau A, Delaplace G. (2011). Influence of calcium on  $\beta$ -lactoglobulin denaturation kinetics: Implications in unfolding and aggregation mechanisms. *Journal of Dairy Science.*, 94, 5794-810.
- Petit J, Herbig AL, Moreau A, Le Page JF, Six T, Delaplace G. (2012). Granulomorphometry: a suitable tool for identifying hydrophobic and disulfide bonds in  $\beta$ -lactoglobulin aggregates. Application to the study of  $\beta$ -lactoglobulin aggregation mechanism between 70 and 95°C. *Journal of Dairy Science.*, 95, 4188-202.
- Perez OE, Pilosof AMR. (2004). Pulsed electric effects on the molecular structure and gelation of  $\beta$ -lactoglobulin concentrate and egg white. *Food Research International.*, 37, 102-10.
- Ramachandra S.S., Wiehe S., Hyland M.M., Chen X.D., Bansal B. (2005). Modification of heating surfaces to reduce the effects of fouling in the dairy industry. *Heat exchanger fouling and cleaning: challenges and opportunities, engineering conferences intl*. Kloster Irsee, Germany, June 5-10. New York, U.S.A.: Engineering Conferences International.
- Rao A.V., Kulkarni M.M., Bhagat S.D. (2005). Transport of liquids using hydrophobic aerogels. *J. Colloid Interf. Sci.* 285, 413.

- Ritter, R. B. (1983). Crystallisation Fouling Studies. *Journal of Heat Transfer*, 105: p. 374-378.
- Rittschof, D. and Parker, K. K. (2001). Cooperative Antifoulant Testing: A Novel Multisector Approach. In *Recent Advances in Marine Biotechnology: Bio-organic compounds: Chemistry and Biomedical Applications*. Fingerman, M., Nagabhuchanam, R. (Eds.). Science Publishers Inc.: Enfield, NH, Vol. 6, pp 239-251.
- Roefs, P. F. and de Kruif, K. G., 1994, A model for the denaturation of  $\beta$ -lactoglobulin, *Eur J Biochem*, 226: 883–889.
- Rosmaninho R, Rizzo G, Müller-Steinhagen H, Melo LF. (2003). The influence of bulk properties and surface characteristics on the deposition process of calcium phosphate on stainless steel. In: *Proceedings of heat exchanger fouling and cleaning—fundamentals and applications*. Santa Fe, New Mexico, U.S.A.; May 18-22. New York, U.S.A.: Engineering Conferences International.
- Rosmaninho R, Rizzo G, Müller-Steinhagen H, Melo LF. (2005). Anti-fouling stainless steel based surfaces for milk heating processes. *Heat exchanger fouling and cleaning: challenges and opportunities, engineering conferences intl*. Kloster Irsee, Germany; June 5-10: New York, U.S.A.: Engineering Conferences International.
- Rosmaninho R, Melo LF. (2006). Calcium phosphate deposition from simulated milk ultrafiltrate on different stainless steel-based surfaces. *Int Dairy J* 16:81–7.
- Rosmaninho R, Santos O, Nylander T, Paulsson M, Beuf M, Benezech T. (2007). Modified stainless steel surfaces targeted to reduce fouling – Evaluation of fouling by milk components. *Journal of Food Engineering.*, 80, 1176-87.

- Rosmaninho R, Melo LF. (2008) Protein-Calcium Phosphate Interactions in Fouling of Modified Stainless-Steel Surfaces by Simulated Milk. *International Dairy Journal*, 18, 72-80.
- Rungraeng N., Cho Y., Yoon S., Jun S. (2012). Carbon nanotube-polytetrafluoroethylene nanocomposite coating for milk fouling reduction in plate heat exchanger. *Journal of Food Engineering*, 111, 218–224.
- Saikhwan P, Mercadé-Prieto R, Chew YMJ, Gunasekaran S, Paterson WR, Wilson DI. (2010). Swelling and dissolution in cleaning of whey protein gels. *Food and Bioproducts Processing.*, 88, 375-83.
- Sakiyama, T., Tanino, K., Urakawa, M., Imamura, K., Takahashi, T., Nagai, T., Nakanishi, K. (1999). Adsorption characteristics of tryptic fragments of bovine  $\beta$ -lactoglobulin on a stainless steel surface. *J. of Biosci. And Bioengin.*, Vol. 88, 5, 536-541.
- Santos O, Nylander T, Paulsson M, Trägårdh C. (2001). Adsorption behavior of  $\beta$ -Lactoglobulin on different types of stainless steel surfaces. In: *Proceedings of heat exchanger fouling—fundamental approaches & technical solutions*. Davos, Switzerland; July 8-13: New York, U.S.A.: United Engineering Foundation, Inc.
- Santos O, Nylander T, Rizzo G, Müller-Steinhagen H, Trägårdh C, Paulsson M. (2003). Study of whey protein adsorption under turbulent flow rate. In: *Proceedings of heat exchanger fouling and cleaning—fundamentals and applications*; Santa Fe, New Mexico, U.S.A.; May 18-22. New York, U.S.A.: Engineering Conferences International.
- Santos O, Nylander T, Rosmaninho R, Rizzo G, Yiantsios S, Andritsos N, Karabelas A, Müller-Steinhagen H, Melo L, Boulangé-Petermann L, Gabet C, Braem C, Trägårdh C, Paulsson M. (2004). Modified

- stainless steel surfaces targeted to reduce fouling—surface characterization. *J Food Eng* 64:63–79.
- Santos, O., T. Nylander, et al., (2006), Effect of surface and bulk solution properties on the adsorption of whey protein onto steel surfaces at high temperature, *J. Food Eng.*, Vol. 73(2), pp. 174.
- Scriven L.E. (1988). Physical and applications of dip coating and spin coating. *Materials Research Society Symposium Proceedings* 121, 717.
- Seo M. K., Park S. J., Lee S. K. (2005). Influence of atmospheric plasma on physicochemical properties of vapor-grown graphite nanofibers. *J. of Colloid Interface Sci.* 285, 306.
- Shang H.M., Wang Y., Limmer S.J., Chou T.P., Takahashi K., Cao G.Z. (2005). Optically transparent superhydrophobic silica-based films. *Thin Solid Films*, 472, 37.
- Skudder, P.J., Brooker, B.E., Bonsey, A.D. and Alvarez Guerrero, N.R. (1986). Effect of pH on the formation of deposit from milk on heated surfaces during ultra-high-temperature processing. *Journal of Dairy Research* 53, 75–87.
- Somerscales, E. F. C., and Knudsen, J. G. (eds.) (1981). *Fouling of Heat Transfer Equipment*. Hemisphere, New York.
- Taneike M., Abe F. and Sawds K. (2003). Creep-strengthening of steel at high temperatures using nano-sized carbonitride dispersions, *Nature*, 424, 294-296.
- Tang S., Kwon O. J., Lu N., Choi H. S. (2005). Surface characteristics of AISI 304L stainless steel after an atmospheric pressure plasma treatment. *Surface Coating Technol.* 195, 298.

- Tay S. N. and Yang C. (2006). Assessment of The Hydro-Ball Condenser Tube Cleaning System, Hydro-Ball Technics Sea Pte. Ltd, Singapore,
- Tisser, J.P., Lalande, M., and Corrieu, G. (1984). A study of milk deposition on a heat exchange surface during ultra-high-temperature treatment. In engineering and food, Vol. 1: Engineering sciences in the food industry, Mckenna B.M., Eds., Applied Science Publishers.
- Thim G.P., Oliveira M.A.S., Oliveira E.D.A., Melo F.C.L. (2000). Sol-gel silica film preparation from aqueous solutions for corrosion protection. *J. Non-Cryst. Solids* 273, 124.
- Thom, R. (1975). Formation of milk deposits in plate heaters. *Milchwissenschaft*, 30 (2), 84-89.
- Toyoda, I., Schreier, P.J.R., Fryer, P.J., (1994). A computational model for reaction fouling from whey protein solutions. Fouling and Cleaning in Food Processing, Jesus College, Cambridge, England, March 23–25.
- Visser, J., & Jeurnink, T. J. M. (1997). Fouling of heat exchangers in the dairy industry. *Experimental Thermal and Fluid Science*, 14(4), 407–424.
- Vyas H.K., and Tong P.S. (2004). Impact of source and level of calcium fortification on the heat stability of reconstituted skim milk powder. *J Dairy Sci* 87:1177–80.
- Wahlgren M., Arnebrant T. (1990). Adsorption of  $\beta$ -lactoglobulin onto silica, methylated silica, and polysulfone. *J Coll Interf Sci* 136:259–65.
- Wahlgren M., Arnebrant T. (1991). Protein adsorption to solid surfaces. *Tibtech* 9:201–8.

- Walker, G., (1982). Degradation of Performance, Industrial Heat Exchangers- A Basic Guide. Hemisphere Publishing Corporation. 213-272.
- Wang L., Li H., He J., He X., Li W., Wang Y. and Li H., (1997). Structure analysis of eflon-like thin films synthesized by ion beam sputtering deposition Mater. Lett. 33, 77.
- Walstra P., Wouters J. T. M. and Geurts T. J. (2006). Dairy Science and Technology (2nd Ed), CRC/Taylor & Francis
- Watanabe K. and Udagawa H. (2001). Drag Reduction of Non-Newtonian Fluids in a Circular Pipe with a Highly Water-Repellent Wall. J. AIChE (Japan) 47 (2), 256.
- Xiong Y. L. (1992) Influence of pH and ionic environment on thermal aggregation of whey proteins. Journal of Agricultural and Food Chemistry 40 380-384.
- Yabu H., Takebayashi M., Tanaka M. and Shimomura M., (2005). Superhydrophobic and Lipophobic Properties of Self-Organized Honeycomb and Pincushion Structures. Langmuir 21, 3235.
- Yang S., Liu C., Su C., Chen H. (2009). Atmospheric-pressure plasma deposition of SiO<sub>x</sub> films for super-hydrophobic application. Thin Solid Films. 517, 5284.
- Yi G. and Sayer M. (1991). Sol-gel processing of complex oxide films. Am. Ceram. Soc. Bull., 70 (1991), pp. 1173.
- Yoon, J. and Lund, D. B. (1989). Effect of operation conditions, surface coatings and pretreatment on milk fouling in plate heat exchanger. In proceeding of third international conference on fouling and cleaning in food processing. University of Munich. Munich, Germany.

- Yoon J., Lund D.B. (1994). Magnetic treatment of milk and surface treatment of plate heat exchangers: effect on milk fouling. *J Food Sci* 59(5):964–9, 980.
- Zhai J, Wooster TJ, Hoffmann SV, Lee TH, Augustin MA, Aguilar MI. (2011). Structural rearrangement of  $\beta$ -lactoglobulin at different oil-water interfaces and its effect on emulsion stability. *Langmuir.*, 27, 9227-36.
- Zhang D., Dongal S. M., Yeganeh M. S. (2000). Effect of UV irradiation and plasma treatment on a polystyrene surface studied by IR-visible sum frequency generation spectroscopy. *Langmuir.* 16, 4528.
- Zhao Q., Müller-steinhausen H. (2001). Intermolecular and Adhesion Forces of Deposits on Modified Heat Transfer Surfaces. Proc. UEFC on Heat Exchangers Fouling., Davos, Switzerland, Session II.

## **CHAPTER TWO**

# ***SURFACE CHARACTERIZATION TECHNIQUES, MATERIAL AND EXPIREMENTAL METHODS***

# ***1. SURFACE CHARACTERIZATION TECHNIQUES***

## ***1.1. Introduction***

A number of surface characterization techniques are used to investigate properties related to adhesion mechanisms and adhesion strength of the coating thin film deposit on the substrate surface.

These include time-of-flight secondary ion mass spectrometry (ToF-SIMS), X-ray photoelectron spectroscopy (XPS), atomic force microscopy (AFM), secondary electron microscopy (SEM), and other microscopy techniques plus methods sensitive to surface energy such as optical contact angle analysis (Zanna et al., 2010; Adraider et al., 2012; Adraider et al., 2013; Arushanov et al., 2013; Duday et al., 2013; Khandelwal et al., 2013; Yi et al., 2013 ; Adraider et al., 2014; Lia and Easton, 2014). Numerous studies have looked at surface properties such as roughness, polarity, chemical composition and surface free energy to describe and explain adhesion phenomena at a surface or interface using the above mentioned techniques (Lin et al., 2011; Al-Hamarneh et al., 2012; Brunelli et al., 2012; Wang et al., 2013; Mei et al., 2012).

## ***1.2. Time-of-Flight Secondary Ion Mass Spectroscopy (ToF-SIMS)***

ToF-SIMS uses mass spectrometry to determine the type and quantity of ionizable chemical groups within nanometer at the top of surface.

ToF-SIMS instruments generate surface mass spectra under clean ultrahigh vacuum conditions. A pulsed, highly focused primary ion beam is directed at the surface causing the emission of secondary charged and neutral fragments from the surface and near-surface region. The primary ion source was formerly monoisotopic Gallium (Ga) but contemporary instruments typically

use Bismuth (Bi) cluster ion sources or C<sub>60</sub> ion sources for superior mass range and spectral yield. Positively or negatively charged secondary ions within a narrow energy band are extracted from the surface region and mass analyzed using a time-of-flight analyzer. The resulting spectrum depicts signal intensity versus mass to charge ratio ( $m/z$ ) and can be used to gauge relative intensities of chemical species. It can also provide two-dimensional chemical maps for use in establishing surface homogeneity (Kingshott et al., 2003) or designing micropatterning for genomic arrays and biosensors (Hyun et al., 2001).

ToF-SIMS provides elemental, isotopic and molecular information at extremely high surface sensitivity (monolayer) (Vickerman and Briggs, 2001; Vickerman, 2003). This molecular information provides the chemistry at the interface, allowing for molecular insight into the adhesive reaction. The detection limit of ToF-SIMS is more sensitive than XPS, on the order of parts per billion, however ionization of surface molecules is dependent on sample matrix, and is therefore not quantitative. ToF-SIMS can be used to complement XPS results by offering identification of chemical species (Sibilia, 1988); it may also be used to differentiate samples that have similar XPS spectra.

ToF-SIMS analysis was performed on the reference steel and coated surfaces. ToF-SIMS spectra measurements were carried out using a ToF-SIMS V instrument (ION-TOF GmbH Germany). This instrument is equipped with a Bi liquid metal ion gun (LMIG). Pulsed Bismuth Bi<sup>+</sup> primary ions have been used for analysis (25 KeV, 1 pA). Charging effects, due to the primary ion beam, were compensated using pulsed low energy electrons

(20 eV). Each analysis was carried out the same day on two samples and on different zones of the sample to confirm the repeatability.

Reference mass spectra have been established recovering both ion polarities of the whey protein tableted for analysis. Surface spectra were taken from an area of 500  $\mu\text{m}$  x 500  $\mu\text{m}$  during 100 sec.

As the  $\text{Ca}^+$  ion can be detected only in positive polarity, depth profiling (non-interlaced mode) were performed only in positive polarity on stainless steel samples after fooling during 1 minute. Cesium ( $\text{Cs}^+$ ) has been used as sputter gun (0.5kV, 35nA) with a raster of 300 $\mu\text{m}$ x300 $\mu\text{m}$ . Secondary ions were generated with  $\text{Bi}^+$  ion gun from an area of 100 $\mu\text{m}$ x100 $\mu\text{m}$  centred on sputter gun crater.

Profiles combined with high lateral resolution secondary ions images were also acquired in the burst alignment mode using  $\text{Bi}^+$  as primary ion gun (Pulse = 100 ns; Mass Resolution = 105 at  $m/z$  40 for  $\text{Ca}^+$ ; lateral resolution  $\approx$  200 nm) and  $\text{Cs}^+$  (0.5 kV) as sputter gun. Raster for  $\text{Cs}^+$  and  $\text{Bi}^+$  were respectively 300  $\mu\text{m}$  x 300  $\mu\text{m}$  and 20  $\mu\text{m}$  x 20  $\mu\text{m}$ .

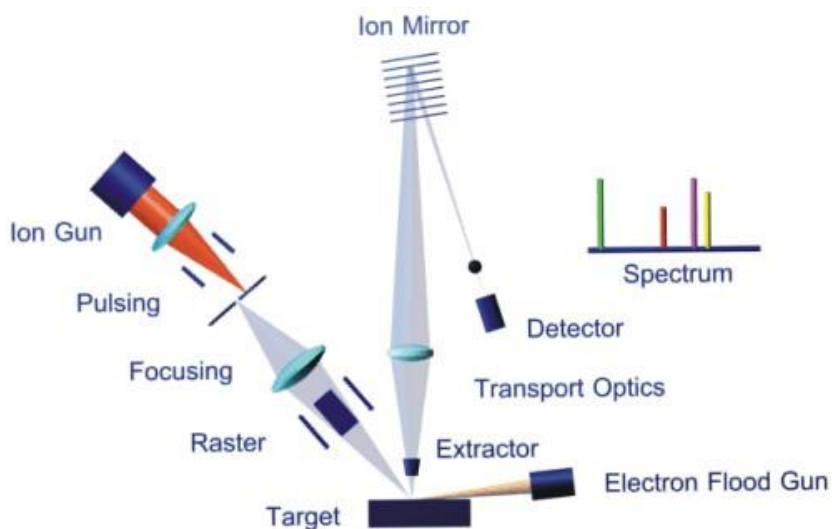


Figure 2.1: Diagram of ToF-SIMS

***Whey protein fragments analyzed:*** Concerning the whey protein (containing mainly  $\beta$ -Lg), different ions can be detected in negative polarity using ToF-SIMS ([Pellegrini et al., 2001](#)). B-lactoglobulin ( $\beta$ -Lg) is a major protein in milk serum. It consists in 162 amino acids. According to its amino acid sequence ([Wei et al., 2003](#)), leucine, alanine, glutamic acid and lysine are the most abundant amino acids.

The most abundant fragments are thus  $\text{CN}^-$  ( $m/z$  26) and  $\text{CNO}^-$  ( $m/z$  42) ([Lalande et al., 1989](#)), arising from the fragmentation of peptide backbone and indicating protein absorption. However, other elements can also be detected. Indeed, the  $\beta$ -Lg conformational structure and its link with temperature have been investigated: literature data show that an increase in temperature initiates a heat denaturation process which leads to different  $\beta$ -Lg protein conformations in addition to the native one, unfolded and aggregated state ([Tolkach and Kulozik, 2007](#)). Today, it is well established that when heated in a neutral aqueous solution, globular molecules of  $\beta$ -Lg unfold with a loss of their tertiary and secondary structure. Such unfolding of the protein exposes reactive sulphhydryl (-SH) groups, which are normally contained within the core of protein, and allows the formation of disulfide bridges with different proteins present in the solution (e.g. casein,  $\alpha$ -lactoglobulin). It results in the formation of aggregates ([Tolkach and Kulozik, 2007](#)). Thus, in negative polarity,  $\text{S}^-$  ( $m/z$  32) is another characteristic ion for  $\beta$ -Lg. However, studies in negative polarity are not really useful for this study, as  $\text{Ca}^+$  ( $m/z$  40) is only detected in positive polarity.

In positive ion polarity, it is delicate to detect characteristic ions of the protein. The major positive fragments that can be generated from the

proteins amino acids are  $C_5H_{12}N^+$  ( $m/z$  86),  $C_2H_6N^+$  ( $m/z$  44),  $C_4H_6NO^+$  ( $m/z$  84) and  $C_5H_{10}N^+$  ( $m/z$  86) (Tsuge et al., 2002).

However the signals obtained from these fragments are very low. To obtain peaks with good resolution during depth profiles it was decided to investigate the couplings between  $CN^+$  ions and cesium. The best signal was obtained for  $CNCs^{2+}$  ( $m/z$  292). This signal will be the one followed in ToF-SIMS analyses for the protein. As the whey protein also contains some calcium, issued from impurities, the  $Ca^+$  ( $m/z$  40) was also followed.

***Steel fragments analyzed:*** The stainless steel used in this study (316L) contains sufficient chromium to form a passive film of chromium oxide at its extreme surface. It prevents further surface corrosion and blocks corrosion from spreading into the metal's internal structure. The first layer of the stainless steel must be thus composed of a chromium oxide. Using ToF-SIMS, it is delicate in positive polarity to detect the steel elements, except  $Cr^+$  ( $m/z$  52) which is well detected and can be taken as a reference for substrate. It is also possible to look at the signal produced by the coupling of the Cesium beam (Cs) with a secondary ion (e.g.  $Fe^+$ ). In our case, the  $Fe^+$  ion of stainless steel is not detected whereas  $CsFe^+$  ( $m/z$  189) shows a significant signal. By the same method, it is possible to detect the oxygen ion  $Cs_2O^+$  ( $m/z$  282) to investigate the chromium oxide layer.

### ***1.3. X-Ray Photoelectron Microscopy (XPS)***

XPS determines the atomic composition with several nanometers at solid surface. Upon exposure to X-ray photons, a surface emits photoelectrons whose binding energies can be compared to known values to identify the elements and its oxidation state (Sabbatini and Zambonin, 1993).

XPS is surface sensitive analytical technique with a depth of analysis of the order of 5–10 nm. The resulting spectrum is a plot of intensity (arbitrary units) versus binding energy (eV). The intensity of the ejected photoelectrons relates directly to the material surface atomic distribution and can therefore be used to quantify percent atomic composition and stoichiometric ratios (Kiss et al., 1987; Sabbatini and Zambonin, 1993). In addition to quantifying change in surface atomic composition, XPS can be used to estimate extents of reaction by dividing measured atomic concentrations by theoretical values calculated by assuming complete conversion (Crombez et al., 2005; Kingshott et al., 2003).

As with ToFSIMS, this surface sensitivity requires that XPS instruments operate ideally at ultrahigh vacuum to minimize undesirable surface contamination. X-ray photons (generally in range 100–2500 eV), derived from monochromated laboratory X-ray sources or soft X-ray synchrotron beam lines, irradiate the sample surface and cause the emission of photoelectrons from the near surface region. The kinetic energy of these electrons is determined, typically using a hemispherical sector analyzer, and the corresponding electron binding energy calculated.

Characteristic peaks in the spectra correspond to the electronic core levels in the atoms in the near surface region and can be used to identify the species present and quantify the relative surface composition. Chemical shifts and curve fitting of peak envelopes with multiple contributions allows the chemical state of surface species to be identified, for example, the oxidation state or bonding environment.

The elemental information along with the bonding states allow for the chemistry at the adhesive interface to be understood. XPS also facilitates quantitative correlations between elemental and functional groups present on

the surface and surface energy or adhesion strength. XPS operating principles are explained in detail in a variety of published works ([Vickerman and Briggs, 2001](#); [Vickerman, 2003](#); [Ratner and Castner, 1997](#)). Because XPS analysis is limited to the top few nanometers of the surface, samples must be handled carefully as even minor surface contamination is pronounced in the resulting spectrum.

XPS analyses were performed on an Axis ultra DLD (Kratos analytical) using a monochromatic Al KR X-ray source ( $h\nu = 1486.6$  eV). The emission voltage and the current of this source were set to 15 kV and 10 mA, respectively. The pressure in the analyzing chamber was maintained at  $10^{-7}$  Pa or lower during analysis, and the size of the analyzed area was  $300 \times 700 \mu\text{m}^2$ , with a depth of 10 nm. Survey (0-1300 eV) and high-resolution spectra were recorded at pass energies of 20 eV with a step of 0.05 eV (the surveys were recorded at pass energies of 160 eV with a step of 1 eV). Data treatment and peak-fitting procedures were performed using Casa XPS software. Obtained spectra were rescaled by shift of C1s C-C at 285 eV. The Ca2p peaks were decomposed using Gaussian-Lorentzian peak shapes.

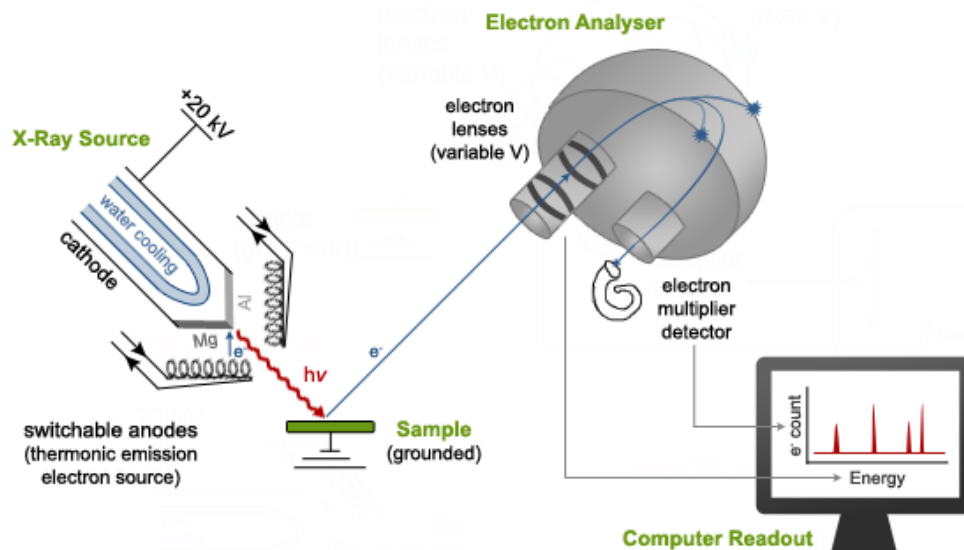


Figure 2.2: Diagram of an X-ray photoelectron spectrometer.

#### 1.4. Atomic Force Microscopy (AFM)

Atomic force microscopy (AFM), is a group of contemporary microscopic techniques that find wide application in the physical, chemical and biological sciences. In AFM, a tip attached to a palpeur moves across the sample surface to measure surface morphology on an atomic scale. The change in surface height is then measured by the location of the reflected laser beam in the quadrant photodetector, and a surface topographical map is generated from which surface roughness values can be calculated ([Alessandrini and Facci, 2005](#)).

AFM is widely used to generate topographic maps of surfaces, whereby cantilever deflections arising from the interaction with surface features are recorded as a function of raster position. AFM is able to achieve atomic resolution in the vertical plane and 0.01 nm spatial resolutions in the horizontal plane ([Vickerman, 2003](#)). This resolution allows for the detection of changes to topography after surface treatment, and can be

measured through roughness values, providing valuable information on contribution of surface roughness to adhesion strength.

AFM was used to analyze the surface morphology and roughness of the nano-thick fouling layers obtained after 1 minute fouling. The AFM device was a Bruker-Veeco Bioscope, which was operated in intermittent contact mode in air at ambient temperature. The membrane surfaces were imaged in different scan sizes (from  $4\mu\text{m} \times 4\mu\text{m}$  to  $200\text{nm} \times 200\text{nm}$ ). A single silicon cantilever (Mikromash NSC15/AIBS typical spring constant:  $46\text{ N/m}$ ) was used at a frequency of  $325\text{ kHz}$ . The limit of detection of the cantilever corresponds to a roughness of  $6\ \mu\text{m}$ .  $R_a$  (average roughness) and quadratic (or RMS) roughnesses  $R_q$  as well as 3D surface pictures were obtained using this technique.

A few images are presented in Phase mode imaging. In this mode, the phase shift of the oscillating cantilever relative to the driving signal is measured. This phase shift can be correlated with specific material properties that affect the tip/sample interaction. The phase shift can be used to differentiate areas on a sample with such differing properties as adhesion and viscoelasticity. The image treatments were carried out using the software WSxM 5.0 and Develop 6.1 from Nanotec.

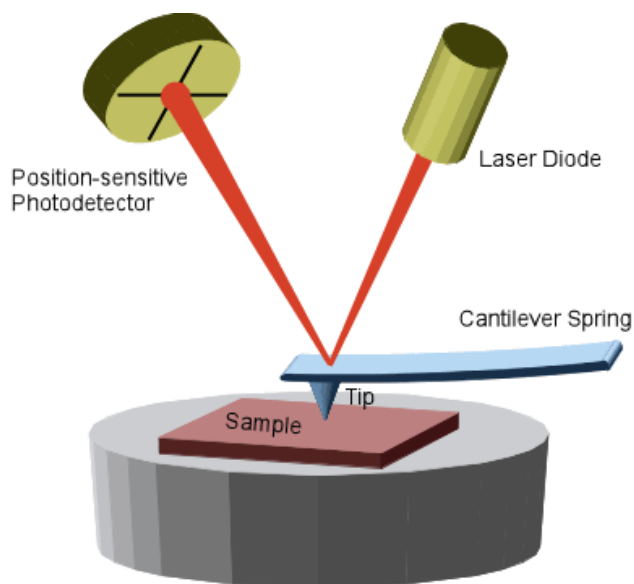


Figure 2.3: Diagram of an AFM.

### ***1.5. Scanning Electron Microscopy (SEM)***

Scanning electron microscopy (SEM) is a well-known electron beam technique in which electron scattering is used to image the topography of the sample surface under investigation. The electron beams across the sample surface (which must be conductive or rendered so by coating) with the signal from the emitted secondary electrons displayed via an electron detector. SEM has the potential to generate images with a few nanometers spatial resolution, and has a relatively large depth of field, in some cases up to 100 times that of an optical microscope (Reed, 1996). This provides topographical information on the sample surface allowing for greater understanding of the reaction between surface treatment and substrate. SEM is not as surface sensitive as other techniques, and non-conducting polymers must be sputter-coated prior to analysis (Kongdee et al., 2005; Dee

et al., 2002). Nevertheless, it is one of the more widely available tools in surface analysis, and it is thus often used to measure surface topography (Bag et al., 1999; Sheng et al., 1995; Desai et al., 2003; Kongdee et al., 2005).

The SEMFEG used to carry out secondary electron images was a Hitachi S4700 used at 6kV acceleration voltage and a current of 15 $\mu$ A at different magnifications. (Until 400 000)

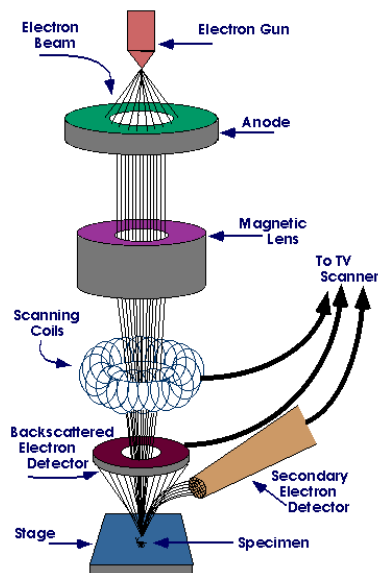


Figure 2.4: Diagram of scanning electron spectrometer.

### ***1.6. Electron Probe Micro Analysis (EPMA)***

An electron microprobe (EMP), also known as an electron probe microanalyzer (EPMA) or electron micro probe analyzer (EMPA), is an analytical tool used to non-destructively determine the chemical composition of small volumes of solid materials. It works similarly to a scanning electron microscope: the sample is bombarded with an electron beam, emitting x-rays at wavelengths characteristic to the elements being analyzed. This enables the abundances of elements present within small sample volumes

(typically 10-30 cubic micrometers or less) to be determined the concentrations of elements from boron to plutonium can be measured at levels as low as 100 parts per million (ppm).

The characteristic X-rays are used for chemical analysis. Specific X-ray wavelengths or energies are selected and counted, either by wavelength dispersive X-ray spectroscopy (WDS) or energy dispersive X-ray spectroscopy (EDS). WDS utilizes Bragg diffraction from crystals to select X-ray wavelengths of interest and direct them to gas-flow or sealed proportional detectors. In contrast, EDS uses a solid state semiconductor detector to accumulate X-rays of all wavelengths produced from the sample. While EDS yields more information and typically requires a much shorter counting time, WDS is generally a more precise technique with lower limits of detection because its superior X-ray peak resolution.

Chemical composition is determined by comparing the intensities of characteristic X-rays from the sample material with intensities from known composition (standards). Counts from the sample must be corrected for matrix effects (depth of production of the X-rays, absorption and secondary fluorescence) to yield quantitative chemical compositions. The resulting chemical information is gathered in textural context. Variations in chemical composition within a material (zoning), such as a mineral grain or metal, can be readily determined.

In our case, samples were embedded into epoxy resin, polished and carbon coated with a Bal-Tec SCD005 sputter coater.

A Cameca SX100 EPMA was used to perform elemental analysis. Back scattered electron images were carried out at 15 kV, 20nA and X-ray mappings were carried out at 15 kV, 40 nA. For mappings, the crystal used

to detect the  $K\alpha$  of Sulphur (S) and Calcium (Ca) was pentaerythritol (PET) and the crystal used to detect the  $K\alpha$  of Fe and Cr was a lithium fluoride (LiF).

**Why protein characteristic elements:** Nitrogen being difficult to detect with a good resolution using EPMA, sulphur will be thus preferred to nitrogen to identify the protein in the fouling layer.

**Steel characteristic elements:** Steel will be identified by the Fe and Cr elements.

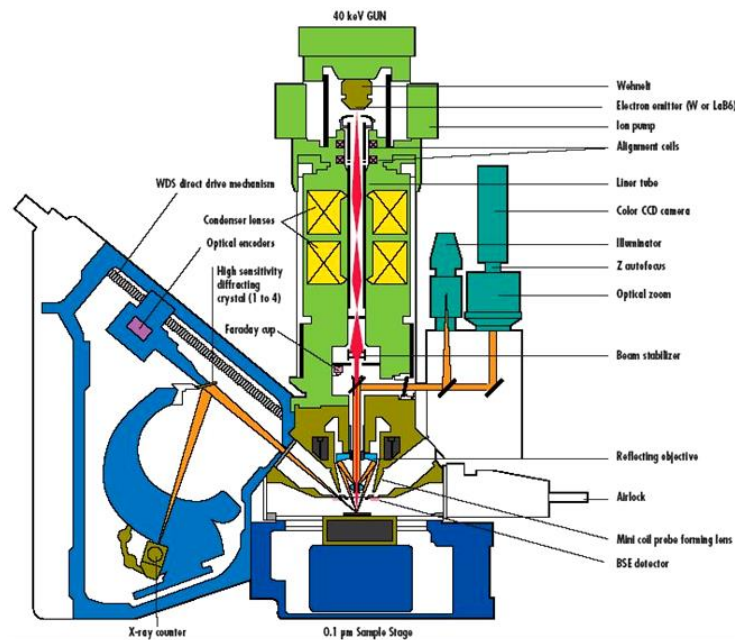


Figure 2.5: Diagram of an EPMA.

### 1.7. Optical Microscopy

The simplest optical imaging system that can be used as a microscope consists of two converging lenses: an objective lens and an eyepiece. The optical train of this microscope and its corresponding ray diagram are shown in Figure 2.6 (a). Illumination light transmitted through the sample is collected by the objective lens and transferred to the eyepiece, forming an

image on the retina of the observer's eyes. Various types of light detecting devices, such as charge-coupled device (CCD) cameras, photodiodes, avalanche photodiodes, photomultiplier tubes, and other optical sensors are nowadays widely used for collecting the image. Electronic scanning systems such as galvano-mirrors and acousto-optic deflectors or fast confocal illumination systems such are often utilized in modern optical microscopes and imaging systems.

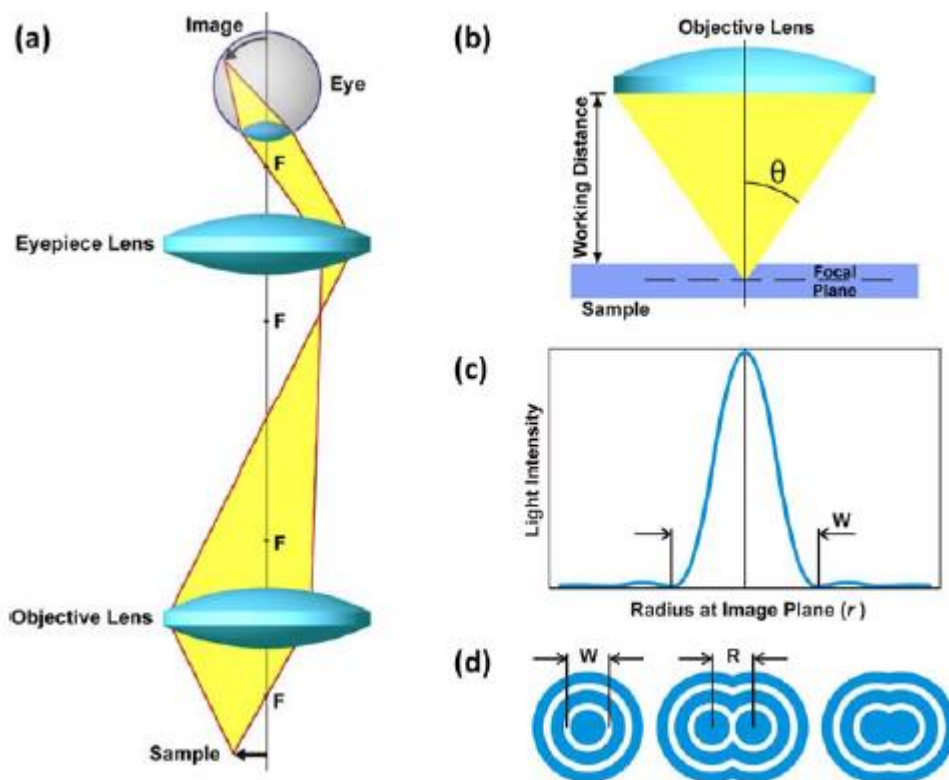


Figure 2.6: Principles of imaging with an optical microscope: (a) ray diagram of the simplest two-lens microscope; (b) definition of parameters of an objective lens; (c) point spread function with the first minimum at  $r=W/2$ ; (d) Airy patterns in the image plane. “F” marks the foci of lenses. “R” shows the separation distance between the centers of Airy discs.

Objective lenses are perhaps the most essential optical components and are characterized by parameters like numerical aperture and working distance, which largely define their performance. The numerical aperture (NA) of the objective determines the range of angles over which the objective lens can accept light and is defined as

$$NA = n \cdot \sin\theta \dots\dots\dots (2.1)$$

Where  $n$  is the refractive index of the medium between the objective lens and the sample, and  $\theta$  is the half-angle of the cone of light accessible for collection by the objective [Figure 2.6 (b)].

Numerical aperture determines important microscope characteristics such as the point spread function (PSF) and, consequently, the resolution. The PSF [Figure 2.6 (c)] can be thought of as the light intensity distribution in the image acquired by the microscope from a point source, and is given by (Jue, 2009)

$$SPF(r) = \left[ \frac{2J_1(ra)}{ra} \right]^2 \dots\dots\dots (2.2)$$

where  $a = 2\pi NA / \lambda$ ,  $J_1$  is the Bessel function of the first kind,  $\lambda$  is the wavelength of light and  $r$  is the distance from the center of the peak in light intensity [Figure 1(c)]. In the image plane of a standard optical system, the PSF is shaped as the Airy diffraction pattern with the first minimum at  $r = W/2$  [Figure 2.6 (d)]. Two Airy discs separated by the distance  $R \geq W/2$  [Figure 2.6 (d)] can be resolved into separate entities, but not at smaller  $R$  (Pawley, 2006). This limit is often called the Rayleigh criterion or the diffraction limit and defines the lateral resolution of the objective as  $r_{lateral} = 61.0\lambda/NA$ , i.e., the resolution in the plane orthogonal to the microscope's optical axis. From the definition of  $r_{lateral}$  it follows that

objectives with higher NA can resolve finer details, however, even for high-NA objectives, the lateral resolution can be only slightly smaller than the wavelength of light used for imaging.

Digital images of the steel plates have been taken using an optical microscope, the Olympus GX 51. Digital images of the steel plates have been taken also by using a Keyence VHX-500F Digital Microscope. The Keyence VHX-500F digital microscope is a high resolution CCD camera based system with a high intensity halogen lamp and image processing capabilities that integrates observation, recording, and measurement functions.

The system is equipped with a VH-Z100R bright field lens (see figure 2.7). Rotating the zoom ring on the lens changes the magnification from roughly ~100x to ~1000x. A separate ring controls the aperture setting. The lens may be tilted to achieve angled images of samples.

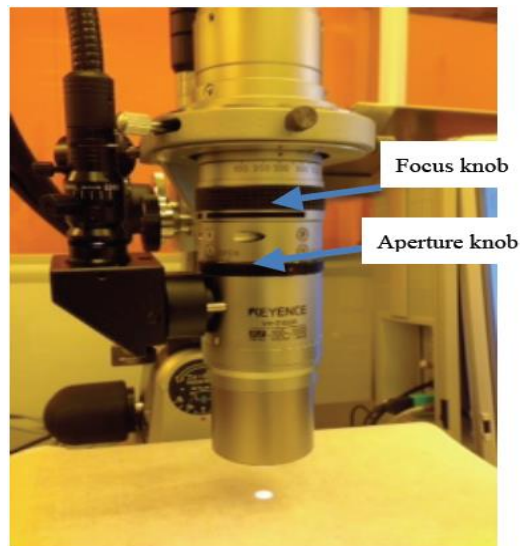


Figure 2.7: The optical column



Figure 2.8: Optical Microscopy.

### ***1.8. Contact Angle Measurement***

The determination of solid-vapor ( $\gamma_{sv}$ ) and solid-liquid ( $\gamma_{sl}$ ) interfacial tensions is of importance in a wide range of problems in pure and applied science. Because of the difficulties involved in measuring directly the surface tension involving a solid phase, indirect approaches are called for. Several independent approaches have been used to estimate solid surface tensions, including direct force measurements (Fogden and White, 1990 ; Pashley et al., 1988 ; Claesson et al., 1986 ) contact angles (Spelt and Li, 1996; Van Oss et al., 1988 a,b; Good and Van Oss, 1992) capillary penetration into columns of particle powder (Kilau and Pahlman, 1987) sedimentation of particles (Vargha-Butler et al., 1987 ; Li et al., 1996); solidification front interaction with particles (Zubko et al., 1973); film flotation (Fuerstenau et al., 1990); gradient theory (Guermeur et al., 1985) ; Lifshitz theory of van der Waals forces (Van Giessen et al., 1997); and theory of molecular interactions (Matyushov and Schmid, 1996).

Among these methods, contact angle measurements are believed to be the simplest.

Contact angle measurement is easily performed by establishing the tangent (angle) of a liquid drop with a solid surface at the base. The attractiveness of using contact angles to estimate the solid-vapor and solid-liquid interfacial tensions is due to the relative ease with which contact angles can be measured on suitably prepared solid surfaces. It will become apparent later that this seeming simplicity is, however, very misleading.

The possibility of estimating solid surface tensions from contact angles relies on a relation which has been recognized by Young (Young, 1805). The contact angle of a liquid drop on a solid surface is defined by the mechanical equilibrium of the drop under the action of three interfacial tensions (Figure 2.9) solid-vapor, ( $\gamma_{sv}$ ), solid-liquid, ( $\gamma_{sl}$ ), and liquid-vapor, ( $\gamma_{lv}$ ). This equilibrium relation is known as Young's equation:

$$\gamma_{lv} \cos \theta_Y = \gamma_{sv} - \gamma_{sl} \dots\dots\dots (2.3)$$

Where  $\theta_Y$  is the Young contact angle, i.e. a contact angle which can be inserted into Young's equation. It will become apparent later that the experimentally accessible contact angles may or may not be equal to  $\theta_Y$ .

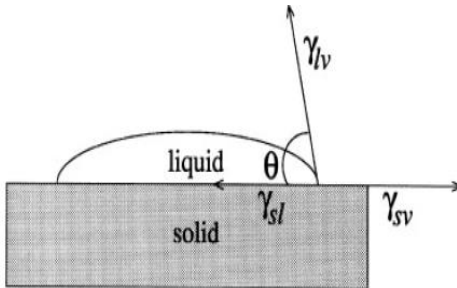


Figure 2.9: Schematic of a sessile-drop contact angle system.

Young's (Eq. 2.3) contains only two measurable quantities, the contact angle  $\theta$  and the liquid- vapor surface tension,  $\gamma_l$ . In order to determine  $\gamma_s$  and  $\gamma_{sl}$ , an additional relation relating these quantities must be sought.

Nevertheless, (Eq. 2.3) suggests that the observation of the equilibrium contact angles of liquids on solids may be a starting point for investigating the solid surface tensions,  $\gamma_s$  and  $\gamma_{sl}$ . This has inspired many studies which attempt to develop methodologies for determining solid surface tensions. A common feature of these approaches is the assumption that contact angle measurement is a trivial task. Since  $\gamma_l$ ,  $\gamma_s$  and  $\gamma_{sl}$  are thermodynamic properties of the liquid and solid, (Eq. 2.1) implies a single, unique contact angle; in practice, however, contact angle phenomena are complicated (Neumann, 1974). In particular, the contact angle made by an advancing liquid ( $\theta_a$ ) and that made by a receding liquid ( $\theta_r$ ) are not identical; nearly all solid surfaces exhibit contact angle hysteresis, H (the difference between  $\theta_a$  and  $\theta_r$ ):

$$H = \theta_a - \theta_r \dots\dots\dots (2.4)$$

Contact angle hysteresis can be due to roughness and heterogeneity of a solid surface. If roughness is the primary cause, then the measured contact angles are meaningless in terms of Young's equation. On very rough surfaces, contact angles are larger than on chemically identical, smooth surfaces (Zettler and Wiess, 2005). Obviously, interpreting such angles in terms of (Eq. 2.1) would lead to erroneous results because the contact angle would inevitably reflect surface topography, rather than exclusively surface energetic. Another important contribution in the field of surface analysis was made by Dupre (Subide, 2011). According to this equation, work of adhesion  $W_A$  between a solid (s) and a liquid (l) can be expressed as,

$$W_A = \gamma_s + \gamma_l - \gamma_{sl} \dots\dots\dots (2.5)$$

This work of adhesion  $W_A$  is the reversible work done in separation of unit area of solid/liquid interface and equals to one half of the work of cohesion when the arrangement of molecules in the surface region is the same as the bulk. Combining equation (3) and (5), gives the Young-Dupre equation which is represented by Eq. (2.6).

$$W_A = \gamma_s (\cos\theta + 1) \dots\dots\dots (2.7)$$

The work of adhesion  $W_A$  can be evaluated from Eq. (2.7) using accessible quantities  $\gamma_l$  and  $\theta$ . Equation (2.7) is the starting point for interpretation of all contact angle data. After the evaluation of  $W_A$ , the surface energy of the solid  $\gamma_s$  can be determined by further use of other models

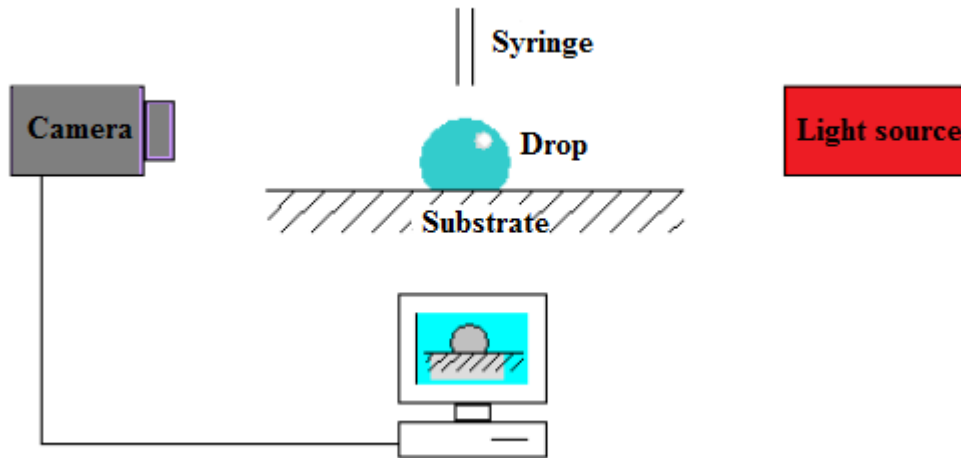


Figure 2.10: Scheme representing a measurement of contact angle.

**1.9. Roughness Measurements**

Surface roughness, often shortened to roughness, is a measure of the texture of a surface. It is quantified by the vertical deviations of a real surface from its ideal form. If these deviations are large, the surface is rough; if they are small the surface is smooth.

Each of the roughness parameters is calculated using a formula for describing the surface.

There are many different roughness parameters in use, but  $R_a$  is by far the most common. Other common parameters include  $R_z$ ,  $R_q$  and  $R_{sk}$ .

$$R_a = \frac{1}{n} \sum_{i=1}^n |y_i| \dots\dots\dots (2.8)$$

The formula assumes that the roughness profile has been filtered from the raw profile data and the mean line has been calculated. The roughness profile contains  $n$  ordered, equally spaced points along the trace, and  $y_i$  is the vertical distance from the mean line to the  $i^{\text{th}}$  data point. Height is assumed to be positive in the up direction, away from the bulk material. Many roughness terms like ( $R_a$ ,  $R_q$ , etc...) and its definition, calculations and uses were found in appendix 1.

The average roughness ( $R_a$ ) was measured by a profilometer (Tencor Alpha- Step IQ, Science) on the various coated stainless steel surfaces. At least three measures were taken for each surface tested. A profilometer is a measuring instrument used to measure a surface's profile, in order to quantify its roughness.

A stylus is moved vertically in contact with a sample and then moved laterally across the sample for a specified distance and specified contact force. A profilometer can measure small surface variations in vertical stylus displacement as a function of position. A typical profilometer can measure small vertical features ranging in height from 10 nanometres to 1 millimetre. The height position of the stylus generates an analog signal which is converted into a digital signal stored, analyzed and displayed. The radius of diamond stylus ranges from 20 nanometers to 50  $\mu\text{m}$ , and the horizontal

resolution is controlled by the scan speed and data signal sampling rate. The stylus tracking force can range from less than 1 to 50 milligrams.



Figure 2.11: Profilometer (Tencor Alpha- Step IQ, Science).

## 2. Material and Experimental Methods

### 2.1. Materials

**Stainless steel:** The steel surface tested in this study is a 316L stainless steel. The detailed chemical composition of the industrial grade (analyzed by Fluorescence X which supplied by ArcelorMittal) is presented in Table (2.1).

Table 2.1: Chemical composition of the stainless steels used, expressed in weight percentage

Element	Ti	Nb	C	S	Co	Si	Cu	Mn	Mo	Ni	Cr	Fe
Wt.-% in 316L stainless steel	0.004	0.014	0.019	0.03	0.19	0.26	0.33	1.36	2.05	10.07	16,9	68.5

Prior to any testing, bare stainless steel plates (1 cm<sup>2</sup>) was degreased first by an acetone/ethanol (50/50) blend, then soaked for 10 min at 50°C in a 2% (v/v) RBS 35 (Société des traitements chimiques de surface, Lambersart, France) and rinsed 2 times for 5 min in distilled water at 50°C and 2 times for 5 min in distilled water at room temperature.

**Fouling fluids:** The first fouling model fluid used in this study was obtained by reconstituting 1% w/w Whey Protein Concentrate (WPC) powder (Promilk 852 FB1, IDI SAS France) in Total Hardness zero (TH0). Tapwater was treated using an exchange ion resin in order to replace the Ca<sup>2+</sup> ions by Na<sup>+</sup> ions. The second fouling model fluid was obtained by reconstituting 1% w/w Whey Protein Concentrate (WPC) powder (Promilk 852 FB1, IDI SAS France) with tapwater containing 90 mg of calcium per litre. Calcium content was determined using an atomic absorption spectrophotometer (Philips, Pye Unicam).

The calcium content of the whey protein issued from impurities due to the protein extraction process was also investigated by diluting the protein in ultrapure water and analysing the calcium content by atomic absorption: the whey protein has a calcium content of 30 ppm. It means that the solution containing TH0 water and whey protein has calcium content of about 30 ppm whereas the solution containing tapwater and whey protein has a global calcium content of 120 ppm.

700 litres of model fluid were prepared the day of experiment. It was prepared carefully to ensure that its physical properties (density, specific heat, thermal conductivity and Newtonian viscosity) remained constant for

all runs. The pH of the fouling product was remained quite constant between 7.3 and 7.7.

## 2.2. Experimental Fouling Equipment

**Experimental runs:** The pilot-plant test ring is displayed in Figure (2.12).

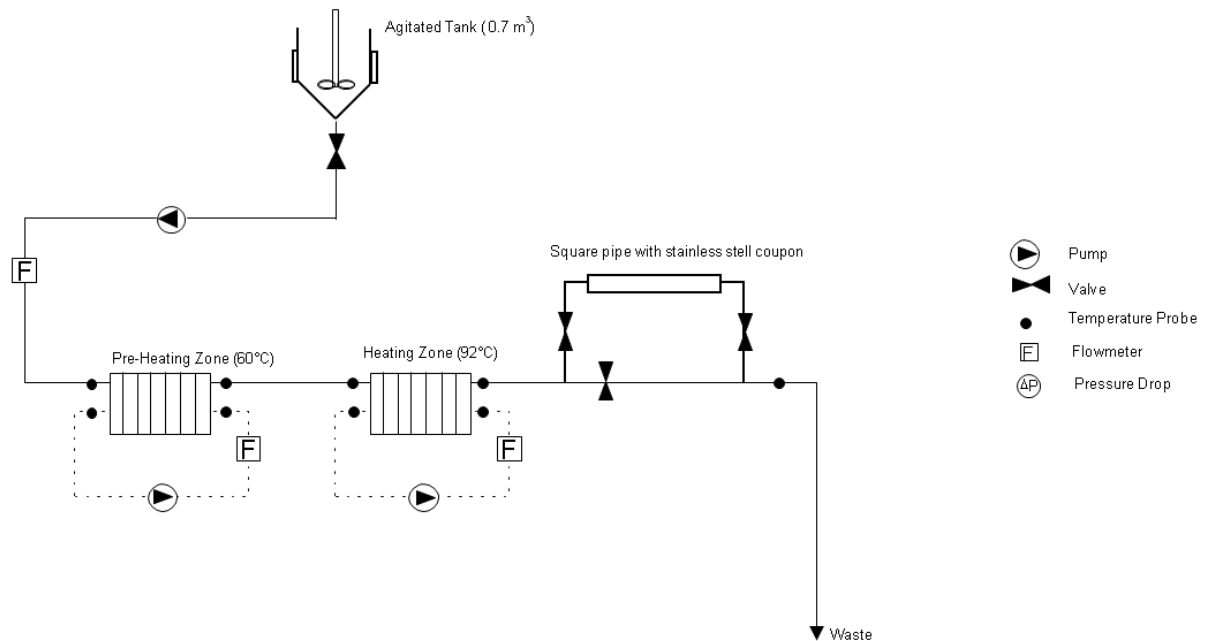


Figure 2.12: Pilot plant test ring for the fouling test (INRA, PIHM).

The pilot plant used for fouling experiments is shown in Figure 2.13.

It consists in 5 main parts:

- (i) A preheating zone with a conventional heat exchanger equipped with Alfa-Laval Vicarb V7 type plates, 8 pass and 1 channel per pass for the two sides of the heat exchanger ;
- (ii) A volumetric pump;
- (iii) A heating zone composed of a heat exchanger equipped with Alfa-Laval Vicarb V7 type plates, 5 passes and 1 channel per pass for the two sides of the heat exchanger ;

- (iv) A holding tube with square cross section which contains the coated surface.

The manual back-pressure valve at the plant outlet allowed maintaining the pressure in the pilot plant equal to 2.5 bar.

During all the experiments, several measurements were controlled, in particular flow rates, inlet and outlet temperatures, and were collected using a data acquisition system (Agilent Technologies 34970A, USA). For all measured parameters, acquisition period was set equal to 15 seconds.

The measurements were the following ones:

- (i) Four temperatures (inlet and outlet of the product and inlet and outlet of the hot water), measured by means of platinum resistance probes (Sensor-Nite, type Pt100) with a precision of 0.1°C ;
- (ii) Two flow rates (fouling product and hot water), measured using an electromagnetic flowmeter (Khrone, type IFM) ;
- (iii) Two pressure drops between the inlet and the outlet of the heating zone, measured by two differential pressure sensors (Siemens and Schlumberger) ;
- (iv) The relative pressure at the outlet of the pump, measured by a relative pressure strain gauge sensor.



Figure 2.13: Heat exchanger pilot (INRA).

First, the fouling solution was pre-heated from 10 to 60°C, then heated from 60 to 93°C and finally cooled from 93 to 20°C according the following kinetic (Figure 2).

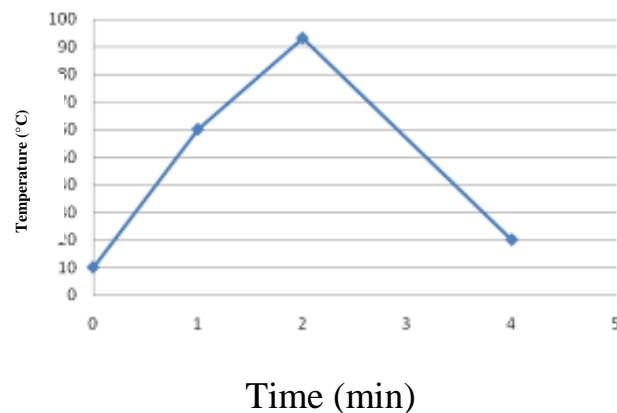


Figure 2.14: Kinetic of the heating process.

A plate heat exchanger (PHE) was used in a counter-current configuration (Model V7 of Alfa-Laval Vicarb, France). It consists in five passes of one channel for the two sides. The length between the two frames was fixed at 47.0 mm which means that the equivalent space between two plates was equal to 3.93 mm. The whey protein concentrate (WPC) solution was passed through a pre-heater composed of V7 type plates, 10 passes and 1 channel

per pass for the two sides of the heat exchanger to ensure the required inlet temperature (62°C) to the test section. The protein solution was not re-circulated to avoid fouling from material which had already been treated. During fouling experiments, the inlet hot water product was adjusted to ensure a constant outlet product temperature close to 92°C, maintained in a holding zone composed of square pipes where stainless steel plates (15\*10\*1 mm<sup>3</sup> and 15\*45\*1 mm<sup>3</sup>) are inserted. The ratio of flow rates of hot water and whey protein solution flow rate was also kept constant to 1,2 and the Reynolds number is 64000, corresponding to a turbulent regime. Duration of fouling experiments was 1 min and 2 hours, and the stainless steel plates were dehydrated using critical point drying method.

### ***2.3. Polishing Process***

#### ***2.3.1. Mechanical polishing***

Stainless steel samples (dimensions 10mm x 16mm x 1mm) were subjected to polishing. The surface roughness and morphology of foils were measured prior to polishing experiment. The ESC 200 GT polishing machine is chosen as the setup for all experiments (Figure 2.15), until it reaches a less rough surface as possible. Grades of paper used for polishing are 80, 180, 240, 320, 400, 600, 800, 1000, 1200, 2400 and ¼ μ (mirror like). The polishing experiments are run in a manual operation. All polishing experiments are lasted for enough time (5–20 min) to ensure the complete removal of surface layer.

Then the polished stainless steel coupons were rinsed with acetone to clean the samples after polishing.



Figure 2.15: Mechanical polishing instrument.

### ***2.3.2. Electropolishing***

Electropolishing (EP) was performed on mirror polished 316L 2B SS samples. The 316L 2B SS sheets were totally immersed into the center of a cylindrical cell containing 500 ml EP solution. The cathode, which was a NSCD stainless steel, was also totally immersed into the solution. The EP solution was composed of H<sub>2</sub>SO<sub>4</sub> (80 ml), distilled water H<sub>2</sub>O (30 ml), C<sub>2</sub>H<sub>5</sub>OH (250 ml) and citric acid (600 mg) with density current (10 A/dm<sup>2</sup>). The EP experiment was conducted by a direct current (dc) power supply (LAMDA, LP-522-FMW). After the EP treatment, the test sheet was rinsed in distilled water for 2 min followed by drying at room temperature.

The average surface roughness factor (RMS) was measured with an area of 20µm x 20µm by an atomic force microscope (AFM).

### ***2.4. Small Scale Fouling Test Development***

As the semi-industrial fouling test described in chapter three takes time to be carried out and necessitates lots of proteins, it was decided to try to develop a small scale fouling test in the laboratory, in order to carry out a screening of the different antifouling coatings we aimed at developing.

This trial involved a one hour immersion of the reference and coated plates in aqueous solutions (200 ml) of protein (1% w/w Whey Protein Concentrate (WPC) powder (Promilk 852 FB1, IDI SAS France) in distilled water) with a concentration of (5 g/l). This test was carried out under static conditions, on the contrary to the semi-industrial test, which was carried out in dynamic conditions. After the immersion period the samples were gently removed from the solution and dried at ambient temperature.

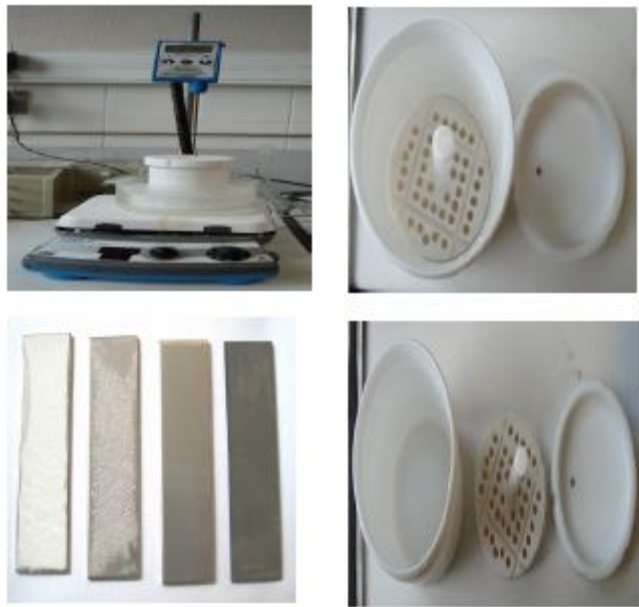


Figure 2.16: Small scale fouling test

### ***2.5 Plasma Coating***

The surface of stainless steel was treated with atmospheric pressure plasma at room temperature, the deposition experiments were carried out using a cold atmospheric plasma torch (ULS AcXys technologies) with a liquid injection system.

The cold plasma torch supplied by AcXys (ULS) is based on a controlled arc discharge, generated with alternative high tension (3 kV) at 120 kHz. Resulting pseudo-arc is confined into a cylindrical nozzle and allows shuffled gas to be homogeneously ionized. A low temperature post-discharge of around 1 cm<sup>2</sup> is then created. By adding another cylinder after the plasma reactor with a nozzle of 4 mm and 4 vertical holes, it is possible to inject the precursors sprayed ( $\mu\text{m}$  droplets) by a carrier gas N<sub>2</sub> (air liquid 99.99%) or air (dry and free of oil) with a Flow rate between 1 and 20 L/min in the plasma beam. Precursors flow is controlled by a peristaltic pump (400F/A Watson Marlow). In this study the plasma and carrier gases (air and nitrogen) flow rates were kept constant at 60 and 8 L/min respectively.

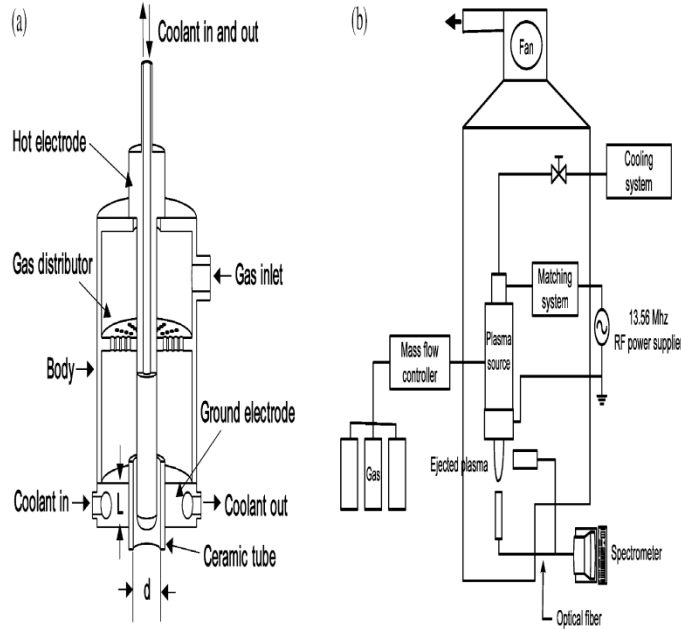


Figure 2.17: (a) Structure of plasma source, and (b) schematic diagram of the experimental setup (Kim et al., 2003).

***Antifouling performances***

The fouling performances of the coatings were evaluated by the pilot-plant tests described earlier in the manuscript. Fouling was determined by weight measurements of the samples before and after fouling and “fouling percentage” was calculated [(Δ deposited of fouling mass/ mass of fouling on uncoated plate) x 100].

$$\% F = \frac{F_{cs} - F_{ss}}{F_{ss}} \times 100 \dots\dots\dots (2.9)$$

Where *F* is the fouling, *F<sub>cs</sub>* is the fouling mass deposited on the coated stainless steel and *F<sub>ss</sub>* is fouling mass deposited on the uncoated stainless steel surface.

## 2.6. Sol-Gel Preparation

For the present study, three different sols (sol S1, sol S2 sol S3 and sol S4) were selected, the main objective being to obtain significant changes in the hydrophobic properties of the resulting silica surfaces.

The details of the composition of these three sols are given below.

Sol-Gel 1 (S1): The following analytical-grade reagents and high-purity raw materials were used to prepare SiO<sub>2</sub> sol: tetraethyl orthosilicate (TEOS) 98% Si [OC<sub>2</sub>H<sub>5</sub>]<sub>4</sub> from Aldrich Chemical Co. and ethyl alcohol absolute.

TEOS/H<sub>2</sub>O/C<sub>2</sub>H<sub>5</sub>OH/HCl with molar ratios 1:4:5:0.25 was prepared: 30 mL of TEOS was added to 32 mL of ethyl alcohol and 0.1 mL of HCl (1M) used as catalyst and then 17 mL H<sub>2</sub>O was added for hydrolysis.

The mixture was stirred for 30 min at room temperature to complete hydrolysis then forming the sol. Soon after, the beaker containing sol was adequately covered with a plastic film to prevent chemical/solvent evaporation ([Latthe et al., 2009](#)).

Sol-Gel 2 (S2): Silica alco-sol was prepared at room temperature by hydrolysis and polycondensation of ethanol (EtOH) diluted tetraethoxysilane (TEOS) in the presence of ammonium hydroxide (NH<sub>4</sub>OH) as a catalyst and trimethylethoxysilane (TMES) as co-precursor. In order to obtain transparent silica films, the molar ratio of TEOS:EtOH:H<sub>2</sub>O was kept constant at 1:38.6:8.68, respectively, with 2 M NH<sub>4</sub>OH throughout the experiments and the TMES/TEOS molar ratio (M) was varied from 0 to 1, 1. This mixture of silica alco-sol and TMES was stirred for at least 20 min before dip-coating ([Hamdy and Butt, 2006](#)).

Sol-Gel 3 (S3): the sol-gel prepared by adding the solution of 0.3 N of Nitric acid (HNO<sub>3</sub>) to the solution of TEOS/EtOH (TEOS solution as ratio

of mass H<sub>2</sub>O: 1.75, 75% mass of ethanol) and stirring until getting clear solution. The final solution was dip coated at least 24 hours after being prepared.

Sol-Gel 4 (S4): The silica sols were prepared by mixing tetramethoxysilane (TMOS), 1,1,1,3,3,3-hexamethyldisilazane (HMDZ) (Acros Organics, USA), methanol (MeOH) and deionized water in proper proportions. Ammonium hydroxide (NH<sub>4</sub>OH, 6 M) was used as a base catalyst to control the rates of hydrolysis and condensation reactions. Sol (S4) was obtained with the TMOS: EtOH: HMDZ: H<sub>2</sub>O molar ratio of 1:36.4:1:6.6, respectively. The sol was stirred for 5 min to obtain a homogeneous reaction mixture (Bhagat et al., 2006).

### ***2.6.1. Dip coating***

This method simply consists in immersing the substrate in the solution containing the “SiO<sub>2</sub> sol” and remove it under very controlled and stable conditions in order to obtain a film of uniform thickness (Figure 2.18). The substrates were withdrawn at a speed of 100mm.s<sup>-1</sup> from the sol. A sample without any surface treatment was used as a reference.

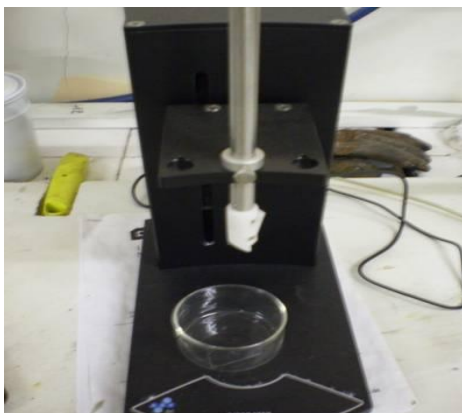


Figure 2.18: Apparatus for dip coating.

Infrared drying (Figure 2.19), following the dip-coating, was necessary to achieve evaporation of water and absolute ethyl alcohol in order to form the gel at the surface of stainless steel plates. This evaporation must be fast and efficient. The substrates were dried three times 10 seconds by Infrared instrument.



Figure 2.19: Infrared instrument

### ***2.6.2. Effect of immersion time***

To study effect of time of immersion on the contact angle, roughness and surface energy of the obtained coating, three immersion times were selected (4, 8, 12 minute) for sol-gel (S2) starting from the time of addition of the base catalyst.

## ***Conclusion***

Many surface characterization techniques exist to investigate adhesion mechanisms and adhesion strength of a thin film coating deposited on a substrate surface.

These include time-of-flight secondary ion mass spectrometry (ToF-SIMS) which uses mass spectrometry to determine the type and quantity of ionizable chemical groups of a surface's top nanometer, X-ray photoelectron spectroscopy (XPS), which determines the atomic composition of a solid's top several nanometers., atomic force microscopy (AFM) used to generate topographic maps of surfaces,. Secondary Electron Microscopy (SEM) is a well-known electron beam technique in which electron scattering is used to image the topography of the sample surface under investigation.

Other microscopy techniques and methods such as EPMA or optical contact angle analysis, profilometer, were used in association with the above mentioned techniques to describe and explain fouling growth and adhesion phenomena at a surface. The type of analysis and information provide by each surface characterization techniques are shown in appendix 2.

These techniques will be used in this thesis to understand the fouling phenomena (Chapter III) and to characterized proposed functional coatings (Chapter IV)

## ***References***

- Adraider Y., Hodgson S.N.B., Sharp M.C., Zhang Z.Y., Nabhani F., Al-Waidh A., Pang Y.X. (2012). Structure characterisation and mechanical properties of crystalline alumina coatings on stainless steel fabricated via sol–gel technology and fibre laser processing. *Journal of the European Ceramic Society*, 32, 4229–4240.
- Adraider Y., Pang Y.X., abhani F.N., Hodgson S.N., Sharp M.C., Al-Waidh A. (2013). Fabrication of zirconium oxide coatings on stainless steel by a combined laser/sol–gel technique. *Ceramics International*, 39, 9665–9670.
- Adraider Y., Pang Y.X., abhani F.N., Hodgson S.N., Sharp M.C., Al-Waidh A. (2014). Laser-induced deposition of alumina ceramic coating on stainless steel from dry thin films for surface modification. *Ceramics International*, 40, 6151–6156.
- Al-Hamarneh I., Pedrow P., Eskhan A., Abu-Lail N. (2012). Hydrophilic property of 316L stainless steel after treatment by atmospheric pressure corona streamer plasma using surface-sensitive analyses. *Applied Surface Science*, 259, 424– 432.
- Alessandrini A., Facci P. (2005). AFM: a versatile tool in biophysics. *Meas. Sci. Technol.*, 16, R65–92.
- Arushanov K.A., Drozdov M.N., Karabanov S.M., Zeltser I.A., Tolstogouzov A. (2013). TOF-SIMS study on surface modification of reed switch blades by pulsing nitrogen plasma. *Applied Surface Science*, 265, 642– 647.
- Bag D.S., Kumar V.P., Maiti S. (1999). Chemical modification of LDPE film. *J. Appl. Polym. Sci.*, 71, 1041–8.

- Brunelli K., Gottardello S., Napolitani E., Dal Bianco B., Bertocello R., Magrini M., Dabalà M. (2012). The effect of surface treatment with atmospheric pressure plasma jet, generated by air, on corrosion properties of AISI 304L stainless steel. *Materials Chemistry and Physics*, 136, 1073-1080.
- Claesson P.M., Blom C.E., Horn P.C., Ninham B.W., (1986). Interactions between water—stable hydrophobic Langmuir—Blodgett monolayers on mica. *J. Colloid Interface Sci.* 114, 234.
- Crombez M., Chevallier P., Gaudreault R.C., Petitclerc E., Mantovani D., Laroche G. (2005). Improving arterial prosthesis neo-endothelialization: application of a proactive VEGF construct onto PTFE surfaces. *Biomaterials*, 26, 7402–7409.
- Dee K.C., Puleo D.A., Bizius R. (2002). *An introduction to tissuebiomaterial interactions*. Hoboken, NJ: Wiley-Liss.
- Desai S., Bodas D., Patil K.R., Patole M., Singh R.P. (2003). Tailormade functional surfaces: potential elastomeric biomaterials I. *J. Biomat. Sci-Polym. E*, 14, 1323–1338.
- Duday D., Vreuls C., Moreno M., Frache G., Boscher N. D., Zocchi G., Archambeau C., Van De Weerd C., Martial J., Choquet P. (2013). Atmospheric pressure plasma modified surfaces for immobilization of antimicrobial nisin peptides. *Surface & Coatings Technology*, 218, 152–161.
- Fogden A., White L.R., (1990). Contact elasticity in the presence of capillary condensation: I. the nonadhesive Hertz problem. *J. Colloid Interface Sci.* 138, 414.

- Fuerstenau D.W., Diao J., Hanson J., (1990). Estimation of the Distribution of Surface Sites and Contact Angles on Coal particles from film flotation data. *Energy Fuels* 4, 34.
- Good R.J., van Oss C.J., (1992). The modern theory of contact angles and the hydrogen bond components of surface energies, in: M. Schrader, G. Loeb\_Eds., *Modern Approaches to Wettability: Theory and Applications*, Plenum Press, New York, pp. 1-27.
- Guermeur R., Biquard F., Jacolin C., (1985). Density profiles and surface-tension of spherical interfaces — Numerical results for nitrogen drops and bubbles. *J. Chem. Phys.* 82, 2040.
- Hyun J., Zhu Y.J., Liebmann-Vinson A., Beebe T.P., Chilkoti A. (2001). Microstamping on an activated polymer surface: patterning biotin and streptavidin onto common polymeric biomaterials. *Langmuir*, 17, 6358–6367.
- Jue T., (2009). *Fundamental Concepts in Biophysics*, Humana Press, New York.
- Kilau H.W. and Pahlman J. E. (1987). Coal wetting ability of surfactant solutions and the effect of multivalent anion additions. *Colloids Surf.* 26, 217.
- Kingshott P., Wei J., Bagge-Ravn D., Gadegaard N., Gram L. (2003). Covalent attachment of poly(ethylene glycol) to surfaces, critical for reducing bacterial adhesion. *Langmuir*, 19, 6912–6921.
- Kiss E., Golander C.G., Eriksson J.C. (1987). Surface grafting of polyethyleneoxide optimized by means of ESCA. *Prog. Coll. Pol. Sci.*, 73, 113–119.
- Khandelwal H., Singh G., Agrawal K., Prakash S., Agarwal R.D. (2013). Characterization of hydroxyapatite coating by pulse laser deposition

- technique on stainless steel 316 L by varying laser energy. *Applied Surface Science*, 265, 30– 35.
- Kongdee A., Bechtold T., Teufel L. (2005). Modification of cellulose fiber with silk sericin. *J. Appl. Polym. Sci.*, 96, 1421–1428.
- Krishnan S., Weinman C., Ober C. (2008). Advances in Polymers for Anti-Biofouling Surfaces. *J. Mater. Chem.* 18, 3405.
- Lalande M., René F. and Tissier J. P. (1989). Fouling and its control in heat exchangers in the dairy industry. *Biofouling*, 1, 233.
- Lia Y., Muir B. W., Easton C. D., Thomsen L., Nisbet D. R., Forsythe J. S. (2014). A study of the initial film growth of PEG-like plasma polymer films via XPS and NEXAFS. *Applied Surface Science*, 288, 288– 294.
- Lin J. and Chang H. (2011). Surface modification of SUS304 stainless steel by atmospheric pressure Ar/N<sub>2</sub>/O<sub>2</sub> plasma. *Nuclear Instruments and Methods in Physics Research, B.* 269, 1801–1808.
- Matyushov D.V., Schmid R., (1996). Calculation of Lennard-Jones energies of molecular fluids. *J. Chem. Phys.* 104, 8627.
- Mei Y., Yao C., Fan K., Li X. (2012). Surface modification of polyacrylonitrile nanofibrous membranes with superior antibacterial and easy-cleaning properties through hydrophilic flexible spacers. *Journal of Membrane Science* 417–418 20–27.
- Neumann A.W., (1974). Contact angles and their temperature dependence: Thermodynamic status, measurement, interpretation. *Adv. Colloid Interface Sci.* 4, 105.
- Pashley R.M., McGuiggan P.M., Horn R.G., Ninham B.W., (1988). Forces between bilayers of cetyltrimethylammonium bromide in micellar solutions. *J. Colloid Interface Sci.* 126, 569.

- Pawley J. B., (2006). Handbook of Biological Confocal Microscopy, 3rd ed. Springer, New York.
- Pellegrini A., Dettling C., Thomas U., Hunziker P. (2001). Isolation and characterization of four bactericidal domains in the bovine beta-lactoglobulin. *Biochim. Biophys. Acta*, 1526, 131.
- Ratner B.D. and Castner D.G. (1997). Electron spectroscopy chemical analysis. John Wiley and Sons.
- Reed S.J.B. (1996). Electron microprobe analysis and scanning electron microscopy in geology. Cambridge: Cambridge University Press.
- Sibilia J.P. (1988). A guide to materials characterization and chemical analysis. New York: VCH Publishers, Inc.
- Sabbatini L., Zambonin P.G. (1993). Surface characterization of advanced polymers. New York: VCH Publishers, Inc.
- Sheng E., Sutherland I., Brewis D.M., Heath R.J. (1995). Effects of the Chromic-Acid Etching on Propylene Polymer Surfaces. *J. Adhes. Sci. Technol.*, 9, 47–60.
- Spelt J.K., Li D., (1996). The equation of state approach to interfacial tensions, in: A.W Neumann, J.K. Spelt \_Eds., *Applied Surface Thermodynamics*, Marcel Dekker Inc., New York, pp. 239-292.
- Subide D. P. (2011). Contact Angle Measurement for the surface Characterization of solids, *The Himalayan physics*, Vol. II.
- Tolkach A. and Kulozik U. (2007). Reaction kinetic pathway of reversible and irreversible thermal denaturation of  $\beta$ -lactoglobulin. *Le Lait*, 87, 301.
- Tsuge H., Tanaka Y., Yoshizawa S. and Kuraishi T. (2002). Rreactive crystallization behaviour of calcium phosphate with and without whey protein addition, *Chemical Engineering Research and Design*, 80, 231.

- Van Giessen A.E., Bukman D.J., Widom B., (1997). Contact angles of liquid drops on low-energy solid surfaces. *J. Colloid Interface Sci.* 192, 257.
- Van Oss, C.J., Good, R.J., Chaudhury, M.K., 1988a. Additive and nonadditive surface tension components and the interpretation of contact angles. *Langmuir* 4, 884–891.
- Van Oss, C.J., Good, R.J., Chaudhury, M.K., 1988b. Interfacial Lifshitz-van der Waals and polar interactions in macroscopic systems. *Chemical Reviews* 88, 927.
- Vargha-Butler E.I., Moy E., Neumann A.W., (1987). Sedimentation behavior of low *surface*-energy powders in different non-polar liquid-systems. *Colloids Surf.* 24, 315.
- Vickerman J.C. and Briggs D. (2001). *Surface analysis by mass spectrometry*. United Kingdom: IM Publications and Surface Spectra Limited.
- Vickerman J.C. 2003. *Surface analysis: the principal techniques*. West Sussex: John Wiley & Sons.
- Wang M., Wang Y., Chen Y., Gu H. (2013). Improving endothelialization on 316L stainless steel through wettability controllable coating by sol-gel technology. *Applied Surface Science*, 268, 73– 78.
- Wei J., Ravn D.B., Gram L. and Kingshott P. (2003). Stainless steel modified with PEG can prevent protein adsorption but not bacterial adhesion. *Colloids and Surfaces B: Biointerfaces*, 32 (4) 275.
- Yi P., Peng L., Zhou T., Wu H., Lai X. (2013). Cr-N-C multilayer film on 316L stainless steel as bipolar plates for proton exchange membrane fuel cells using closed field unbalanced magnetron sputter ion plating. *International journal of hydrogen energy*, 38, 1535-1543.

- Young T., (1805). An essay on the cohesion of fluids. *Philos. Trans. R. Soc. London* 95, 65.
- Zanna S., Saulou C., Mercier-Bonin M., Despax B., Raynaud P., Seyeux A., Marcus P. (2010). Ageing of plasma-mediated coatings with embedded silver nanoparticles on stainless steel: An XPS and ToF-SIMS investigation. *Applied Surface Science*, 256, 6499–6505.
- Zettler, H. U., M. Wiess, et al., (2005), Influence of surface properties and characteristics on fouling in plate heat exchangers, *Heat Transfer Eng.*, Vol. 26(2), pp. 3.
- Zubko A.M., Lobonov V.G., Nikonova V.V., (1973). Reaction of foreign particles with a crystallization front. *Sov. Phys. Crystallogr.* 18, 239.

## ***CHAPTER THREE***

# ***FUNDAMENTAL COMPREHENSION OF THE FOULING MECHANISM AT THE STAINLESS STEEL SURFACE***

## ***1. Introduction***

The formation of unwanted deposits on the surfaces of heat exchangers, known as fouling, is still a serious issue in dairy industries: most of the cleaning procedures necessitate stopping the heat transfer process, leading to a high cost in terms of production losses and labour.

Milk is a complex biological fluid composed of several components including whey proteins and calcium. The deposition of whey proteins (mainly  $\beta$ -lactoglobulin –  $\beta$ -Lg) and calcium are the two major mechanisms of fouling during the heat treatment of milk, which results respectively from protein denaturation and from the decrease of calcium solubilisation upon heating ([Changani et al., 1997](#)). Fouling starts as soon as a dairy product is brought into contact with a stainless steel surface, even if it is invisible to the naked eye. A recent study ([Blanpain-Avet et al., 2012](#)) shows that the mass distribution of the fouling deposited in a plate heat exchanger is primary controlled by the distribution of the unfolded protein generated by the denaturation process. The presence of calcium and phosphate also contribute to fouling in an important manner. Upon heating of milk, part of these ions will tend to precipitate and ultimately will form a mineral deposit on the stainless steel surface ([Bansal and Chen, 2006](#); [Rosmaninho and Melo, 2007](#)) in a typical crystallization fouling process ([Rosmaninho et al., 2007](#)), depending on the surface energy of the substrate ([Rosmaninho and Melo, 2008](#); [Santos et al., 2004](#); [Yoon and Lund 1994](#)). It was also showed very recently that a relationship exists between substrate roughness and fouling amount ([Jimenez et al., 2012](#)).

However, only few studies have tried to investigate the interfacial behaviour of proteins and calcium at a stainless steel surface. An electrochemical

impedance spectroscopy study was carried out by Omanovic et al. (2000) to investigate the interfacial behaviour of  $\beta$ -Lg at an austenitic stainless steel surface over the temperature range 299 to 343 K to an open circuit potential: the electrode/electrolyte interface and corresponding surface processes were successfully modelled by applying an equivalent-electrical-circuit approach. It was confirmed that  $\beta$ -Lg strongly adsorbs onto the stainless steel surface via chemisorption. Another study (Blanpain-Avet et al., 2012), using micro Raman spectroscopy (MRS), on the conformational structure of whey proteins constituting fouling deposits during the processing in a heat exchanger was also recently published. MRS analyses at different depths of the deposit reveal a loss of  $\alpha$ -helix structures of  $\beta$ -Lg without detection of aggregate signatures. For a range of calcium content of 90 to 160 mg/L, no effect of calcium ions on the molecular conformation of  $\beta$ -Lg within the deposit was shown.

Two types of fouling exist: a predominantly mineral fouling, with formation of calcium phosphate aggregates, and a predominantly organic fouling, with formation of a protein layer containing calcium particles (Daufin et al., 1987; Lalande et al., 1989; Mantus et al., 1993; Xie et al., 2001; Tsuge et al., 2002). Our objective was thus to set a characterization procedure to investigate a predominantly organic fouling mechanism, i.e. the adsorption phenomena of protein and calcium particles after long and very short fouling times, when no fouling can be seen with naked eyes. To investigate the fouling deposit as well as the interface with stainless steel, Scanning Electron Microscopy (SEM), Electron-Probe Micro Analysis (EPMA), Time-of-Flight Secondary Ion Mass Spectroscopy (ToF-SIMS) and Atomic Force Microscopy (AFM) were carried out on 316L stainless steel submitted to different fouling solutions in a heat exchanger for two hours and for

1 minute. It is the first time in literature that these nano-thick fouling layers are investigated.

## 2. Fouling Characterization

### 2.1. Stainless steel analysis:

The Figure (3.1) shows the depth profiles obtained for  $\text{Ca}^+$ ,  $\text{Cr}^+$ ,  $\text{CsFe}^+$ ,  $\text{Cs}_2\text{O}^+$  and  $\text{CNCs}^{2+}$  ( $m/z$  292).  $\text{Ca}^+$  and  $\text{CNCs}^{2+}$  signals were followed to confirm that the virgin stainless steel does not contain or only contains traces of these elements, so that the further fouling analyses can be relevant.

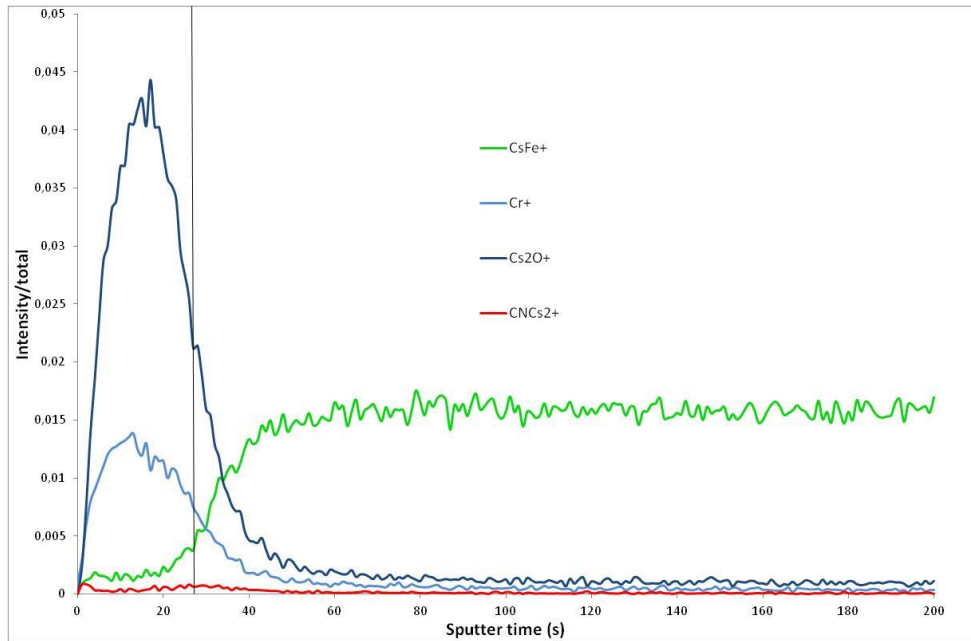


Figure 3.1: Depth profiles (ToF-SIMS) in  $\text{Cr}^+$ ,  $\text{CsFe}^+$ ,  $\text{Cs}_2\text{O}^+$  and  $\text{CNCs}^{2+}$  of the stainless steel

The  $\text{Cr}^+$  layer is, as assumed, first detected. The  $\text{Cr}^+$  signal is well correlated with the oxygen signal ( $\text{Cs}_2\text{O}^+$ ). These peaks are characteristic of the chromium oxide passive film. Then the  $\text{CsFe}^+$  signal increases. The interface

between the chromium oxide and the iron layers is detected after around 30 s erosion.

No  $\text{Ca}^+$  signal is detected in the steel that is why it is not represented in the Figure 3.3 very low  $\text{CNCs}^{2+}$  signal is surprisingly observed, may be due to contaminations on the steel surface.

The steel surface was also investigated by AFM. The Figure (3.2) presents an image taken on a surface of  $4\mu\text{m} * 4\mu\text{m}$ .

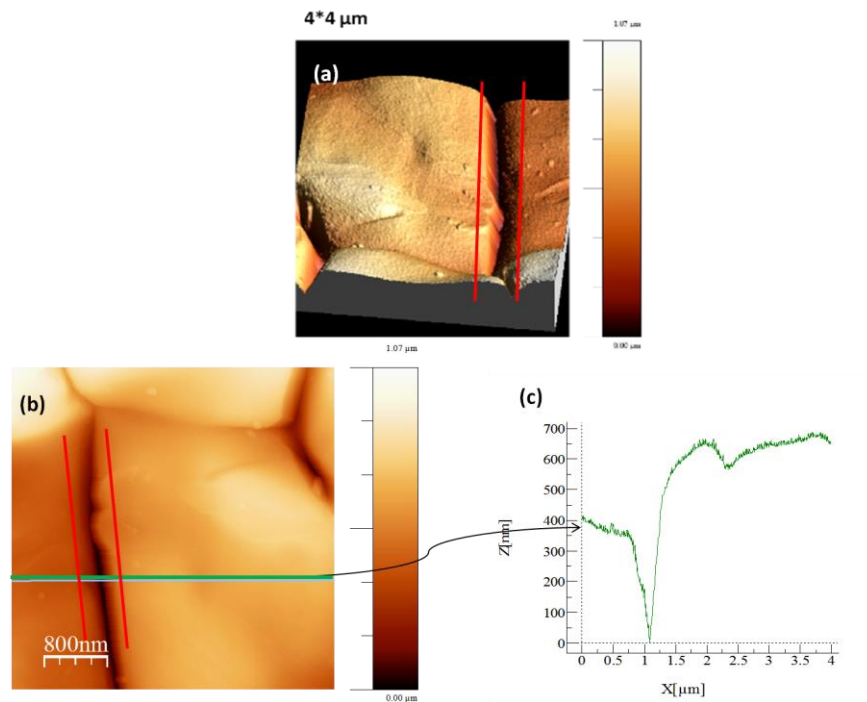


Figure 3.2 : AFM image of virgin stainless steel surface on a  $4\mu\text{m} * 4\mu\text{m}$  surface: 3D representation (a) with a zoom around the steel fissure (b) and profile analysis of the failure (c)

The image taken on the  $4\mu\text{m} * 4\mu\text{m}$  surface shows a quite homogeneous surface (Figure 3.2a), with some fissures (outlined by red lines) of around 700 nm depth (Figure 3.2b, c). These defects can be due to surface scratches, or to grain boundaries. To elucidate this point, an optical image of the steel plate was taken (Figure 3.3)

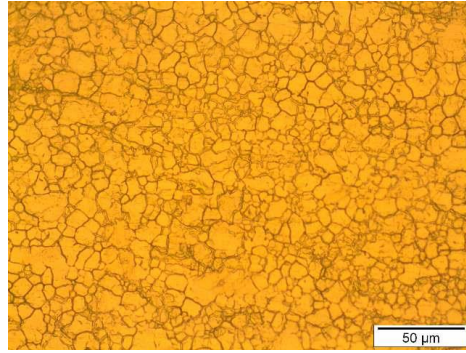


Figure 3.3: Optical picture of the steel plate surface

On the picture the steel grain boundaries are well identified. It confirms that the fissure observed come from the steel grain boundaries. Quadratic roughness calculated on Figure 3.3b is equal to 150 nm. The rest of the surface presents some heterogeneity, as shown by the profile in Figure 3.3c. When a zoom is made on the picture without taking into account the grain boundary, the quadratic roughness is around 64 nm. Another AFM picture was taken on a 200 nm\*200 nm surface in order to investigate the steel roughness on a nano-scale (Figure 3.4).

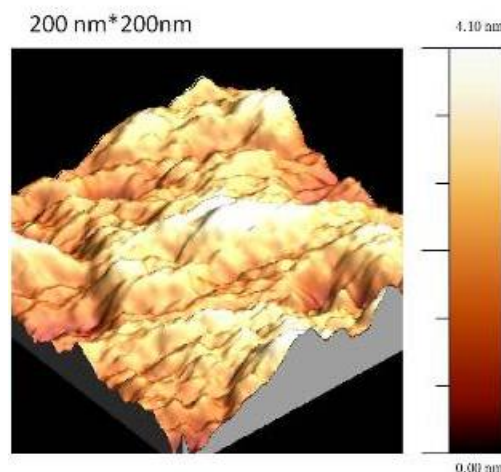


Figure 3.4: AFM picture of the steel plate on a 200 nm \*200 nm surface

Looking at Figure (3.4) in the homogeneous zone, the image taken on a surface of 200 nm\* 200 nm reveals a homogeneous morphology and a smooth surface, with an Rq of 4 nm.

To conclude this preliminary study, steel shows a surface not so homogeneous (Rq=64 nm) on a micrometer scale but very smooth on a nanometer scale (Rq=4 nm) with deep fissures (around 700 nm depth) that are dispatched on the surface and that come from the steel grain boundaries. In the next part, fouling layers obtained after 2 hours fouling in both fouling solutions will be investigated.

## ***2.2. Analysis of the fouling layer after 2 hours fouling:***

The steel samples were submitted to two dairy solutions, made of whey protein (30 ppm calcium) and TH0 water (FM 1) (without calcium) or tapwater (FM 2) (containing 90 ppm calcium), during two hours. The results obtained are completely different. The Figure3.5 shows the difference in terms of visual aspect between the two fouling layers obtained.

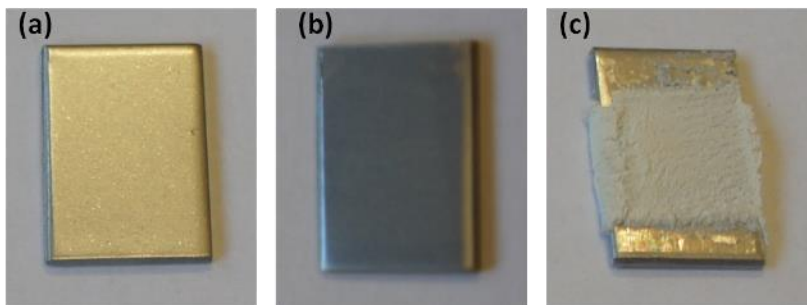


Figure 3.5: comparison of the numerical pictures of the samples before fouling (a) and after two hours fouling in solutions containing whey protein in (FM 1) (b) or in (FM 2) (c).

After two hours fouling in the solution containing whey protein and TH0 water, the plate shows homogeneous blue reflects which are

characteristic of the fouling layer; when tap water is used, the fouling layer is completely different: it is very thick, white, and it seems very rough. Both fouling layers were investigated using different techniques in order to investigate their morphology and composition.

### ***3.2.1. Study of the fouling layer after fouling in a solution containing whey protein and TH0 water (FM 1):***

When TH0 water is used, the fouling layer is quasi-invisible to the naked eye. The main difference with the virgin stainless steel consists mainly in a difference of surface colour: the plate shows homogeneous blue reflects which are characteristic of the thin fouling layer.

An optical picture was first taken to see if the layer was hiding the grain boundaries (Figure 3.6).

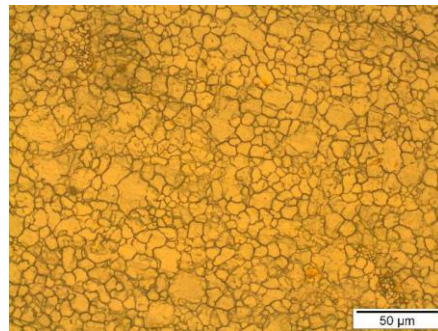


Figure 3.6: Optical picture taken after 2 hours fouling in the fouling solution (FM 1) containing whey protein and TH0 water.

It is clear that the fouling layer is too thin to hide the grain boundaries with the optical microscope resolution. It was also not possible to carry out a cross-section analysis using EPMA: the electron interaction volume is  $1\mu\text{m}^3$  and the layer is too thin to be detected.

A SEM analysis was carried out on the surface of the fouling layer (Figure 3.7).

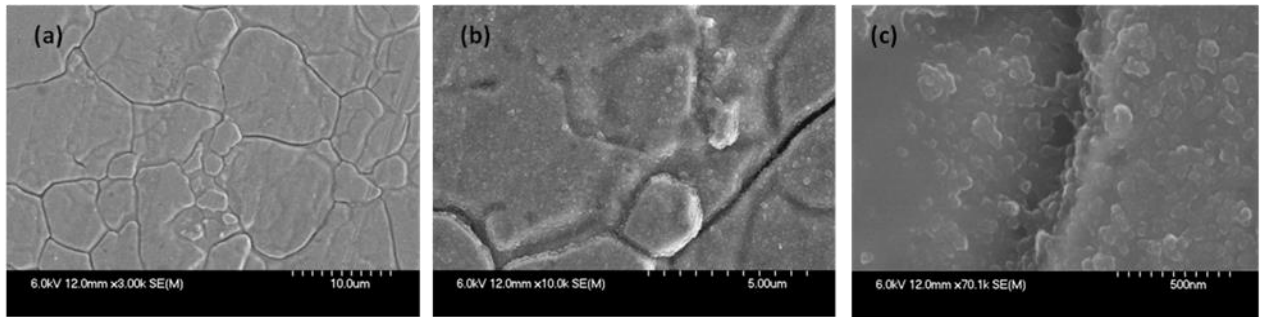


Figure 3.7: SEM images of the surface fouling layer at different magnifications (a)X3000, (b)X10000, (c)X70000

On the first picture (Figure 3.7a), the fouling layer is hardly detected and the grain boundaries are well visible. On the Figure 3.7b taken at higher magnification, the surface is covered with a homogeneous layer and the grain boundaries are also partly covered. The last image (Figure 3.7c) shows that the grain boundaries are filled in with the fouling layer, consisting in small clusters, also covering the surface.

An AFM analysis was finally carried out on a  $2\ \mu\text{m} * 2\ \mu\text{m}$  surface to better investigate the deposit morphology and roughness. The Figure (3.8) presents the corresponding pictures.

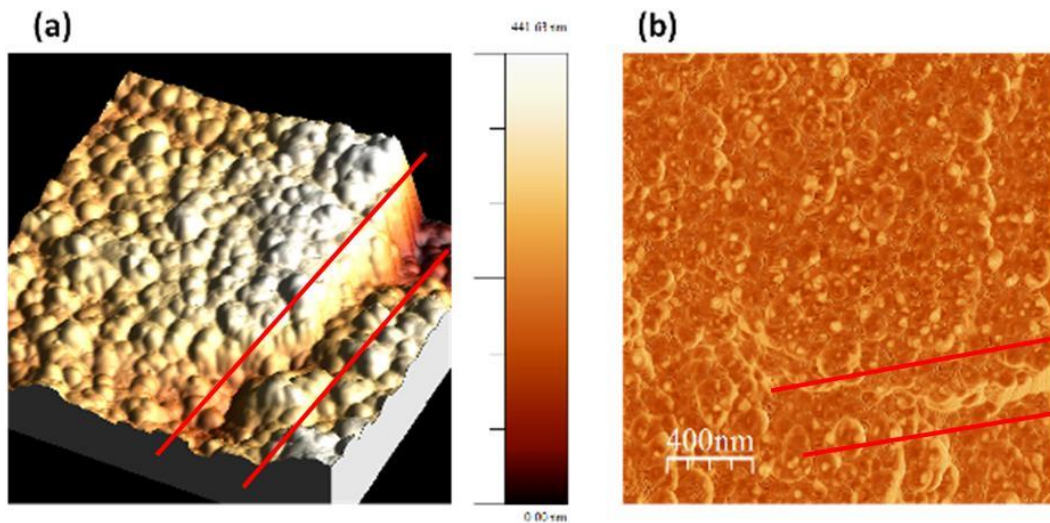


Figure 3.8 : AFM image of the  $2\ \mu\text{m} * 2\ \mu\text{m}$  surface after two hours fouling with TH0 water: 3D representation(a) and picture obtained using phase imaging (b)

The fouling layer is quite homogeneous, and the deposit covers the steel surface as well the steel fissures, as it can be well observed in the phase imaging. It is composed of regular clusters covered with small particles. Complementary images were taken on the smooth part of the sample and are presented in the Figure (3.9).

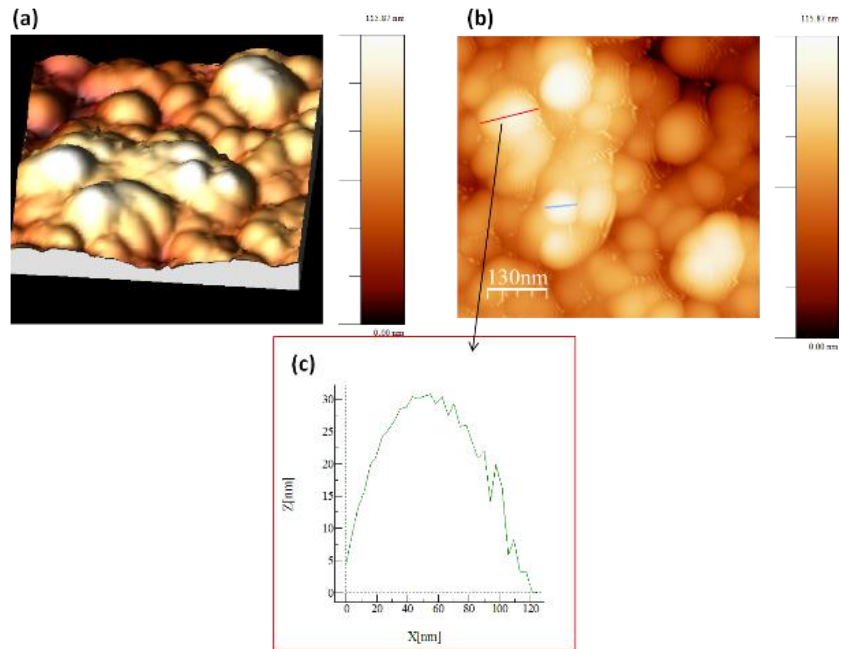


Figure 3.9: AFM pictures taken on the plane part of the  $2\ \mu\text{m} * 2\ \mu\text{m}$  surface: 3D picture (a), picture obtained using phase imaging (b) and particle profile (c).

The surface layer has a quadratic roughness  $R_q$  of 32 nm. The fouling layer is composed of a juxtaposition of clusters of different sizes (Figure 3.9 a and b), varying from 120 nm inside the layer (Figure 3.9 c) to 60 nm in extreme surface.

The whey protein contains mainly  $\beta$ -Lactoglobulin ( $\beta$ -Lg).  $\beta$ -Lg is a 18,400 dalton retinol binding protein with a  $\beta$ -barrel structure characteristic of the lipocalin superfamily which is stabilised by two intra-molecular disulphide bonds (Cys106- Cys119, and Cys66- Cys160) (Figure 3.10) together with a single free cysteine residue (Cys121) (Brownlow et al., 1997).

1	Leu Ile Val Thr Gln Thr Met Lys Gly Leu Asp Ile Gln Lys Val	15
16	Ala Gly Thr Trp Tyr Ser Leu Ala Met Ala Ala Ser Asp Ile Ser	30
31	Leu Leu Asp Ala Gln Ser Ala Pro Leu Arg <sub>40</sub> Val Tyr Val Glu Glu	45
46	Leu Lys Pro Thr Pro Glu Gly Asp Leu Glu Ile Leu Leu Gln Lys	60
61	Trp Glu Asn Gly Glu Cys <sub>66</sub> Ala Gln Lys Lys Ile Ile Ala Glu Lys	75
76	Thr Lys Ile Pro Ala Val Phe <sub>82</sub> Lys Ile Asp Ala Leu Asn Glu Asn	90
91	Lys Val Leu Val Leu Asp Thr Asp Tyr Lys Lys Tyr Leu Leu Phe	105
106	Cys <sub>106</sub> Met Glu Asn Ser Ala Glu Pro Glu Gln Ser Leu Ala Cys <sub>119</sub> Gln	120
121	Cys <sub>121</sub> Leu Val Arg Thr Pro Glu Val Asp Asp Glu Ala Leu Glu Lys	135
136	Phe Asp Lys Ala Leu Lys Ala Leu Pro Met His Ile Arg Leu Ser	150
151	Phe Asn Pro Thr Gln Leu Glu Glu Gln Cys <sub>160</sub> His Ile	

Figure 3.10: Primary sequence of  $\beta$ -lactoglobulin (Brownlow et al., 1997)

On heating  $\beta$ -Lg first dissociates into monomers which then partially-unfold before associating into threadlike clusters of around 50nm in diameter (Carrotta et al., 2001; Relkin, 1996). Unfolding reveals the buried Cys121 which is then able to catalyse disulphide interchange to form a non-native monomer in which Cys119 is exposed (Croguennec et al., 2004) allowing the protein to become linked to other food proteins, such as caseins (Smits and Vanbrouwershaven, 1980).

The size of the clusters observed corresponds well to the unfolded protein. We can then assume that the proteins in denatured and unfolded states, and not in aggregated state, deposit on the steel surface during fouling and finally form a homogeneous thin fouling layer. This confirms an observation recently made by Blanpain-Avet et al. (2012).

### ***3.2.2. Study of the fouling layer after fouling in a solution containing whey protein and tapwater (FM 2)***

When tapwater is used, the fouling layer is completely different: it is very thick, white, and it seems very rough (Figure 3.11). A SEM analysis was carried out on the surface of the fouling layer.

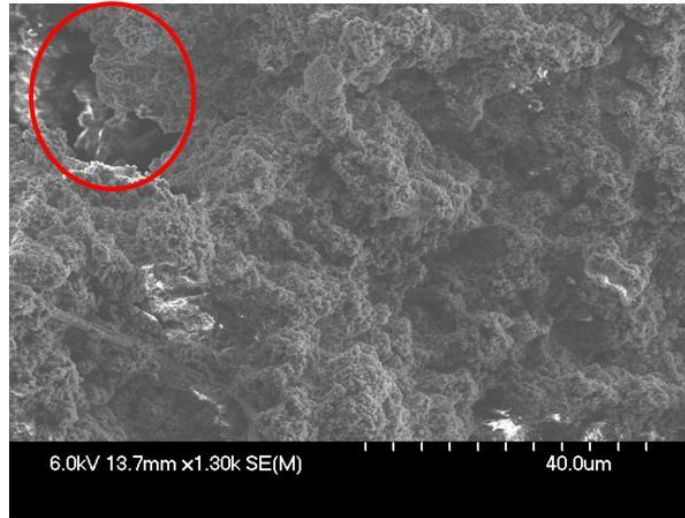


Figure 3.11: SEM image of the fouling layer obtained after 2 hours fouling in (FM 2).

This SEM image confirms the important roughness of the fouling layer, in which some voids and heterogeneities are also visible (red circle in Figure 3.11).

Moreover, a complementary SEM picture was taken on the steel surface after having removed using a cutter the main part of the fouling layer (Figure 3.12).



Figure 3.12: SEM analysis of the steel surface when the main fouling layer has been removed

This picture is very interesting as it shows that the fouling layer covers not only the plate surface but also the inside of the grain boundaries. It means that the fouling is well anchored to the steel plate through the grain boundaries, which can explain the fact that it is then very difficult to remove the fouling during the cleaning procedures.

The aim was then to investigate the chemical composition and morphology of the fouling layer, and EPMA was chosen as analyzing tool.

First a Back Scattering Electron (BSE) image of the cross-section was carried out. It is presented in Figure (3.13).

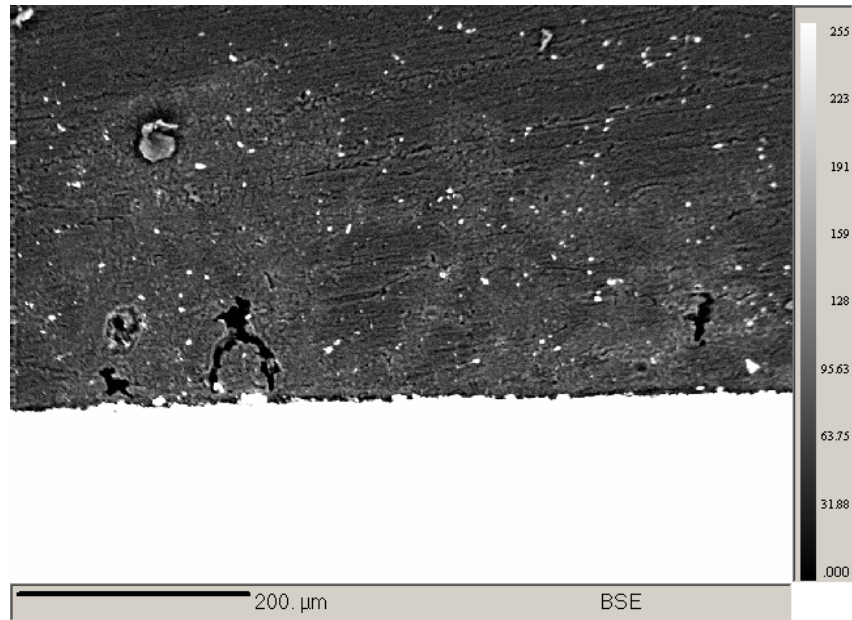


Figure 3.13: BSE cross-section image of the fouling layer obtained after 2 hours fouling (FM 2)

BSE images highlight the contrasts between different chemical species. This is why steel appears completely white compared to the fouling layer (light grey) and the embedded epoxy resin (dark grey). The part of the fouling layer analyzed has a thickness of more than 200 μm, which is huge compared to the thickness of the fouling layer obtained from the solution using TH0 water.

In order to look at the repartition of the calcium (Ca) and of the elements characteristic of the protein (S) and of the steel plate (Cr, Fe), X-Ray mappings of these elements were carried out (Figure 3.14).

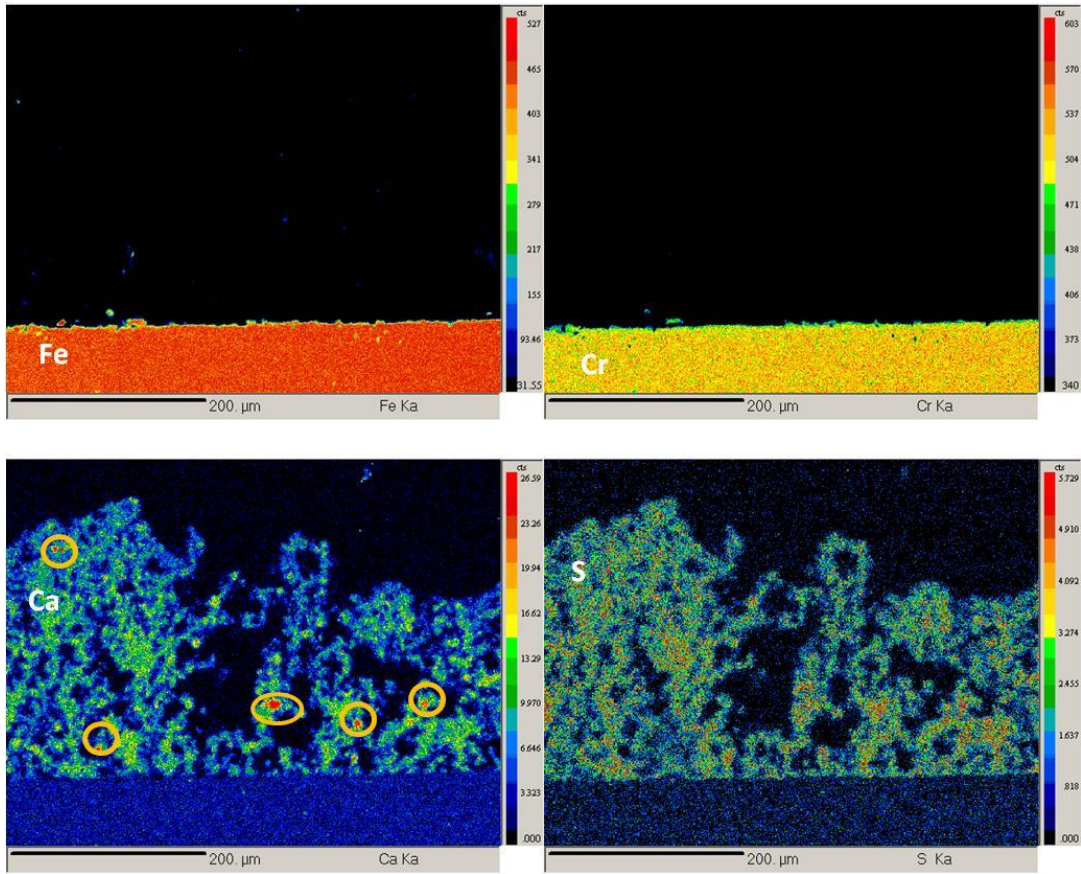


Figure 3.14: Fe, Cr, Ca and S X-Ray mappings of the cross section of the fouling layer (FM 2)

First of all, Fe and Cr are both detected in the steel plate. It is not possible using EPMA to look at the chromium oxide very thin passive layer as the electron interaction volume of EPMA is about  $1 \mu\text{m}^3$ .

Looking at the Ca and S mappings, it can be stated that the layer has developed following an arborescence growth. What is interesting is that both Ca and S are detected at the same places in the fouling layer. The protein is quite homogeneously dispatched. This is not really the case for the calcium: some well visible big calcium aggregates (orange circles) are visible inside the layer

The different analyses of the fouling layers obtained after 2 hours fouling in different solutions (water TH0 and tap water) show complete different behaviours. When no calcium is present in the water (TH0) (FM 1), the layer obtained is thin, homogeneous, with low roughness. On the contrary, when calcium is present at 90 ppm (tap water), the layer is very thick (more than 200  $\mu\text{m}$ ), white, very rough, not homogeneous and shows a growth in arborescence.

The EPMA electron interaction volume is however of 1  $\mu\text{m}^3$  and the resolution might be not high enough to look at the interface on a thickness of a few nanometers. As a consequence, it was decided to make complementary other analyses, using ToF-SIMS and AFM, allowing investigating nano-thick layers, in order to try to determine if the protein first deposits on the surface or if there is a competition between calcium and protein during fouling. This is why it was decided to analyse samples after a fouling duration of only 1 minute in both fouling solutions. After 1 minute the fouling layers are quasi invisible to naked eyes. However they can be detected by AFM and ToF-SIMS.

### ***2.3. Analysis of the fouling layer after 1 minute fouling***

#### ***2.3.1 Solution containing whey protein and TH0 water (FM 1)***

First of all the fouling layer obtained after 1 minute using TH0 water was investigated using AFM on different surface scales. The Figure (2.15) presents the AFM images obtained for surfaces of 4  $\mu\text{m}$  \*4  $\mu\text{m}$ , 2  $\mu\text{m}$  \*2  $\mu\text{m}$  and 500 nm \*500 nm.

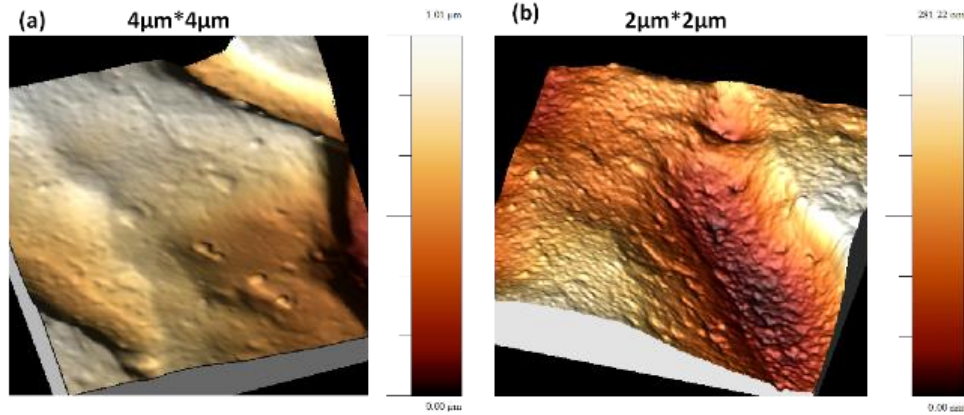


Figure 3.15: AFM 3D pictures of the fouling layer obtained after 1 min in a fouling solution using TH0 water (FM 1) on 4 μm \*4 μm (a) and 2 μm \*2 μm (b) surfaces.

The fouling layer obtained after 1 minute is well detected. The image obtained on a 4 μm \*4 μm surface (Figure 3.15 a) shows that the fouling layer is homogeneous and seems to fit the roughness defects. Again, a grain boundary is visible. The calculated Rq including the grain boundary is equal to 116 nm, whereas it is around 26 nm when it is not taken into account. On the image taken on the 2 μm \*2 μm surface (Figure 3.15b) it is possible to observe a homogeneous layer with no evident imperfection, except the steel imperfections. A last analysis was carried out on a 500 nm\*500 nm surface (Figure 3.16).

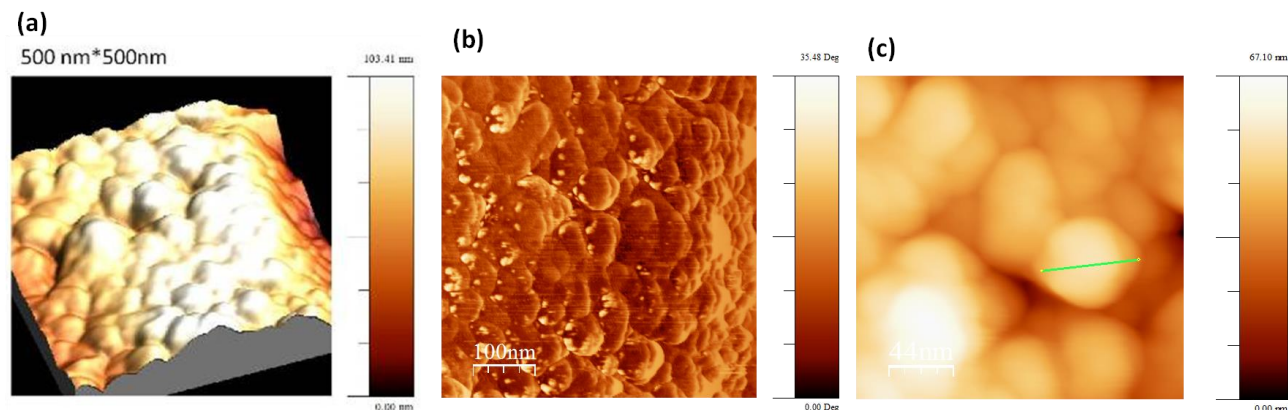


Figure 3.16: AFM images of the fouling layer obtained after 1 min in a fouling solution using TH0 water on a 500 nm\*500 nm surface (a) 3D representation, (b) picture obtained using phase imaging (c) zoom on some particles.

The 3D picture taken on the 500 nm\*500 nm surface (Figure 3.16a) shows a regular structure, with clusters, probably issued from whey proteins, with sizes comprised between 40 and 60 nm. This observation is correlated with the AFM picture taken after 2 hours fouling (Figure 3.8 and Figure 3.9). In this previous image, the fouling layer showed a similar surface structure with bigger clusters (about 120 nm size) inside the layer and 60 nm particles on the extreme surface. The sizes of the particles obtained after 1 minute fouling and on the extreme surface after 2 hours fouling are well correlated, which confirms the fact that the denatured unfolded protein rapidly deposits on the steel surface.

ToF-SIMS was then carried out on same the sample, on a bigger surface (100  $\mu\text{m}$  \*100  $\mu\text{m}$ ), like ToF-SIMS on stainless steel sample without fouling. The speed of erosion were the same for all ToF-SIMS analyses.

First of all erosion depth profiles from the surface layer to the steel plate were carried out, obtained in positive polarity analyses. The ions detected

were  $\text{CNCs}^{2+}$ ,  $\text{Ca}^+$ ,  $\text{Cr}^+$ ,  $\text{Cs}_2\text{O}^+$  and  $\text{CsFe}^+$ . The Figure (3.17) presents the depth profiles plotted against the sputter time after 1 minute fouling in the solution made of whey protein and THO water. The intensity of the different peaks again is not representative of their amount, ToF-SIMS being a non-quantitative analysis.

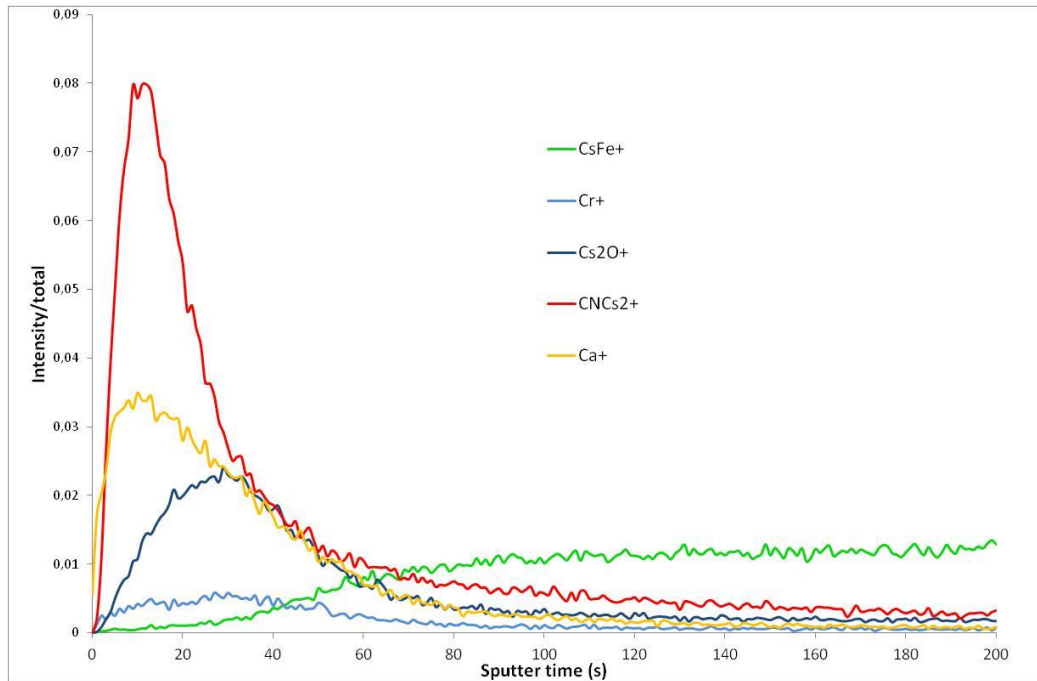


Figure 3.17: ToF-SIMS depth profiles of the fouling layer obtained after 1 minute fouling in THO water (FM 1).

The first remark is that some calcium is detected. As the THO water does not contain any calcium, this one comes from impurities issued from the whey protein, which was analysed and contains 30 ppm calcium. On the ToF-SIMS depth profiles the fouling layer is clearly visible as peaks of  $\text{CNCs}^{2+}$ , characteristic of the protein, and the  $\text{Ca}^+$  peak, are identified during the first 30 s of erosion. The interface with the passive chromium layer is detected after 30 s of erosion, as well as the  $\text{CsFe}^+$  which begins to appear firmly after 60 s of erosion. It is difficult to interpret the depth

profiles as they show a global evolution of each ion on a  $100\ \mu\text{m}^2$  surface: it was observed earlier that the steel can have deep imperfections and a global depth profile does not make a difference between the different roughnesses. This is why the depth profiles presented in Fig 3.19 were not further analysed. To obtain a better resolution, analyses on a  $20\ \mu\text{m} * 20\ \mu\text{m}$  surfaces were carried out, using the “burst alignment” mode of the ToF-SIMS. Using these analyses, it is then possible to reconstruct a 3D picture of the different species detected. The 3D reconstructed pictures obtained for  $\text{Ca}^+$  and  $\text{CNCS}_2^+$  ions from the burst alignment analysis are presented in Figure (3.18).

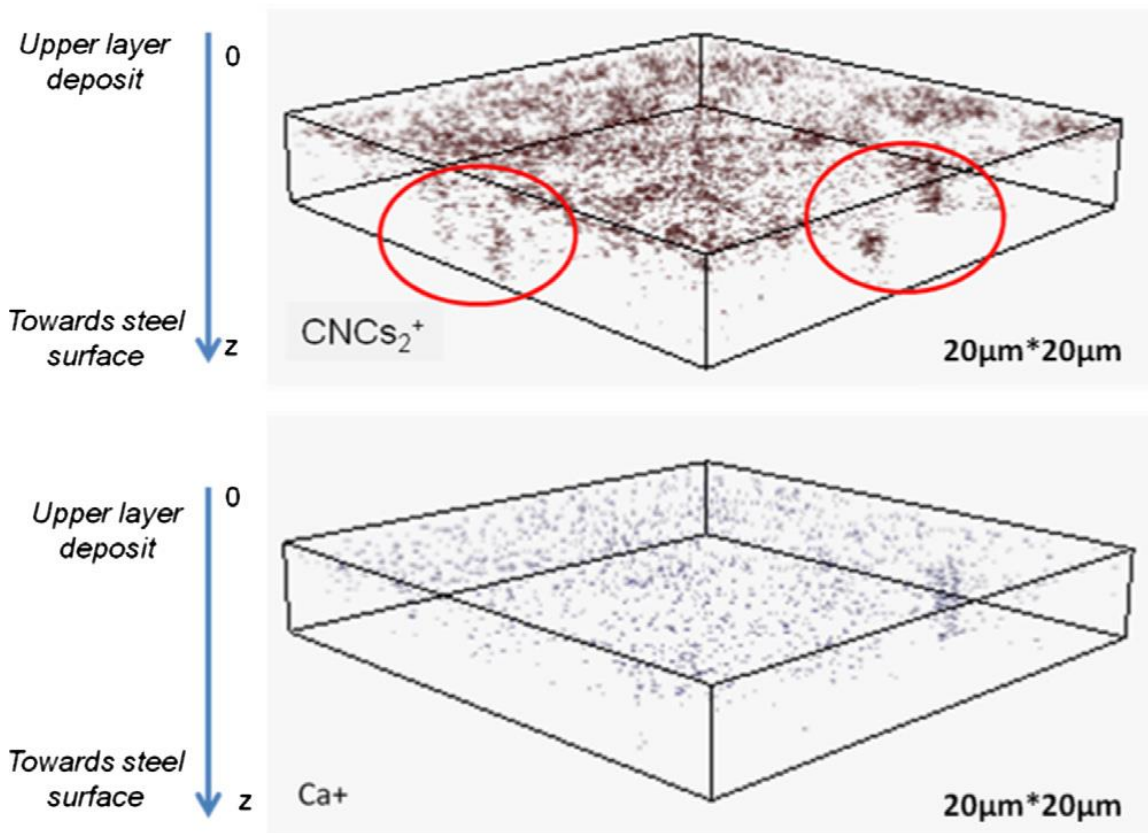


Figure 3.18: 3D ToF-SIMS reconstructed pictures of the fouling layer after 1 minute fouling in the solution using TH0 water (FM 1)

It is clear on those pictures that the protein is deposited quite homogeneously in important amount on the surface as well as inside steel defects (red circles). The calcium is less present but appears at the same place than the protein. However it does not seem to play a role on the fouling layer roughness, as its presence is not evidenced by AFM, which shows a very homogeneous surface.

The fouling layer obtained after 1 minute fouling in the solution using tapwater has then been studied using the same techniques.

### ***2.3.2. Analysis of the fouling layer after 1 minute fouling in the solution using tapwater (FM 2)***

First of all the fouling layer obtained after 1 minute in the solution containing both protein and tapwater was investigated using AFM on different surface scales. The Figure (3.19) presents the AFM images obtained for a surface of 4  $\mu\text{m}$  \*4  $\mu\text{m}$ .

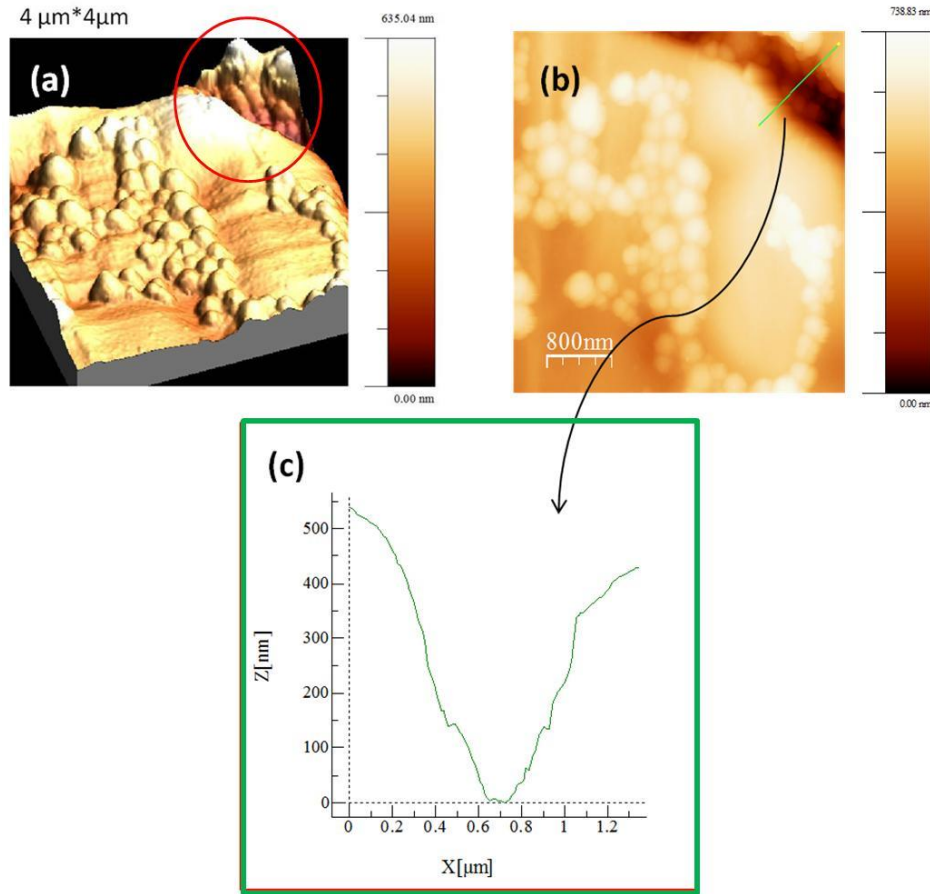


Figure 3.19: AFM images of the fouling layer obtained after 1 min in a fouling solution containing protein and using tapwater on a  $4\ \mu\text{m} \times 4\ \mu\text{m}$  surface: 3D representation (a), picture obtained using phase imaging (b) and profile of the fissure (c).

On certain parts of the picture, the surface is covered with a homogeneous smooth layer. However, grapes of quite round particles appear on the surface, thus increasing the roughness. They seem to be mostly concentrated inside the surface imperfections as well as inside the steel grain boundaries (red circle Figure 3.19a). The fissure visible on Figure (3.19b) was measured (profile in Figure 3.19c) and its size is about  $1\ \mu\text{m}$  with a depth around 600 nm.

These particles were detected nowhere when THO water is used. To better investigate the particles size and morphology, as well as the surface roughness, other pictures were taken on  $2\ \mu\text{m} \times 2\ \mu\text{m}$  surfaces (Figure 3.20).

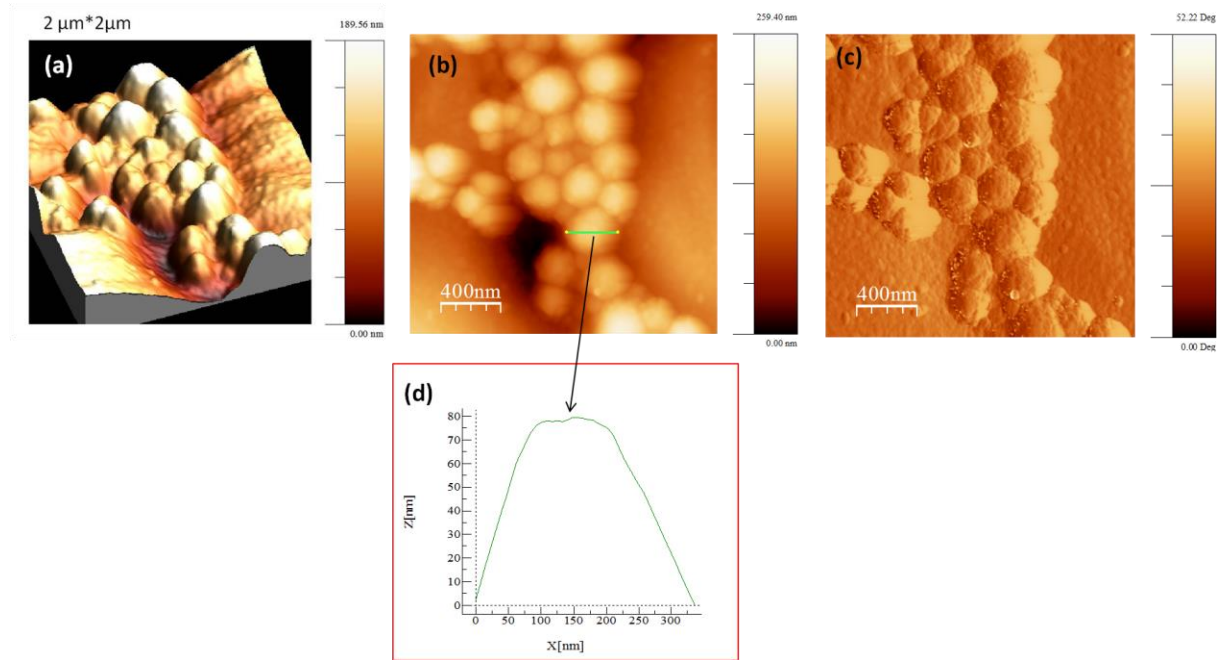


Figure 3.20: AFM images of the fouling layer obtained after 1 min in a fouling solution containing protein and using tapwater on a  $2\ \mu\text{m} \times 2\ \mu\text{m}$  surface : 3D representation (a), imaging mode (b), picture obtained using phase imaging (c), particle profile (d).

The Figure (3.20a) shows that the particles are concentrated in a steel surface defect. The sizes of particles (Figure 3.20b) were measured by profiles, and particle of sizes comprised between 150 nm to 350 nm (Figure 3.20d) could be detected. These particles are much bigger than the protein deposits (60 nm size after 1 min fouling), and looking at the previous EPMA results we assume that these are calcium containing particles.

Roughness measurements were also carried out both on the part containing particles and on the smooth part. When particles are present, a quadratic roughness of 50 nm is obtained. In the smooth layer,  $R_q=11$ , corresponding to the data obtained when only a protein layer is present.

On the phase picture (Figure 3.20c) it seems that the particles show a certain surface roughness or that they are covered by a thin rough layer. This is why 500 nm\*500 nm pictures were taken, both on the smooth part (Figure 3.21a) and on a particles containing part (Figure 3.21b) with a further zoom on one particle.

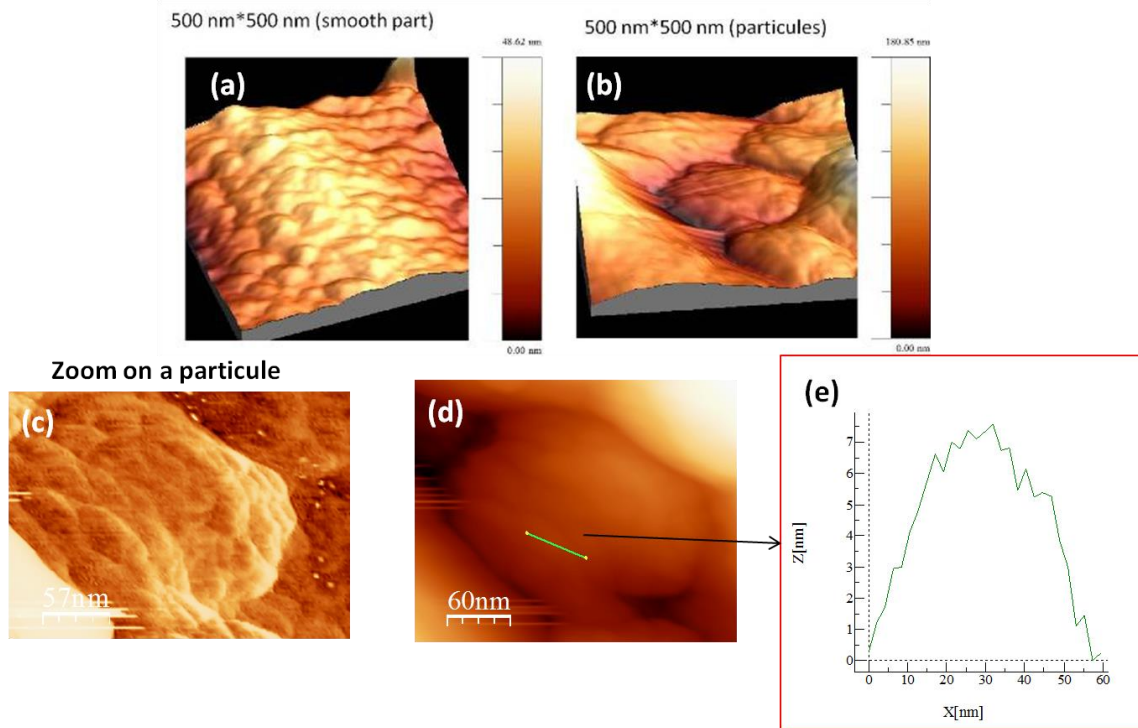


Figure 3.21: AFM images of the fouling layer obtained after 1 minute in a fouling solution containing protein and using tapwater on a 500 nm\*500 nm surface: on the smooth part (a), on the particles containing part (b), with a zoom on one particle using phase mode (c) and imaging mode (d) including a profile on the particle roughness (e).

Looking at the picture of the particles taken on a 500 nm\*500 nm surface (Figure 3.21b and Figure 3.21c), these ones also seem to be re-covered by a layer having the morphology of the protein deposit (Figure 3.21a). When the size of one grain covering the particle is measured, the same size (60 nm) as the size of protein clusters is obtained (Figure 3.21d and Figure 3.21e). The hypothesis is that some calcium-containing particles are deposited in the surface steel defects and that the protein then again covers these particles. However, looking at all these images, it is not possible to confirm if the calcium is directly deposited on the steel plate and then covered by the protein, or if the protein layer first appears and then the calcium particles deposit in the surface defects.

This is why ToF-SIMS analyses were carried out on this layer. First of all, depth profiles in  $\text{Ca}^+$ ,  $\text{CNCs}^{2+}$ ,  $\text{CsFe}^+$ ,  $\text{Cr}^+$  and  $\text{Cs}_2\text{O}^+$  were investigated on a 100  $\mu\text{m}$  \*100  $\mu\text{m}$  surface.

The profiles obtained (not shown in the paper) are quite surprising: looking at the  $\text{Ca}^+$  and  $\text{CsCN}^{2+}$  profiles compared to the  $\text{Cr}^+$  curve, it seems that both the calcium and the protein are present inside the steel, which is impossible. Again, as depth profiles show a global evolution of the species inside the 100  $\mu\text{m}$  \*100  $\mu\text{m}$  surface, they don't take into account the surface roughnesses or the deposit heterogeneity. This is why again these profiles were not analyzed further. It was preferred -as in previous measurements- to carry out a complementary analysis in the burst alignment mode on a 20  $\mu\text{m}$  \*20  $\mu\text{m}$  surface, to obtain higher resolution and allowing 2D and 3D reconstruction of the fouling layer.

Some 2D images were reconstructed on a section of the sample (Figure 3.22), showing the repartition of the  $\text{CsFe}^+$ ,  $\text{Ca}^+$  and  $\text{CNCs}^{2+}$  on this cross-section.

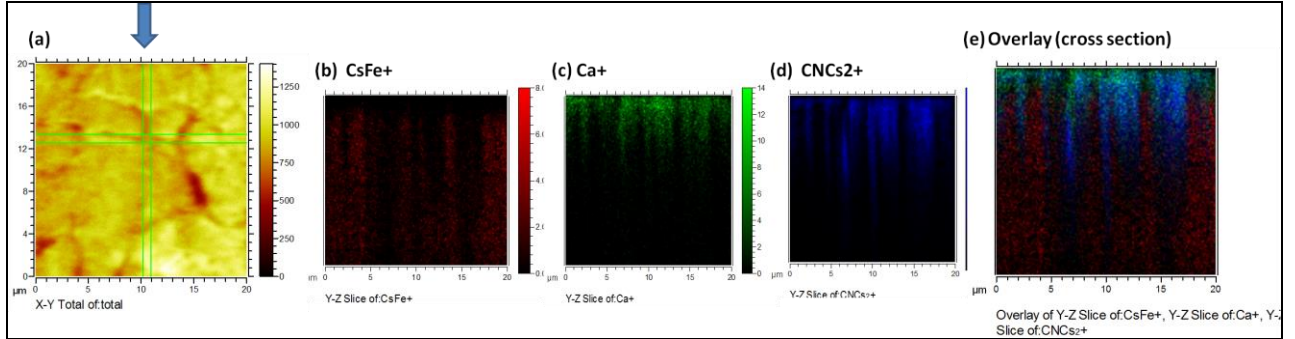


Figure 3.22: (a) imaging mode on a  $20\mu\text{m} \times 20\mu\text{m}$  surface, (b)  $\text{CsFe}^+$  2D reconstruction, (c)  $\text{Ca}^+$  2D reconstruction, (d)  $\text{CNCs}^{2+}$  2D reconstruction, (e) Overlay of the three reconstructions.

The Figure (3.22a) shows the image observed using ToF-SIMS on the  $20\mu\text{m} \times 20\mu\text{m}$  surface analyzed. The grain boundaries are visible. We chose reconstructing the 2D pictures of  $\text{CsFe}^+$  (Figure22b),  $\text{Ca}^+$ (Figure22c), and  $\text{CNCs}^{2+}$  (Figure22d) ions on a cross-section layer of the fouling layer (blue arrow).The results are very interesting: in the  $\text{CsFe}^+$  picture, the red parts show the presence of this ion and the black parts evidence the steel grain boundaries. The  $\text{Ca}^+$  and  $\text{CNCs}^{2+}$  pictures indicate the presence of these ions both on the surface and inside the grain boundaries. However the  $\text{Ca}^+$  ions are mostly concentrated in the upper part of the grain boundaries whereas  $\text{CNCs}^{2+}$  ions are present deeper in the fissures. This is perfectly visible on the overlay of the three 2D pictures: the grain boundaries are completely filled in with protein, whereas the calcium deposit appears mostly next to the surface.

The 3D reconstructed pictures obtained for  $\text{Ca}^+$  and  $\text{CNCS}_2^+$  ions from the burst alignment analysis are presented in Figure (3.23).

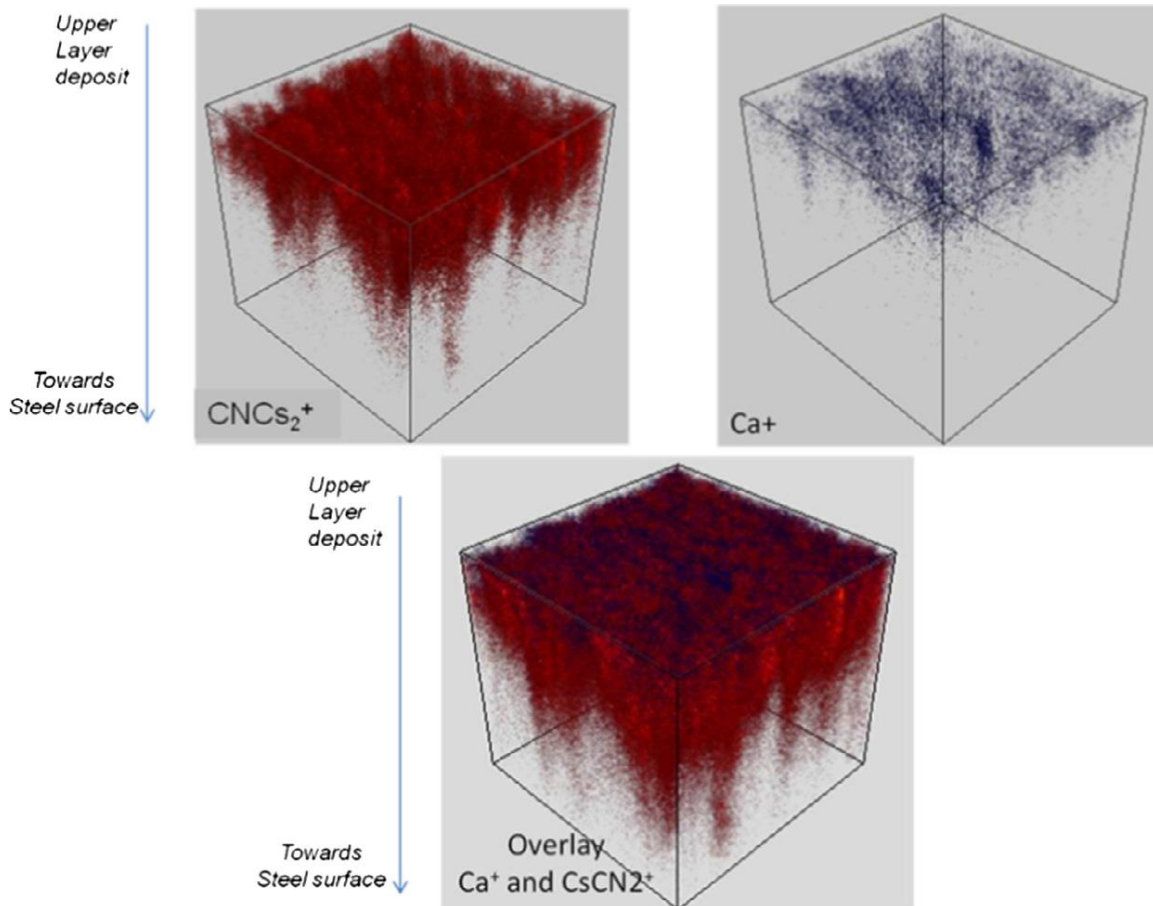


Figure 3.23: 3D ToF-SIMS reconstructed pictures of the fouling layer after 1 minute fouling in the solution using tapwater (FM 2).

These images confirm the previous observations: it is clear that the protein (in red colour) is homogeneously present on the surface, as well as in the steel defects and inside the grain boundaries. The calcium (blue colour) is however mainly present at the surface of the fouling layer and also detected inside the grain boundaries but it can be noticed that it is mainly concentrated in the upper side of the grain boundary. It can also be observed that on the major part of the extreme surface the calcium is covered by the protein, which is well correlated with the AFM observations (Figure 3.21c).

#### ***4. Growth Mechanism***

The fundamental growth mechanism of the first fouling layers obtained in the case of a predominantly organic dairy fouling has never been studied in literature. This study, combining different surface analysis techniques, such as AFM, EPMA and ToF-SIMS, allows identifying very clearly the protein-based layer and the calcium-containing particles.

##### ***4.1. Fouling growth mechanism in presence of whey protein and TH0 water (FM 1)***

When TH0 water is used, the deposit is thin, homogeneous and gives a blue aspect to the steel plate. A low amount of calcium is detected by ToF-SIMS, but no particles are detected by AFM inside or on the protein layer.

A schematic representation of the fouling growth mechanism in presence of whey protein and TH0 water is presented in Figure (3.24).

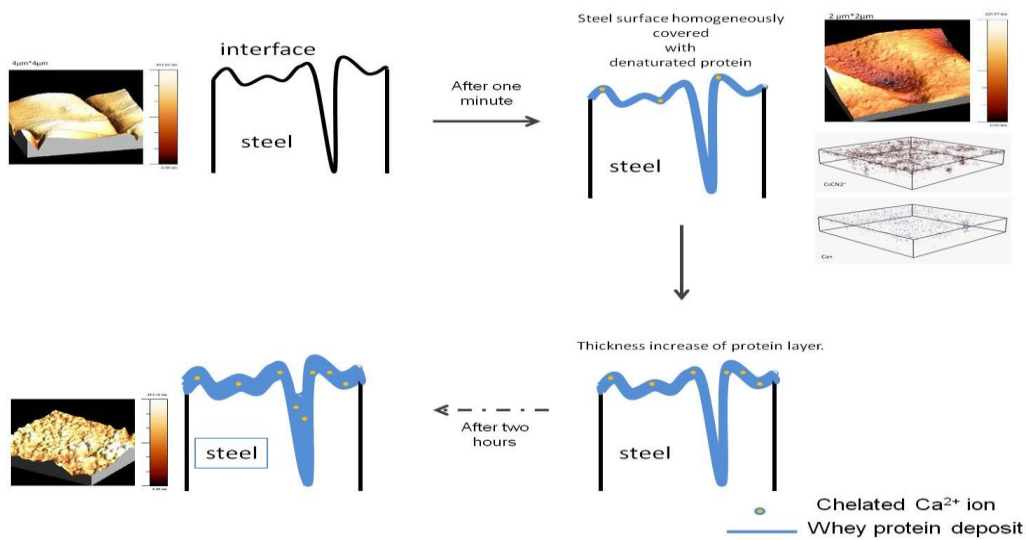


Figure 3.24: Schematic representation of the fouling growth mechanism in presence of whey protein and THO water

AFM after 1 minute fouling shows a deposit covering homogeneously the steel surface. The morphology of the deposit is similar after 1 minute and after 2 hours. It consists in the juxtaposition of small size (60 nm) clusters, coming from denatured and unfolded protein (Carrotta et al., 2001). The clusters are however bigger after 2 hours (120 nm) than after 1 minute (60 nm), leading to the assumption that the proteins are aggregating on the steel plate during long time fouling. Using ToF-SIMS, the whey protein is identified by the  $CNCs^{2+}$  signal. The 3D reconstruction profiles confirm that the protein homogeneously covers the steel surface and that it is also present inside grain boundaries. Calcium is also detected by ToF-SIMS, coming from impurities contained in the whey protein. It seems well dispersed in the protein layer and it does not affect the fouling layer roughness. After 2 hours of fouling, the whole surface is covered and the grain boundaries are partly or completely filled in with the protein fouling layer.

#### 4.2. Mechanism in presence of whey protein and tapwater (FM 2)

The growth mechanism in presence of whey protein and tapwater -total calcium content 120 ppm, is different than the previous one. A schematic representation of this mechanism is shown in Figure (3.25).

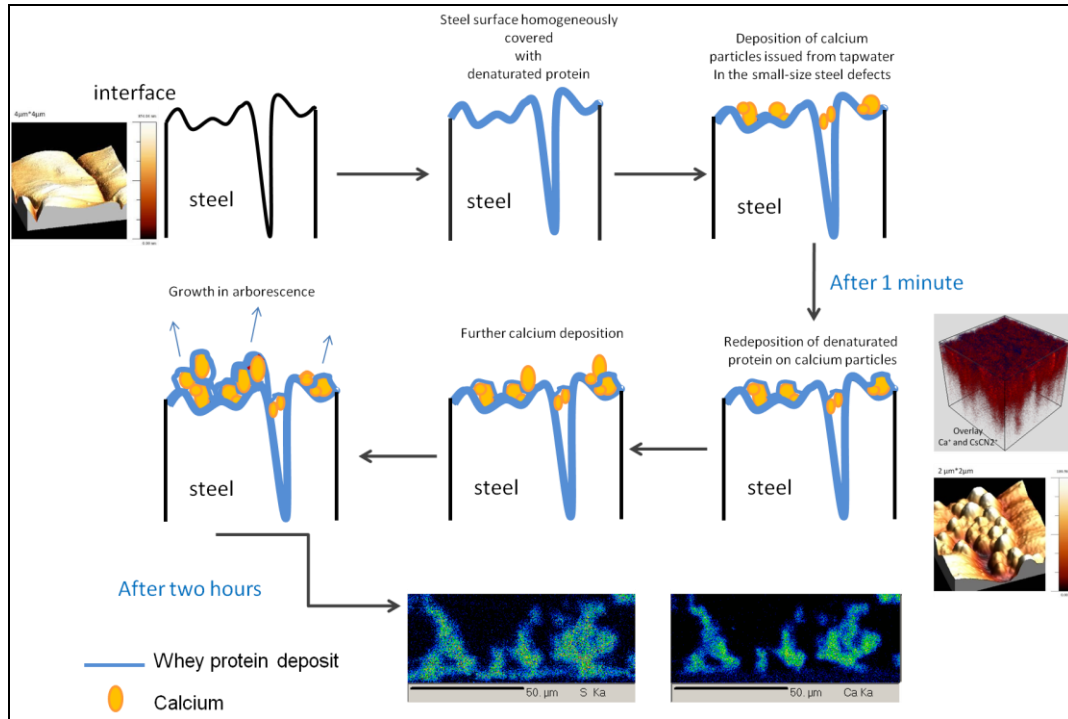


Figure 3.25: Schematic representation of the fouling growth mechanism in presence of whey protein and tapwater (FM 2).

SEM analyses after 2 hours fouling show a thick fouling layer, dispatched both on the surface and inside the grain boundaries. EPMA and SEM also allow detecting an important amount of calcium in the fouling layer. This observation is correlated with AFM observations after 1 minute fouling: on the protein layer (same morphology as when THO water is used), grapes of big round particles are observed, corresponding to calcium-containing particles. These particles of important dimensions (300-400 nm) compared to the protein clusters are mainly dispatched in the steel surface

valleys and are then covered again by protein. AFM and 3D reconstructed ToF-SIMS pictures show that calcium particles are also present in the grain boundaries, but not in the whole depth: they are mainly concentrated in the upper side of the grain boundary, being possibly trapped inside the protein layer before going further inside. The protein layer would be thus the first one being deposited during fouling. The presence of calcium containing particles in the fouling layer would thus increase the total roughness of the sample. This roughness increase favours further deposition of other calcium particles, thus creating preferential fouling pathways. This explains perfectly the arborescent structure observed by EPMA after two hours fouling.

#### ***4.3. Chemical form of calcium particles***

Some questions however remain: some differences are visible between the samples, mainly due to the calcium-containing particles that are not visible inside the layer obtained using TH0 water, even if some calcium is detected by ToF-SIMS. Is the calcium under the same chemical form in the whey protein and in the tapwater? Why calcium particles are only visible when the calcium content is 120 ppm and absent when it's content is 30 ppm?

To try to answer these questions, XPS analyses were in a first step carried out on samples treated 1 minute in both solutions. The signals obtained for Ca2p detected in both fouling layers are represented in Figure (3.26).

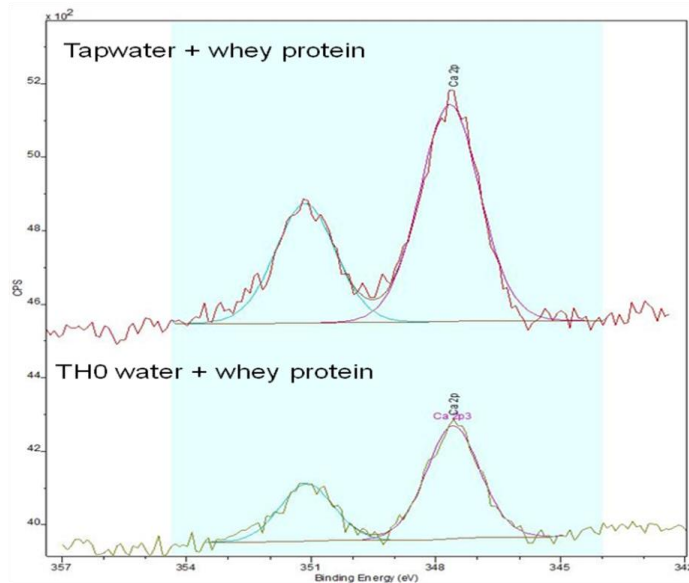


Figure 3.26: XPS spectra of Ca2p for both fouling solutions

The peaks are detected in both cases at the same binding energies (347.7 and 351.2 eV). The profiles obtained for both fouling layers are similar and correspond to the ionic form of Calcium ( $\text{Ca}^{2+}$ ). The energies correspond to the binding energy of  $\text{Ca}^{2+}$  in the calcium carbonate ( $\text{CaCO}_3$ ) form.

One of the most abundant minerals in nature and thus one of the most intensively examined systems is in fact calcium carbonate,  $\text{CaCO}_3$  (Mann, 2001; Sikes and Wheeler, 1988). Calcium carbonate precipitates in the form of several distinct solid phases: hydrated and anhydrous amorphous calcium carbonate (ACC), two hydrates (monohydrate and hexahydrate), and three anhydrous polymorphs (calcite, aragonite, and vaterite) (Mann, 2001; Sikes and Wheeler, 1988; Falini et al., 1996).

When saturated in water,  $\text{Ca}^{2+}$  and  $\text{CO}_3^{2-}$  spontaneously form a rather amorphous unstable precursor consisting of quite spherical particles of calcium carbonate. According to Ostwald's step rule, amorphous calcium carbonate (ACC) will be the first form to rapidly precipitate from

a supersaturated solution, the nanoparticles developing through homogeneous nucleation or spinodal decomposition and rapid aggregation (Tester et al., 2011), and will rapidly crystallize into one of the more stable polymorphs (Brecevic and Nielsen, 1989; Kawano et al., 2002; Xu et al., 2005; Meldrum et al., 2008), if not stabilized by another element. Amorphous calcium carbonate is also the smallest of the polymorphs, averaging spherules of 50 to 400 nm diameter compared to a normal CaCO<sub>3</sub> crystal of 1 to 10 μm.

Although its structure is not fully understood, ACC has been described as a nanoscale framework that includes channels (~1 nm diameter) that contain water, CO<sub>3</sub><sup>2-</sup>, and other substances (additives) derived from the parent fluid (Goodwin et al., 2010; Rodriguez-Blanco, Shaw and Benning, 2011). Goodwin et al. (2010) suggested that such additives are important because numerous experiments have shown that they can influence ACC stability. ACC has been divided into “transient” and “stable” types (Addadi et al., 2003). Transient ACC is anhydrous whereas stable ACC is hydrated with up to 15% water (Xu et al., 2008). ACC is usually observed as a transient modification, with a remarkable exception as a biomineral (Aizenberg et al., 2002): calcium carbonate biominerals are natural biocomposites in which the mineral is the principal component with the organic matrix being present as a minor fraction. It was found that the organic matrix has a unique ability to control nucleation/growth of certain polymorph(s) and to organize their growth into desired patterns by controlling hierarchically their structure, shape, size, and orientation (Mann, 1993; Lakes, 1993; Hernandez-Hernandez et al., 2008).

Additives in the parent solution can thus influence the rate of precipitation, ACC stability, and its subsequent conversion to one of the crystalline CaCO<sub>3</sub>

polymorphs (Jones and Peng, 2012). Such additives include magnesium, macromolecules, triphosphate ions, polymers, various polysaccharides and amino acids (Tester et al., 2011; Rodriguez-Blanco et al., 2011; Addadi et al., 2003; Loste et al., 2003; Ajikumar et al., 2005; Kontrec et al., 2008; Meiron et al., 2011). Certain organisms have for example been found to produce molecules, such as chitin, that temporarily stabilize amorphous calcium carbonate (Zhang and Gonsalves, 1998).

A recent study (Njegić-Džakula et al., 2010) on the addition of amino acids in solutions of different calcium concentrations indicate that the presence and nature of organic polymers such as acidic polypeptides affect the nucleation, crystal growth, and aggregation of the CaCO<sub>3</sub> polymorphs. The initial solution supersaturation may also play a decisive role during the process of formation of the certain polymorphic CaCO<sub>3</sub> modification. The experiments suggest that the concentration of dissolved CaCO<sub>3</sub>, corresponding to the solubility of ACC, is a threshold supersaturation level that should be considered when carrying out the processes (Lasaga et al., 1998).

In this study, the whey protein solution contains in majority β-Lg, which is composed of 162 amino acid residues. The solution containing whey protein and TH0 water has a Calcium content of 30 ppm, corresponding to a calcium concentration in water of 0.75 mmol/L. This solution cannot be considered as supersaturated, and thus nucleation of calcium carbonate particles does not, or only slightly, occurs. As ToF-SIMS analyses show the presence of some calcium, the calcium ions must be simply trapped or chelated in the protein fouling layer, but no distinct particles are detected by AFM.

On the contrary, the solution constituted with whey protein -and thus amino acids- dissolved in tapwater contain approximately 120 ppm calcium

(corresponding to 3 mmol/L) and can be considered as supersaturated. As this solution is also heated at 90°C for fouling tests, degassing of carbon dioxide and further precipitation of calcium carbonate particles are also favoured.

The whey protein used contains amine groups as well as carboxylic acid and thiol groups: according to the previously cited literature, the protein can thus stabilize the amorphous calcium carbonate nuclei, preventing their further crystallisation in calcite or vaterite. The fouling solution then contains both the unfolded proteins and the CaCO<sub>3</sub> nuclei stabilized by the protein, as well as protein aggregates. This solution can be represented by the following Figure (3.27):

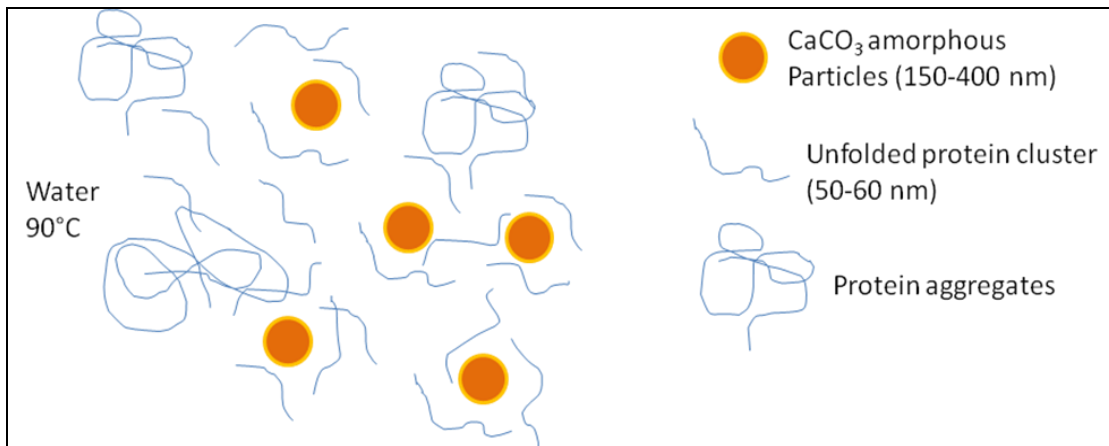


Figure 3.27: Fouling solution “appearance” when put in contact with steel

A recent study ([Blanpain-Avet et al., 2012](#)) shows that - in the conditions used in the paper, which are similar to our conditions-, the mass distribution of the fouling deposited in a plate heat exchanger is primary controlled by the distribution of the unfolded protein generated by the denaturation process, and not by the deposit of aggregated proteins. This is confirmed in

our study, as the size of the protein clusters observed by AFM is of about 50 nm, corresponding to the size of the unfolded  $\beta$ -Lg (Carrotta et al., 2001). These proteins have high affinity with the passive oxidized steel surface, by ionic bindings (electrostatic interactions), hydrophobic interactions or electron exchanges. Omanovic et al. (2000) showed that complexes can be created between the protein and the metallic ions present in the oxide layer (Cr, Fe). The unfolded proteins, carrying the amorphous calcium carbonate particles as well, then deposit on the steel surface. The ACC particles deposit preferentially inside steel roughnesses: once they are trapped in the surface defects and in contact with the protein layer, they cannot easily be dragged away by the water flow and remain on the protein layer. The mineral fouling would be due both to mechanical factors (surface roughness) and chemical interactions (the ACC are dredged by the protein to the surface by ionic interactions). To confirm this, a complementary experiment was carried out: steel plate was submitted during 1 minute only to a tapwater flow in the same experimental conditions than fouling. No mineral fouling can be detected by AFM, no particles are observed.

The protein is thus proven to play a major role in the mineral fouling by dredging and stabilizing the amorphous calcium carbonate particles.

#### ***4.4. Fouling mechanism during the first minutes of experiment***

The Figure (3.28) summarizes all these hypotheses of fouling mechanism during the first minutes of experiment in our experimental conditions.

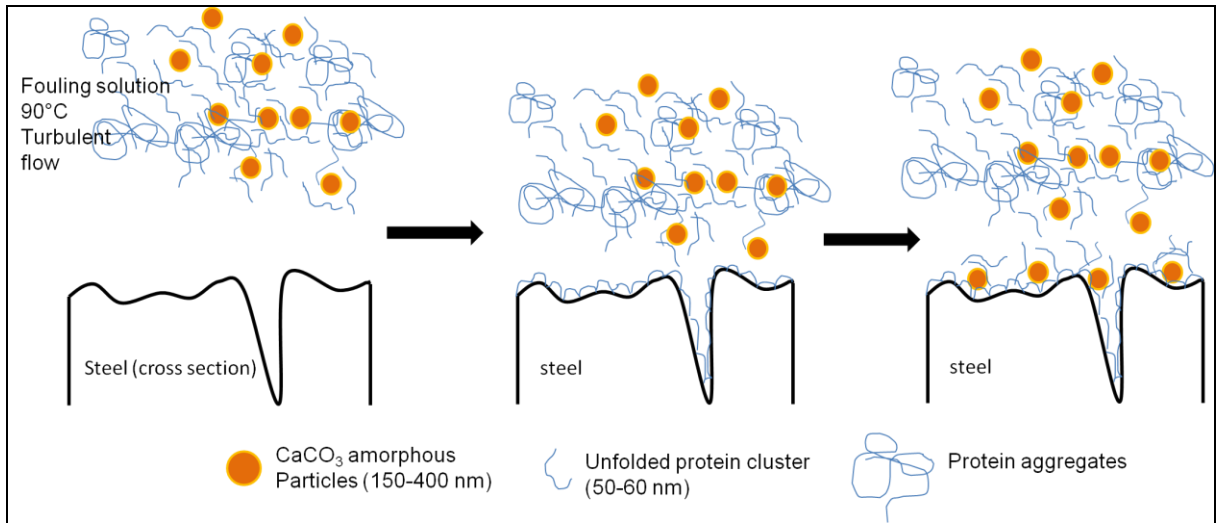


Figure 3.28: Deposition mechanism of the first fouling layers when they protein and tapwater are present in the fouling solution (FM 2).

As the ACC particles are immediately covered by the protein, there is no time to initiate the crystallization of vaterite or calcite, and this explains why at the end of the fouling experiments only ACC is found in the fouling layer. As shown above, the roughness has a great effect on fouling. Indeed, the ACC mainly deposit in the cavity of the surface. Thus, we can assume that removing the cavities of the stainless steel surface would prevent, or at least limit, the fouling to occur. In order to verify this hypothesis we decided to compare the fouling of samples with different grades of polishing.

## ***5. Influence of Roughness of Surface on Fouling Process***

### ***5.1. Mechanical Polishing***

#### ***5.1.1. Surface morphology and roughness of unpolished stainless steel***

Figure (3.29) shows the optical image of the as received stainless steel 316L 2B surface, illustrating the rough surface of this sample. Figure (3.30) is the SEM images of the same sample, as already seen before it contains concave regions and rugged traces. Figure (3.31) exhibits the AFM

morphological image (Imaging conditions: Scan: 20  $\mu\text{m}$  \*20  $\mu\text{m}$ ; Scan rate: 1Hz, 0,5Hz; Resolution: 512 px) of the steel, and the RMS (root mean square) roughness is 140.4 nm in area of 20  $\mu\text{m}$  \*20  $\mu\text{m}$

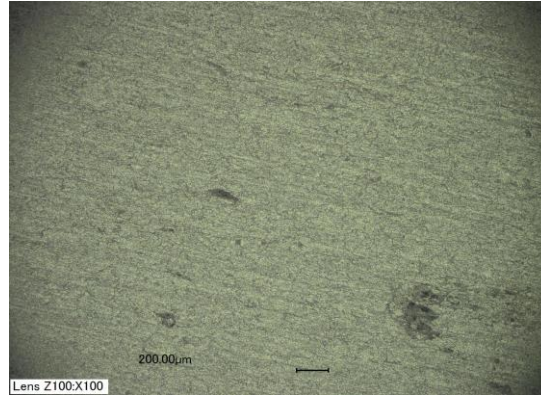


Figure 3.29: The optical microscopic photograph of stainless steel surface

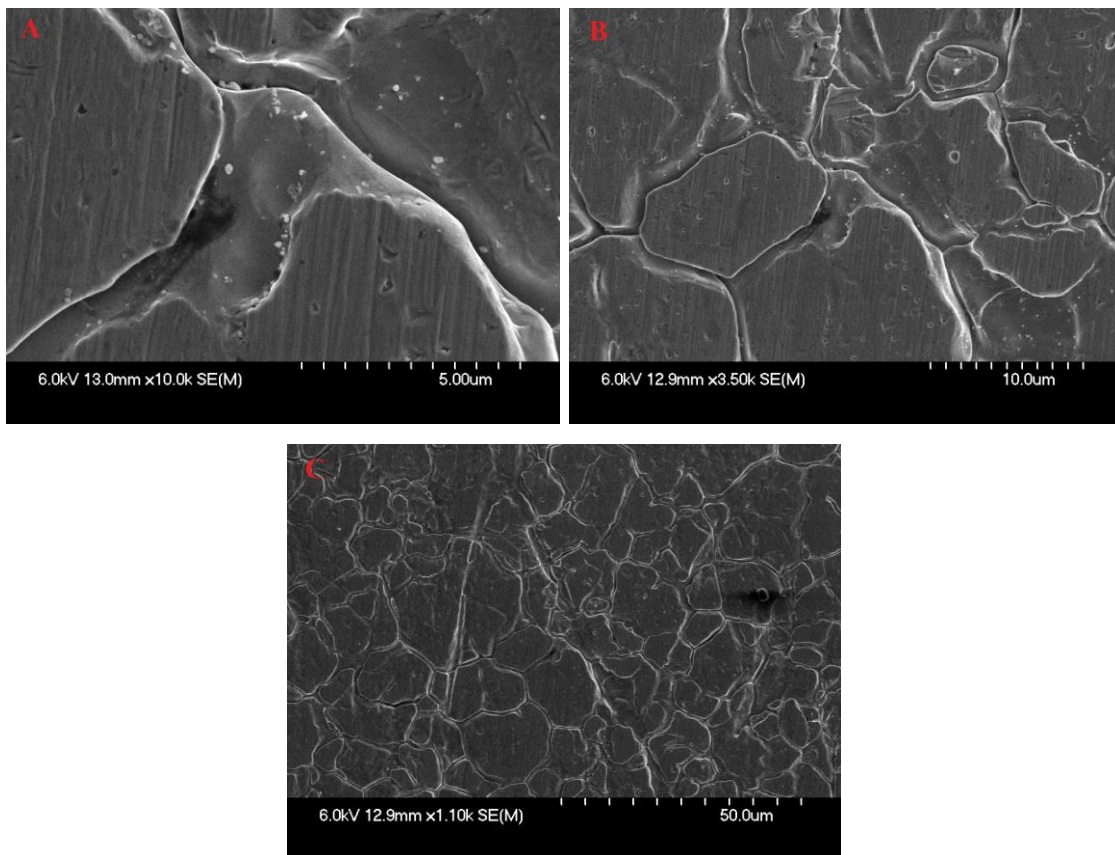


Figure 3.30: The SEM images of stainless steel surface, A) 5  $\mu\text{m}$ ; B) 10  $\mu\text{m}$  and C) 50  $\mu\text{m}$ .

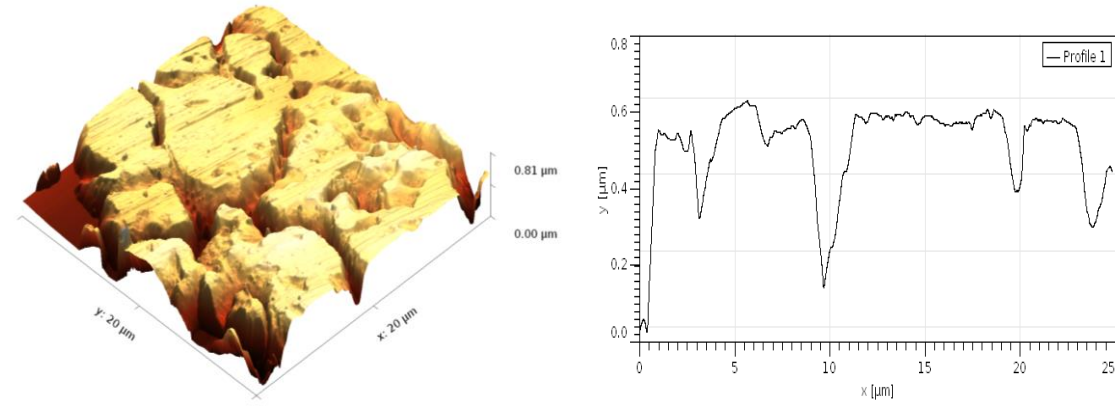


Figure 3.31: The AFM morphological image of the stainless steel surface, (a) 3D image, (b) Profile chart.

### 5.1.2. Surface morphology and roughness of polished stainless steel

Figure (3.32) shows the optical image of stainless steel polished up to a 1000 grade polishing paper.

The AFM image of the surface is displayed in Figure (3.33), the polishing lines are clearly observed on the surface.

The RMS roughness is 28.7 nm in area of 20\*20 μm, much lower than the unpolished one (140.4 nm).

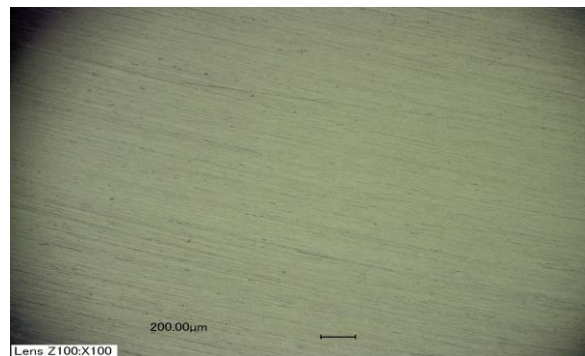


Figure 3.32: The optical image of stainless steel 1000 grade polished

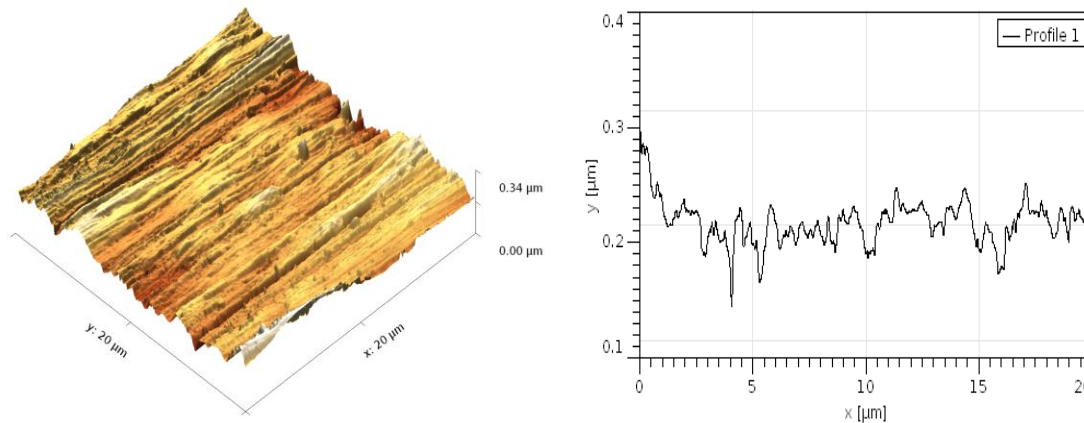


Figure 3.33: The AFM image of the stainless steel 1000 grade polished, (a) 3D image, (b) Profile chart

Figure (3.34) depicts the optical magnified image of a mirror like polished stainless steel surface. The coarseness of original surface is eliminated, however, some black spots appear. Figure (3.34) shows a SEM image of the mirror like surface. The polished surface is very smooth, as compared with the unpolished one (Figure 3.30) or polished with the 1000 grade paper (3.32).

The AFM image of a typical polished surface is displayed in Figure (3.36). The RMS roughness is 6.1 nm in area of 20\*20 μm, much lower than the unpolished steel (140.4 nm) or polished with 1000 grade paper (28.7 nm).



Figure 3.34: The optical microscopic photograph of mirror like stainless steel.

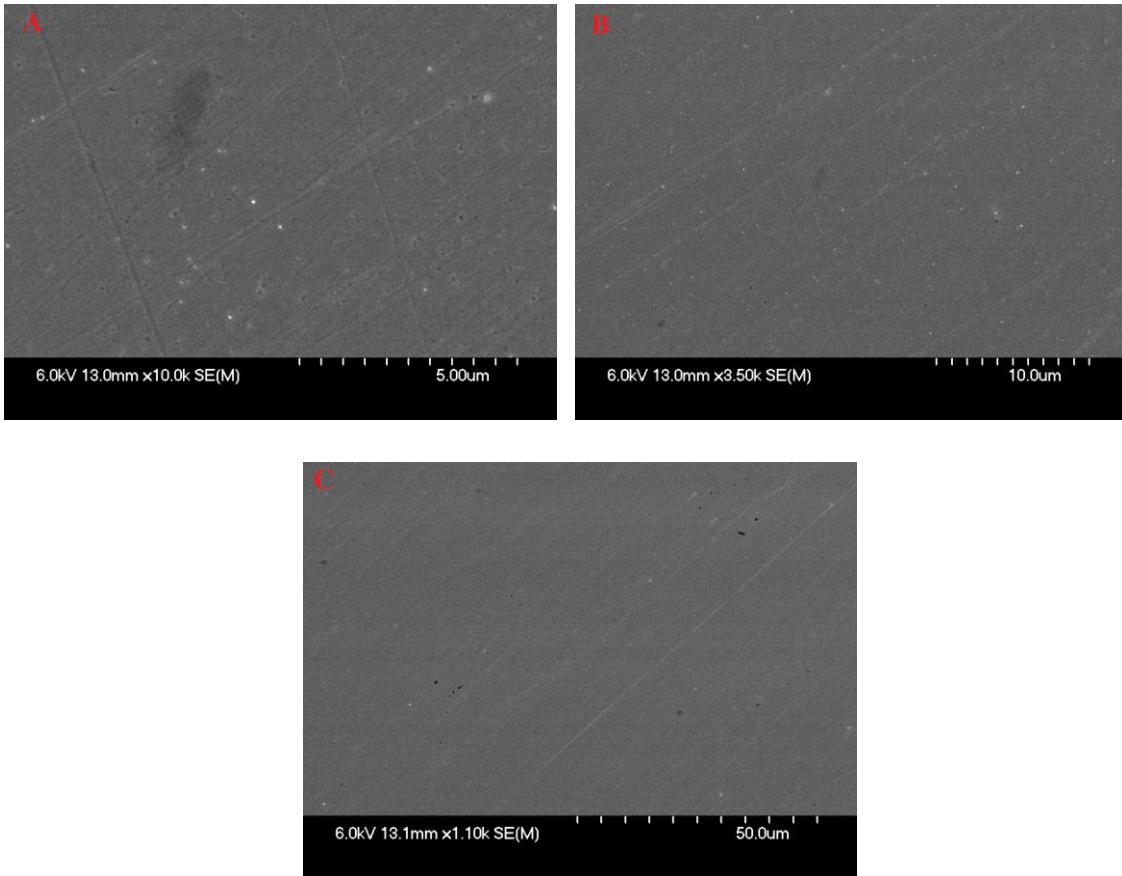


Figure 3.35: The SEM images of mirror like stainless steel, A) 5  $\mu\text{m}$ ;  
 B) 10  $\mu\text{m}$  and C) 50  $\mu\text{m}$ .

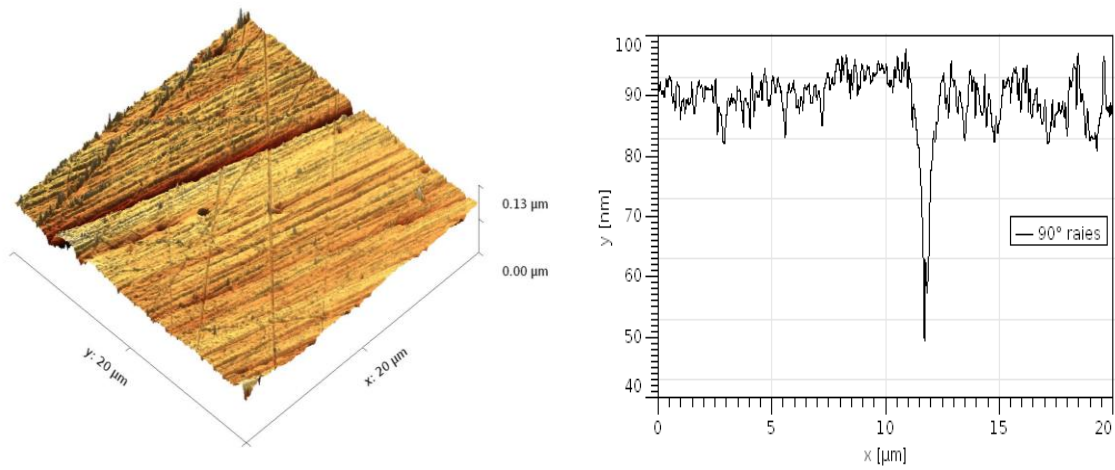


Figure 3.36: The AFM image of mirror like stainless steel, (a) 3D image,  
 (b) Profile chart

## ***5.2. Electropolishing***

Mechanical polishing or grinding is a good polishing method, but it has the disadvantage of hardening the surface, inducing a degree of residual tension and oxide incorporation, introducing scratch marks and damaged layers (Lee, 2000). On the other hand, chemical polishing does not induce surface tensions and removes the contaminations on the surface by chemical dissolution, promoting the smoothening of the surface, but at relatively slow rates. In electrochemical polishing, or electropolishing (EP), the dissolution rate of the metallic surface is significantly increased by the application of anodic currents (Tegart, 1959; Sheir et al., 1994).

The current stainless steel electropolishing process is performed worldwide on a commercial scale and is based on concentrated phosphoric acid and sulfuric acid mixtures.

The optical microscopic micrograph obtained for an electropolished steel sample (Figure 3.37) shows that the steel surface obtained is quite uniform and leveled, practically without any roughness whatsoever.

The morphologies of the raw material are also shown in Figures (3.29, 3.30, 3.31) for a comparison purpose. The comparison between samples before and after EP reveals the enhancement of surface uniformity after EP. Small scratches were eliminated and deep cavities were filled up.

The AFM images (Figure 3.38) shows the morphology of a 316L 2B stainless steel sheet with a low RMS value of 5 nm in area of 20\* 20  $\mu\text{m}$ .

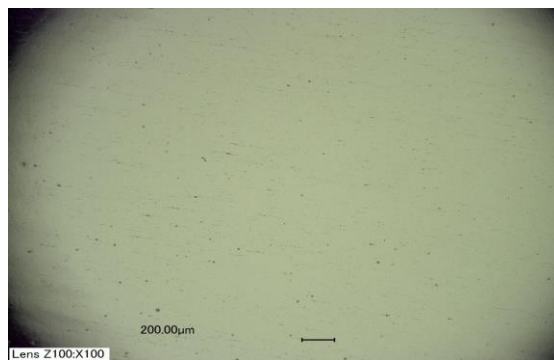


Figure 3.37: The optical microscopic photograph of electropolished stainless steel.

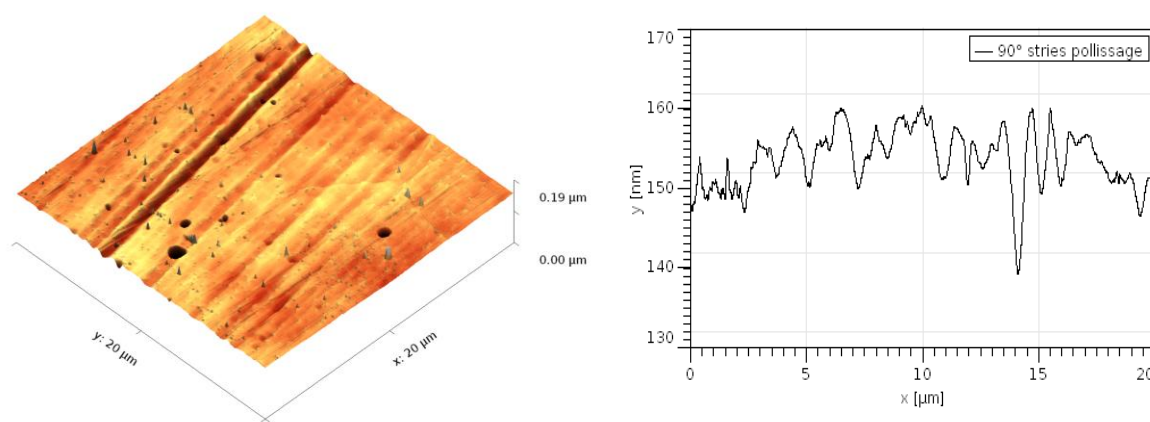


Figure 3.38: The AFM image of electropolished stainless steel, (a) 3D image, (b) Profile chart

## 6. Water Contact Angle and Surface Energy

WCAs of non-polished stainless steel (Ref.), polished with 1000 grade paper, mirror polished and electropolished surfaces were measured by sessile droplets of deionized water. The following WCAs were obtained:  $84 \pm 0.1$ ,  $80.1 \pm 1.06$ ,  $80.6 \pm 2.2$  and  $81.7 \pm 1.9^\circ$ , respectively. Surface energy measurements (by Van Oss method, solvents used were: deionized water, Diiodomethane and Formamide) were also carried out on the same samples, and the following results were obtained:  $1.7 \text{ mN m}^{-1}$ ,  $2.14 \text{ mN m}^{-1}$  and  $9.9 \text{ mN m}^{-1}$  and  $1.8 \text{ mN m}^{-1}$ , respectively.

Table (3.1): Water contact angles, surface energies and roughness values of plate surfaces.

Sample	WCA	$\gamma^{\text{Totale}}$ (Nm/m)	$\gamma^{\text{LW}}$ (Nm/m)	$\gamma^{\text{AB}}$	$\gamma^-$ (Nm/m)	$\gamma^+$ (Nm/m)	$R_a$ (nm)	$R_q$ (nm)
Ref.	84.0 ± 0.1	42.2	36.7	3.2	1.7	1.5	83.9 ± 21.1	106.3 ± 26.1
1000	80.1 ± 1.06	48	42.6	5.4	2.1	0.3	23.1 ± 5.2	28.9 ± 5.4
mirror like	80.6 ± 2.2	35.5	34.3	1.2	9.9	0	0.92 ± 0.28	1.5 ± 0.8
Electropolished	81.7 ± 1.9	42.7	38.5	3.2	1.8	1.5	7.5 ± 3.4	11.2 ± 7.5

### 7. Fouling Test

The following section describes the experimental results based on the pilot – test. Indeed, comparison of the weight of test plates were carried out before and after fouling experiments on each of the unpolished or polished plate to see the influence of the roughness on the fouling rate.

Looking at Figure 3.39, it can be observed that the percentage of fouling decreases for all polished samples compared to the reference steel plate. The best result is obtained for the mirror like sample, with decrease of 30% of the fouling amount (compared to the reference plate fouling) (Figure 3.39). As a consequence, this result confirms our theory developed in the precedent part. The lower roughness prevents the ACC particles of being trapped in the cavities and thus the fouling growth.

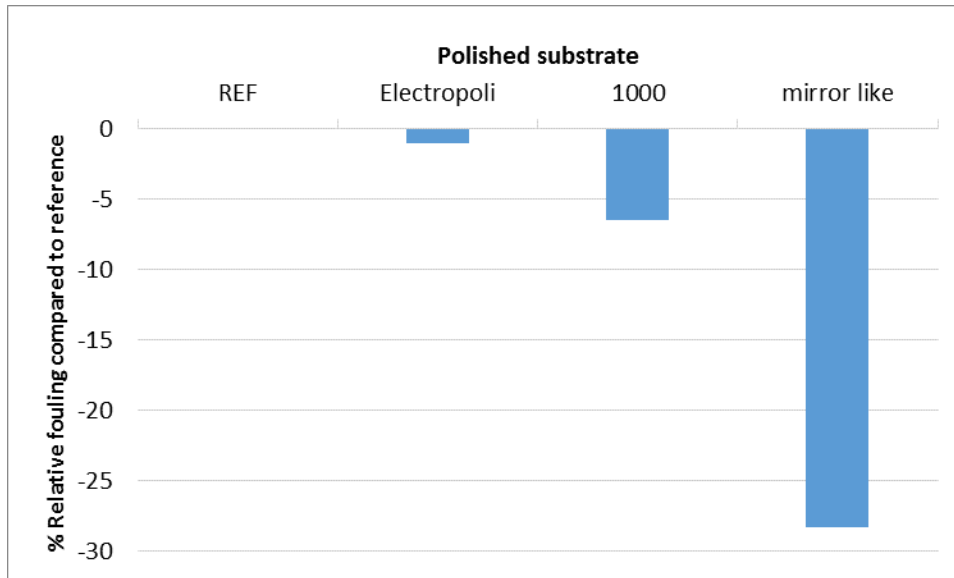


Figure 3.39: deposition masses on different plate surfaces (FM 2).

These results show that the fouling is generally decreased with the decrease of surface roughness. However, the decrease of fouling is not entirely correlated with roughness because the fouling on the electropolished sample does not decrease as much as expected.

The figure (3.40) show a clear relationship between the surface energy (the electron donor component,  $\gamma^-$ ) and the fouling mass deposited on the surface of the substrate.

The surface energy values showed a noticeable difference among the polished and non-polished surfaces. All of the polished surfaces showed a total surface energy higher than the non-polished surface. The electron donor component ( $\gamma^-$ ) of the surface energy has been reported as the most important factor in the interactions of fouling deposits (Andritsos et al., 2002; Rosmaninho and Melo, 2008; Rosmaninho et al., 2004). It was used to establish relationships between the mass of fouling deposits and the modification of surfaces.

As the electropolished sample has the same kind of value of surface energy than the reference (1.8 versus 1.7), it has the same kind of behavior and thus does not decrease the fouling as much as the other polished samples.

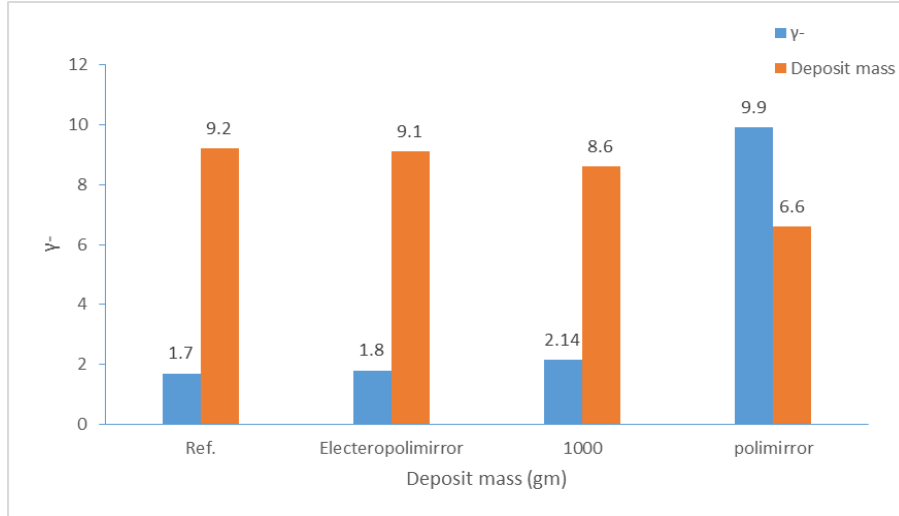


Figure 3.40: The relationship between the surface energy ( $\gamma^-$ ) and the fouling mass deposit on the plate surfaces.

Thus, surfaces with higher Ra values are believed to be of poorer antifouling quality. Hence, it could be anticipated that lower Ra values, resulting in smoother surfaces, would improve the antifouling characteristics. Then, it was also possible to observe that smooth surface with low surface energy improve the antifouling effect.

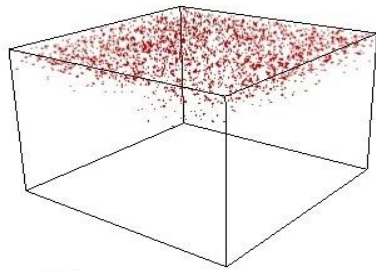
### 7.1. Initial deposition behavior

To better understand the effect of the surface mentioned earlier, a deeper analysis of the initial deposition phase on each surface was carried out by ToF-SIMS after 1 minute fouling.

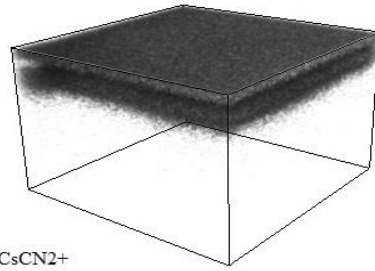
ToF-SIMS was carried out on these plates in the same conditions as previously. The main fragments detected were  $\text{CNCs}_2^+$  (fragment characteristic of the protein) and  $\text{Ca}^+$ . The 3D reconstructed

pictures obtained for  $\text{Ca}^+$  and  $\text{CNCs}_2^+$  ions from the burst alignment analysis are presented in fig. 3.41.

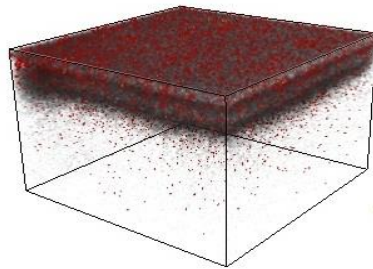
(A)



$\text{Ca}^+$

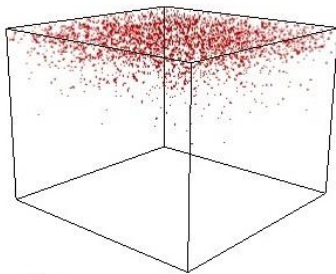


$\text{CsCN}_2^+$

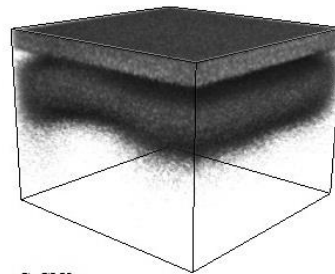


Overlay  $\text{Ca}^+$  and  $\text{CsCN}_2^+$

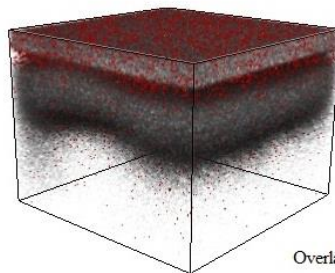
(B)



$\text{Ca}^+$



$\text{CsCN}_2^+$



Overlay  $\text{Ca}^+$  and  $\text{CsCN}_2^+$

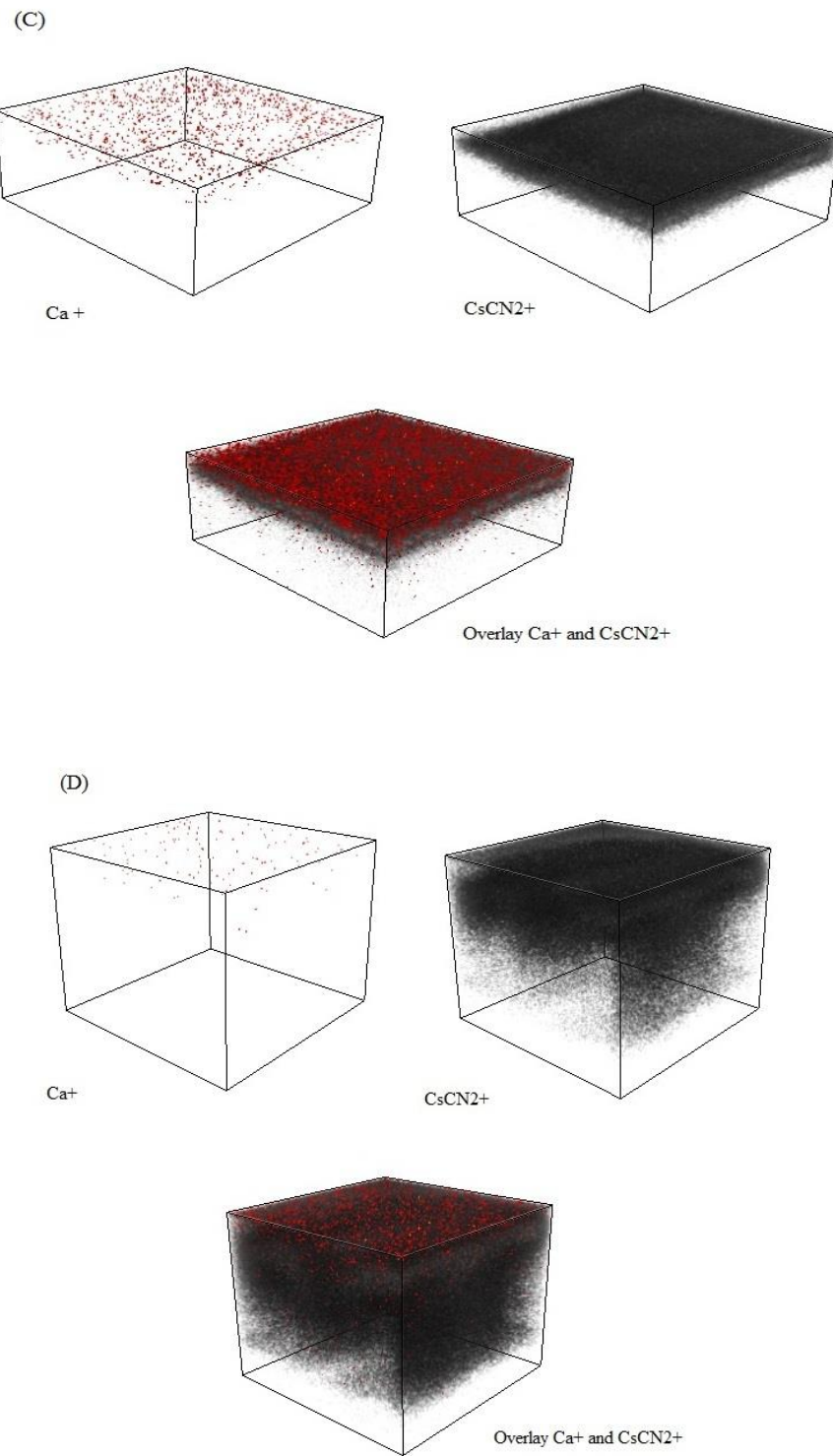
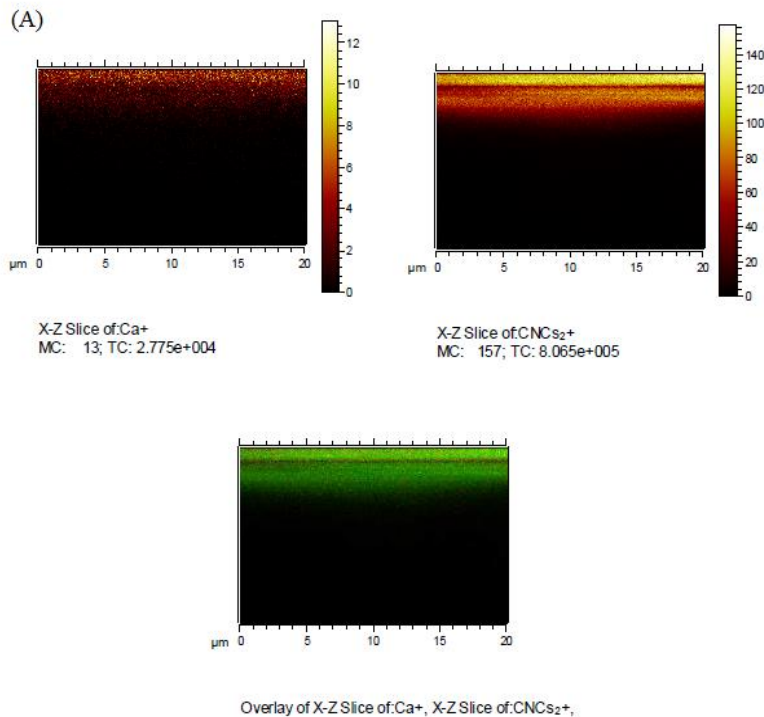
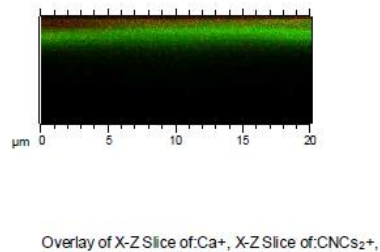
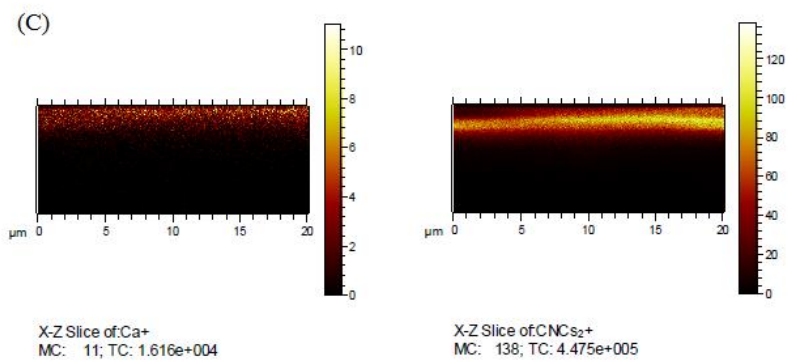
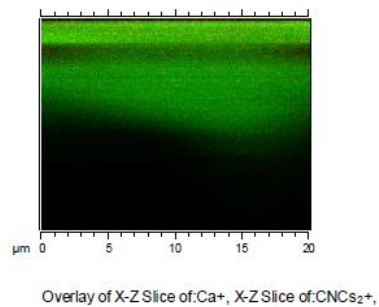
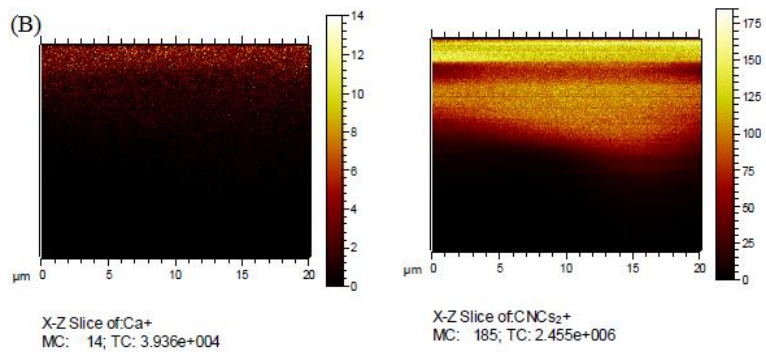


Figure 3.41: 3D images of ToF-SIMS (A) mirror polished, (B) Electropolished, (C) paper 1000, (D) Ref.

It is clear on those pictures that the protein is deposited quite homogeneously in significant amount on the surface, as well as inside the steel defects. The calcium is less present but appears at the same places than the protein.

We chose reconstructing the 2D pictures of  $\text{Ca}^+$ , and  $\text{CNCs}_2^+$  fragments on a cross-section of the fouling layer Figure 3.42. In all polished samples, the  $\text{Ca}^+$  ions are mostly concentrated in the upper part of fouling layer whereas  $\text{CNCs}_2^+$  ions are present. The result obtained for polished plates is different from the results obtained for the reference plate, where  $\text{Ca}^+$  was present everywhere, and particularly in the grain boundaries.





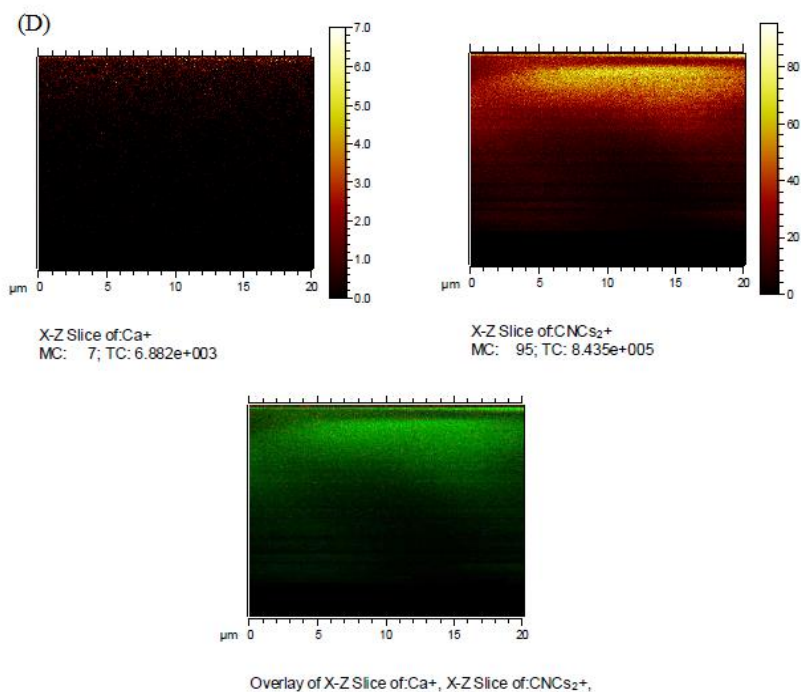


Figure 3.42: 2D images of ToF-SIMS (A) Mirror like, (B) Electromirror like, (C) 1000, (D) Ref.

For the four samples analyzed, the nature of the initial deposition was shown to be dependent on the surface state (roughness and surface energy). Generally, the surfaces having a lower roughness than the reference, and showing no grain boundaries, show less fouling due to a lower amount of ACC particles on the surface. Moreover, the surface having higher surface energy (mirror like) seems to be more prone to adhesion since they show an initial fouling layer composed by a higher number of smaller aggregates than the materials having lower surface energy properties. This result confirms the assumptions of [Rosmaninho and Melo, 2008](#). This type of phenomenon resembles the one described by the theory of heterogeneous nucleation ([Mullin, 1993](#)) and has been reported also by other authors concerning

calcium phosphate nucleation from pure mineral solutions (Wu & Nancollas, 1997, 1998).

Consequently, the first layer of deposition will have more or less adhesion strength depending on the nature of the surface. Taking into account the results of the amount of deposit formed after 2 hours deposition, it can be concluded that the nature of the surface will affect not only the nature of the initial fouling layer, but also the amount of the deposit that subsequently builds up.

|

## ***Conclusion***

The aim of this study was to evidence the growth mechanism of fouling layers obtained in heat exchangers in dairy industries. Two fouling solutions were used: one containing a low amount of calcium (30 ppm), the second one containing 120 ppm calcium.

In the first case, the smooth fouling layer obtained is due to the proteins. Calcium is only detected by ToF-SIMS inside the protein layer but no particles are visible using AFM. As the fouling solution is not saturated in calcium, this one ( $\text{Ca}^{2+}$ ) might be mostly chelated or trapped in the protein layer, without creating a particular roughness effect. The fouling growth mechanism in this configuration is quite simple: particles (size 60 nm) of denatured and unfolded proteins (mainly  $\beta$ -Lg) deposit on the steel plate and inside the grain boundaries in the first fouling seconds and accumulate on and in these places during fouling. After 2 hours some grain boundaries are totally filled in with the protein and the surface is completely covered with a homogeneous protein layer.

In the second case, the fouling layer is thick, white and rough. After 2 hours the fouling is present both on the surface and inside the grain boundaries: it thus creates strong anchorage points and this can explain why it is so difficult to further remove the fouling layer by cleaning. In this fouling configuration the calcium plays a major role. We evidenced by ToF-SIMS that the fouling was initiated by the unfolded protein (size of 60 nm) in the first seconds of exposition to the fouling solution. The unstable amorphous calcium carbonate nuclei (size 150-400 nm) formed in the tapwater at 90°C are stabilized and dredged by the unfolded proteins. They then precipitate preferentially in the steel roughnesses and grain boundaries, in which they

are mechanically trapped. The unfolded protein covers again these calcium particles, etc. This leads to a final thick arborescent growth structure.

We also showed that the nature of the initial deposition is dependent on the surface state (roughness and surface energy). The surfaces having a lower roughness than the reference, and showing no grain boundaries, show less fouling due to a lower amount of ACC particles on the surface. Moreover, the surface having higher surface energy (mirror like) seemed to be more prone to adhesion since they show an initial fouling layer composed by a higher number of smaller aggregates than the materials having lower surface energy properties. More details are shown in appendix 3 which summarizes the physical tests and chemical analysis carried up on each sample.

In the next parts of this study we will try to modify the surface of stainless steel by chemical or physical surface treatment in order to obtain antifouling coatings.

## ***References***

- Addadi L., Raz S., Weiner S. (2003). Taking Advantage of Disorder: Amorphous Calcium Carbonate and Its Roles in Biomineralization. *Advanced Materials*, 15, 959.
- Aizenberg J., Lambert G., Weiner S., Addadi L. (2002). Factors Involved in the Formation of Amorphous and Crystalline Calcium Carbonate: A Study of an Ascidian Skeleton. *J. Am. Chem. Soc.*, 124, 32.
- Ajikumar P.K., Wong L.G., Subramanyam G., Lakshminarayanan R., Valiyaveetil S. (2005). Synthesis and Characterization of Monodispersed Spheres of Amorphous Calcium Carbonate and Calcite Spherules. *Crystal Growth and Design*, 5, 1129.
- Bansal B. and Chen X. D. (2006). A Critical Review of Milk Fouling in Heat Exchangers. *Comprehensive Reviews in Food Science and Food Safety* 5 (2) 27.
- Blanpain-Avet P., Hédoux A., Guinet Y., Paccou L., Petit J., Six T. and Delaplace G. (2012). Analysis by Raman spectroscopy of the conformational structure of whey proteins constituting fouling deposits during the processing in a heat exchanger. *Journal of Food Engineering*, 110 (1) 86.
- Brecevic L., Nielsen A.E. (1989). Solubility of amorphous calcium carbonate. *J. Cryst. Growth*, 98, 504.
- Brownlow S., Cabral J.H.M., Cooper R., Flower D.R., Yewdall S.J., Polikarpov I., North A.C.T. and Sawyer L. (1997). Bovine beta-lactoglobulin at 1.8 Å resolution--still an enigmatic lipocalin. *Structure*, 5, 481.

- Carrotta R., Bauer R., Waninge R. and Rischel C. (2001). Conformational characterization of oligomeric intermediates and aggregates in  $\beta$ -lactoglobulin heat aggregation. *Protein Science*, 10, 1312.
- Changani S. D., Belmar-Beiny M. T. and Fryer P. J. (1997). Engineering and chemical factors associated with fouling and cleaning in milk processing. *Experimental Thermal and Fluid Science* 14 (4) 392.
- Croguennec T., Molle D., Mehra R. and Bouhallab S. (2004). Spectroscopic characterization of heat-induced non-native beta-lactoglobulin monomers. *Protein Science*, 13, 1340.
- Daufin, G., Labbé, J.P., Quemerais, A., Brulé, G., Michel, F., Roignant, M., Priol, M. (1987). Fouling of a heat exchange surface by whey, milk and model fluids. An analytical study. *Le Lait*, 67, 339.
- Falini G., Albeck S., Weiner S., Addadi L. (1996). Control of Aragonite or Calcite Polymorphism by Mollusk Shell Macromolecules. *Science*, 271, 67.
- Goodwin A.L., Michel F.M., Phillips B.L., Keen D.A., Dove M.T., Reeder R.J. (2010). Nanoporous Structure and Medium-Range Order in Synthetic Amorphous Calcium Carbonate. *Chemistry of Materials*, 22, 3197.
- Hernandez-Hernandez A., Gomez-Morales J., Rodriguez-Navarro A.B., Gautron J., Nys Y., Garcia-Ruiz J.M. (2008). Identification of some active proteins in the process of hen eggshell formation. *Cryst. Growth Des.*, 8, 4330.
- Jimenez M., Hamze H., Allion A., Ronse G., Delaplace G. and Traisnel M. (2012) Antifouling stainless steel surface: Competition between roughness and surface energy. *Materials Science Forum*, 706-709 2523.

- Jones B., Peng X. (2012). Amorphous calcium carbonate associated with biofilms in hot spring deposits. *Sedimentary geology*, 269-27058.
- Kawano J., Shimobayashi N., Kitamura M., Shinoda K., Aikawa N. (2002). Formation process of calcium carbonate from highly supersaturated solution. *Journal of Crystal Growth*, 237, 419.
- Kontrec J., Kralj D., Brečević L., Falini G. (2008). Influence of some polysaccharides on the production of calcium carbonate filler particles. *Journal of Crystal Growth*, 310, 4554.
- Lakes R.S. (1993). Materials with structural hierarchy. *Nature*, 361, 511.
- Lasaga A.C. (1998). *Kinetic theory in the earth sciences*, Princeton University press, Princeton N.J.
- Loste E., Wilson R.M., Seshadri R., Meldrum F.C. (2003). The role of magnesium in stabilizing amorphous calcium carbonate and controlling calcite morphologies. *Journal of Crystal Growth*, 254, 206.
- Mann S. (2001). *Biom mineralization: Principles and Concepts in Bioinorganic Materials Chemistry*, Oxford University Press, New York.
- Mann S. (1993). *Biom mineralization: the hard part of bioinorganic chemistry*. *J. Chem. Soc., Dalton Trans.*, 1, 1.
- Mantus D.S., Ratner B.D., Carlson B. A., Moulder J. F. (1993). Static secondary ion mass spectrometry of adsorbed proteins. *Anal. Chem.*, 65, 1431.
- Meldrum F.C. and Cölfen H. (2008). Controlling mineral morphologies and structures in biological and synthetic systems. *Chemical Reviews*, 108, 4332.
- Meiron O.E., Bar-David E., Aflalo E.D., Shecter A., Stepensky D., Berman A., Sagi A. (2011). Solubility and bioavailability of stabilized

- amorphous calcium carbonate. *Journal of Bone and Mineral Research*, 26(2), 364.
- Mullin, J. W. (1993). *Crystallization* (3rd ed.). London, UK: Butterworths.
- Njegić-Džakula B., Falini G., Brečević L., Stoko Ž., Kralj D. (2010). Effects of initial supersaturation on spontaneous precipitation of calcium carbonate in the presence of charged poly-l-amino acids. *Journal of Colloid and Interface Science*, 343, 553.
- Omanovic S. and Roscoe S. G. (2000). Interfacial Behavior of  $\beta$ -Lactoglobulin at a Stainless Steel Surface: An Electrochemical Impedance Spectroscopy Study. *Journal of Colloid and Interface Science*, 227 (2) 452.
- Rosmaninho R. and Melo L. F. (2007). Effect of proteins on calcium phosphate deposition in turbulent flow as a function of surface properties. *Experimental Thermal and Fluid Science* 32 (2) 375.
- Relkin P. and Mulvihill D. M. (1996). Thermal unfolding of  $\beta$  - lactoglobulin,  $\alpha$  - lactalbumin, and bovine serum albumin. A thermodynamic approach. *Critical Reviews in Food Science and Nutrition*, 36, 565.
- Rodriguez-Blanco J.D., Shaw S., Benning L.G. (2011). The kinetics and mechanisms of amorphous calcium carbonate (ACC) crystallization to calcite, *viavaterite*. *Nanoscale*, 3, 265.
- Rosmaninho R. and Melo L. F. (2008). Protein-calcium phosphate interactions in fouling of modified stainless steel surfaces by simulated milk. *International Dairy Journal* 18 (1) 72.
- Rosmaninho R., Santos O., Nylander T., Paulsson M., Beuf M., Benezech T., Yiantsios S., Andritsos N., Karabelas A., Rizzo G., Müller-Steinhagen H. and Melo L. F. (2007). Modified stainless steel surfaces

- targeted to reduce fouling – Evaluation of fouling by milk components. *Journal of Food Engineering* 80 (4) 1176.
- Santos O, Nylander T, Rosmaninho R, Rizzo G, Yiantsios S, Andritsos N, Karabelas A, Müller-Steinhagen H, Melo L, Boulangé-Petermann L, Gabet C, Braem C, Trägårdh C, Paulsson M. (2004). Modified stainless steel surfaces targeted to reduce fouling—surface characterization. *J Food Eng* 64:63–79.
- Sikes C.S., Wheeler A.P. (1988), biopolymers from biominerals as regulators of mineralization. *Chemtech*, 18, 620.
- Smits P. and Vanbrouwershaven J.H. (1980). Heat-induced association of beta-lactoglobulin and casein micelles. *Journal of Dairy Research*, 47, 313.
- Tester C.C., Brock R.E., Krejci M.R., Weigand S., Joester D. (2011). In vitro synthesis and stabilization of amorphous calcium carbonate (ACC) nanoparticles within liposomes. *Cryst. Eng. Comm.*, 13, 3975.
- Xie J., Riley C. and Chittur K. (2001). Effect of albumin on brushite transformation to hydroxyapatite. *Journal of Biomedical Materials Research*, 57, 357.
- Wu, W., and Nancollas, G. H. (1997). Nucleation and crystal growth of octacalcium phosphate on titanium oxide surfaces. *Langmuir*, 13, 861–865.
- Wu, W. J., and Nancollas, G. H., (1998). Crystallization kinetics of calcium phosphates on anatase and rutile surfaces. *Journal of Dental Research*, 77, 111.

- Xu X., Cai A., Liu R., Pan H., Tang R., Cho K. (2008). The roles of water and polyelectrolytes in the phase transformation of amorphous calcium carbonate. *Journal of Crystal Growth*, 310, 3779.
- Xu X., Han J.T., Cho K. (2005). Deposition of amorphous calcium carbonate hemispheres on substrates. *Langmuir*, 21, 4801.
- Yoon J., Lund D.B. (1994). Magnetic treatment of milk and surface treatment of plate heat exchangers: effect on milk fouling. *J Food Sci* 59(5):964–9, 980.
- Zhang S., Gonsalves K.E. (1998). Influence of the Chitosan Surface Profile on the Nucleation and Growth of Calcium Carbonate Films. *Langmuir*, 14, 6761.

## ***CHAPTER FOUR***

### ***DEVELOPMENT OF ANTI-FOULING COATINGS***

- *Physical method by atmospheric pressure plasma*
- *Chemical method by Sol-Gel technics*

## ***1. Introduction***

The unavoidable attachment and adhesion of fouling components to the surface during the thermal food processing is influenced by the interaction between heat transfer surface and process fluid.

One approach to reduce fouling and to increase the removal of formed deposits is the defined modification of the energetic and topographic surface properties.

To reduce milk fouling deposition on processing surfaces, various techniques such as modification of processing parameters, addition of fouling inhibiting chemicals and modification of processing equipment design have been studied ([Belmar-Beiny et al., 1993](#); [Bradley and Fryer, 1992](#); [Chen et al., 2004](#); [Delplace et al., 1994, 1997](#); [Elofsson et al., 1997](#); [Jeurnink et al., 1996](#); [Visser and Jeurnink, 1997](#)). Since alteration in the processing parameters and addition of fouling inhibiting chemicals may affect product quality, nutritional and functional properties and legal requirements ([Müller-Steinhagen, 1998](#)), they cannot be modified easily. Hence, alteration in one or more of surface properties of the processing surface, such as surface roughness, free surface energy, surface chemistry and/or topography is one possible technique to mitigate milk fouling with potentially less impact on process conditions or product quality. Surface properties can be altered by a number of different surface modification techniques, such as deposition of a coating through physical or chemical vapour deposition, electroplating or by ion implantation, DLC (diamond-like carbon), Silica, SiOX, Ni-P-PTFE, Excalibur\_ and Xylan\_ coating, as well as SiF<sup>+</sup> and MoS<sub>2</sub> ion implantation were analyzed. No significant difference

regarding fouling mitigation was found between unmodified and modified stainless steel.

Amongst the techniques that have been used to mitigate organic and or inorganic fouling, the latter coatings are preferred due to their non-toxic properties and relative ease of application (Choi et al., 2007; Stein et al., 2003). Their “fouling release” ability is based on a non-stick surface which exhibits self-cleaning properties with a sufficient flow of fluid over the surface.

Siloxanes and fluoropolymers exhibit low surface energy, characterized by high contact angles which reduce wettability and thus the molecular interaction between the fouling and the surface (Malayeri et al., 2009; Stein et al., 2003). Hydrophobic coatings such as polydimethyl siloxane, (PDMS) and hydrophilic coatings such as polyethylene glycol (PEG), have previously been suggested to reduce intermolecular interactions; as a result of their low (PDMS) and high (PEG) surface energies respectively (Krishnan et al., 2008).

The anti-fouling studies were largely focused on mixed fluoropolymer and siloxane polymers as these have demonstrated superior mechanical properties compared with polymer coatings deposited using the individual monomers (Nwankire et al., 2010). It has also been demonstrated previously that the addition of tetraethylorthosilicate (TEOS) into siloxanes can enhance the coating adhesion to steel substrates (Nwankire et al., 2009). In this study coatings will be deposited using atmospheric pressure plasma coatings.

➤ *Physical method by atmospheric pressure plasma*

**2. Effect of Stainless Steel Pre-treatment on Its Surface Energy**

The surface modification is used to create a high degree of adhesion property between the surface of material and the coating film without affecting the overall mechanical properties of the material.

In the first set of experiments, the surface pre treatments were performed using N<sub>2</sub> and clean and dry air as reactive gases. To determine the optimal processing condition, the experiments were carried out using various values of torch-to-sample distance and number of passes. The influence of aging was investigation as well.

**2.1. Effect of the distance between plasma source and substrate**

In order to determine the most effective plasma pre-treatment for stainless steel, the effect of distance between the plasma source and substrate was first investigated in terms of water contact angle (WCA) and surface energy. The reference water contact angle (WCA) is the WCA of the stainless steel plate before any treatment, i.e. 56.4°. Figure 4.1 shows the various water contact angles plotted versus distance between the plasma source and substrate. It shows that the hydrophilic properties of the surface increase when distance plasma-substrate decreases whatever the gas used. The best results are obtained for N<sub>2</sub> (70° at 4 cm to 33° at 2 cm) which means that the WCA reached the minimum value at distance of 2 cm. The pretreated stainless steel becomes more hydrophilic than the stainless steel without pretreatment. We can thus conclude that when the distance between the plasma source and substrate is too high, the plasma flame is hardly able to touch the surface of the substrate, and thus no significant influence on the contact angle is observed.

Thus the surface hydrophilicity of stainless steel can be significantly improved with atmospheric plasma treatment. Indeed, the high energy particles in the plasma lead to the formation of activated sites on the stainless steel (like activated oxygen and nitrogen species sites).

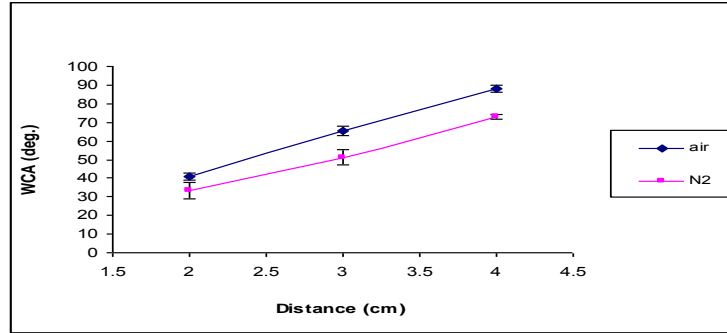


Figure 4.1: Effect of distance on water contact angle

## 2.2. Effect of Aging time:

In industrial applications, taking into account aging of samples is important. Plasma treatments have usually a short time effect and samples have to be used rapidly after treatment. A long time exposure to air could often lead to reverse effect (Dowling et al., 2009). Thus, the influence of time on the WCA (Figure 4.2) was studied. No real changes occur for both plasma treatments (air and N<sub>2</sub>) (after 5, 10 and 60 mn), so it is possible to conclude that the surface state remains stable for at least 60 mn and to have good adhesion, it should be necessary to coating just after the activation.

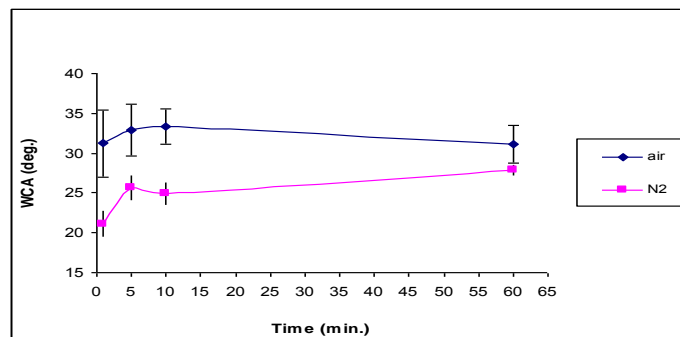


Figure 4.2: Aging time effect on water contact angle.

### 2.3. Effect of the number of passes

The most effective distance to obtain a hydrophilic surface was found to be 2 cm. Thus, this condition was used to try to find out if successive treatments could even more affect the surface of the samples. To study the effect of the number of passes on the surface energies of the samples, six consecutive passes were made at 100 mm/s at a distance of 2 cm between the source and the substrate. Figure (4.3) shows the WCA results. The WCA reaches its minimum values after the 5<sup>th</sup> and the 4<sup>th</sup> passage for plasma treatment with air (20°) and nitrogen (13°) respectively. The number of passes improves the hydrophylicity of the stainless steel surface.

Consequently, we chose the conditions of the surface pre-treatment as follow: distance 2 cm, 5 passages for plasma treatment with air and 4 passages for plasma treatment with nitrogen.

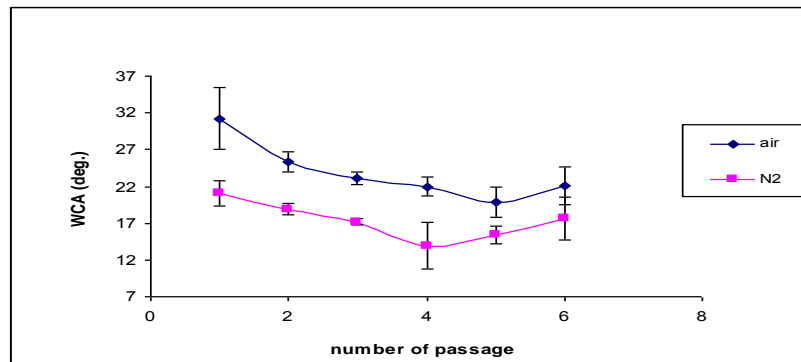


Figure 4.3: effect of the number of passes on the water contact angle

### ***3. Antifouling Efficiency of the Different Coating***

#### ***3.1. Plasma Coating***

##### ***3.1.1. Fluorosilane based precursor***

The precursor mixtures investigated were:

- Perfluorooctyltriethoxysilane ( $C_{14}H_{19}F_{13}O_3Si$ ) PS with Tetraethylorthosilicate ( $C_8SiH_{20}O_4$ ) TEOS,
- Tetramethylcyclotetrasiloxane ( $C_4Si_4H_{16}O_4$ ) TC with TEOS,
- TC with PS,
- PS with Hexamethyldisiloxane ( $(CH_3)_3SiOSi(CH_3)_3$ ) HMDSO,
- PS/TC with HMDSO
- PS/TC/HMDSO with TEOS.

The coating mixtures were obtained by mixing 50/50 by volume of the two precursors.

The PS/TC/HMDSO coating has the highest water contact angle of  $133^\circ$ . The PS/TC, PS/HMDSO, TC/HMDSO. PS/TC/HMDSO and PS/TC/HMDSO/TEOS coatings are hydrophobic with water contact angles above  $90^\circ$ .

The antifouling performances of the coatings were evaluated with the pilot-plant tests and results are presented in Figure 4.4. It is noticeable that the TC, PS/HMDSO, TC/HMDSO and the PS/TC/HMDSO/TEOS surfaces show less deposit formation than the unmodified surface, while the other surfaces promoted the formation of more deposit than the unmodified stainless steel.

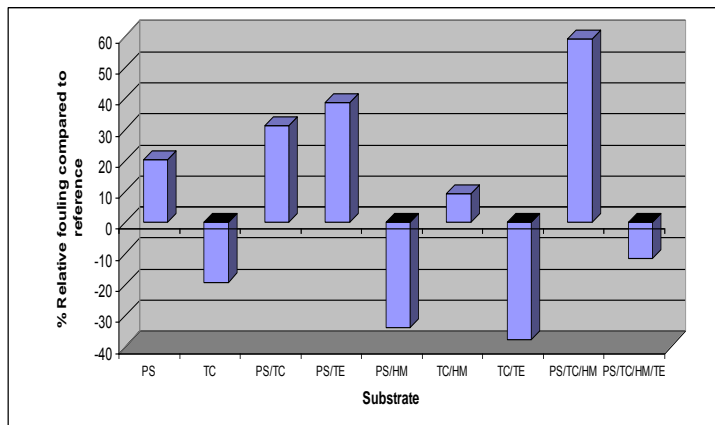


Figure 4.4: Pilot-plant fouling tests results for fluorosilane based precursor.

It can be seen from figure (4.4) that the fouling test results of fluorosilane based precursor substrates were in most cases in the positive side, which means that the fouling masses on the modified surfaces were higher than on the unmodified stainless steel surface. The fouling results were not encouraging; however, based on the literature survey we chose the silicon based products as precursor.

### 3.1.2. Silicon based precursor

The precursors investigated were:

- Hexamethyldisiloxane ( $((\text{CH}_3)_3\text{SiOSi}(\text{CH}_3)_3)$  HMDSO,
- Tetramethyldisiloxane ( $[(\text{CH}_3)_2\text{SiH}]_2\text{O}$ ) TMDSO,
- Hexamethyldisilazane ( $((\text{CH}_3)_3\text{SiNHSi}(\text{CH}_3)_3)$  HMDS,
- Tetraethyl orthosilicate  $\text{Si}(\text{OC}_2\text{H}_5)_4$  TEOS
- Methyltrimethoxysilane  $(\text{CH}_3\text{Si}(\text{OCH}_3)_3)$  MTES.

These precursors were deposited on stainless steel substrates. All the obtained coatings are hydrophobic; indeed, the water contact angles were all above  $90^\circ$ .

The fouling test carried out on the different modified surfaces and compared to the unmodified one, allows to conclude that the HMDSO, HMDS, MTES, DMP/HM, Phos./HM and the TTMSP/HM surfaces showed less fouling than the others which promoted the formation of more deposit than the unmodified stainless steel.

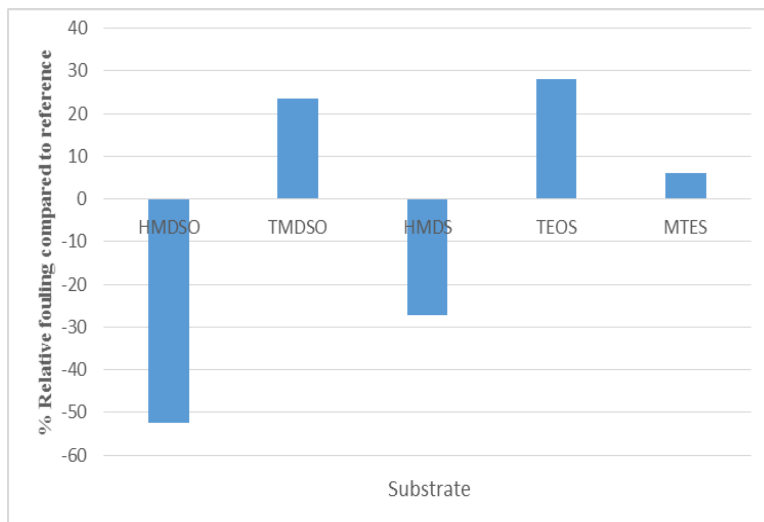


Figure 4.5: Pilot-plant fouling tests results for silicon based precursor.

The HMDSO results shows the best and more repeatable antifouling result, and for this reasons we will focused on this product as the main precursor to get an antifouling coating layer on the surface of stainless steel.

### ***3.1.3. HMDSO Coatings***

The HMDSO precursor was deposited at a flow rate of (8L/min.), a distance plasma-substrate of (2 cm) and a plasma source speed of (100 mm/s), after an activation step. By varying the gases used for

activation, as well as the plasma and carrying gases, six different experiments were carried out (Table 4.1).

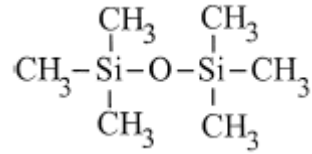


Figure 4.6: The structure of hexamethyldisiloxane (HMDSO).

The activation conditions were the following ones: 5 passes using air or 4 passes using nitrogen, both at 100 mm/s and a distance plasma-substrate of 2 cm.

Table 4.1: Plasma coating gas condition using HMDSO

Activation (60L/min.)	Coating (60L/min.)	Gas carrier (8L/min.)	symbol
Air	Air	Air	AAA
Air	Air	N2	AAN
Air	N2	N2	ANN
Air	N2	Air	ANA
N2	N2	N2	NNN
N2	Air	Air	NAA

From the Figure (4.7), we can see that the highest WCA (103°), which correspond to a surface energy of 23.4 (mN/m<sup>2</sup>), is obtained when nitrogen is used both as activation, precursor and carrying gas (NNN conditions).

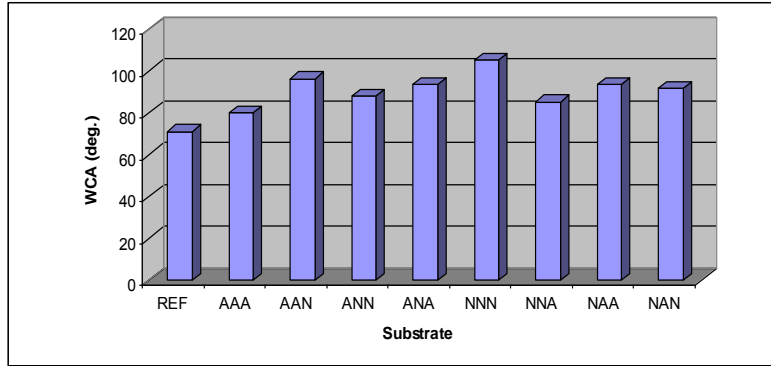


Figure 4.7: The water contact angle versus plasma coating experiment.

The roughness properties of plasma treated surfaces are directly related to the chemical and physical reactions which take place during the treatment process.

In this study, the surface roughness characteristics of the treated 316L 2B stainless steel were investigated using profilometry.

The surface roughnesses of the untreated substrate are ( $R_a=97.13$ ,  $R_q=126$ ) nm. The roughness  $R_a$  and  $R_q$  (table 4.2) of the samples after coating have also been evaluated and most of them have a lower roughness.

Table 4.2: The values of roughness and surface free energy for the different plasma coatings.

Symbol	$R_a$ (nm)	$R_q$ (nm)	Surface free energy ( $mN/m^2$ )
AAA	28.6	37.7	22
AAN	394.4	481.8	26.6
ANN	91.1	114.1	32.9
ANA	354.3	433.9	23.5
NNN	84.2	108.8	23.4
NNA	61.8	81.3	25.2
NAA	84.08	107.1	28.3
NAN	80.3	102.4	27.6

### 3.1.3.1 Surface characterization of HMDSO coatings

In the manuscript, the surface characterizations are presented only for one sample, the NNN coating, but they were carried out on all samples.

#### 1. AFM

The AFM image of HMDSO coating deposited using the condition NNN is given in Figure (4.8). This picture demonstrates that the coating exhibits a nano-textured (needle-like) morphology, which is most likely due to precursor fragmentation and gaseous phase reactions in the plasma. The WCA measured is  $102^\circ$ , the coating surface free energy is ( $22 \text{ mN/m}^2$ ), while  $R_a$  and  $R_q$  are estimated at  $84.2 \text{ nm}$  and  $108.8 \text{ nm}$ , respectively.

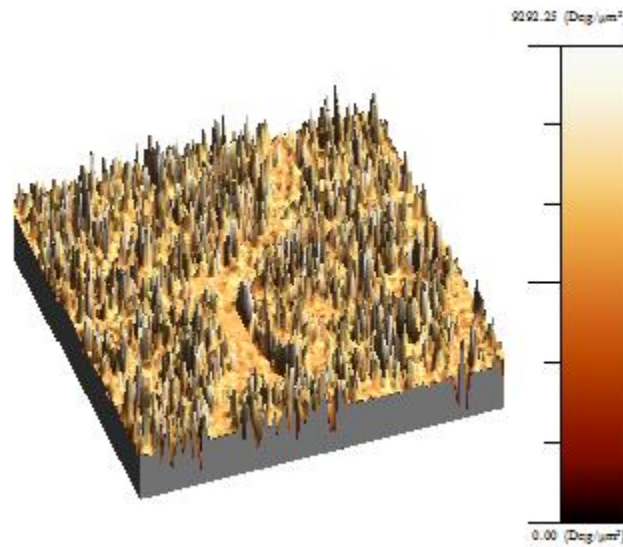


Figure 4.8: AFM image of HMDSO coating.

This morphology has been shown in a previous work of our lab to decrease the fouling deposition rate ([Jimenez et al., 2012](#)).

## 2. ToF-SIMS

HMDSO coatings (NNN sample) were analyzed by ToF-SIMS (see depth profiles in Figure 4.9). The distributions of  $\text{Si}^+$ ,  $\text{Fe}^+$ ,  $\text{Cr}^+$  and  $\text{SiO}$  ions, measured with the time of flight spectrometer are plotted versus the  $\text{Cs}^+$  ion sputtering time. In the recorded profiles, two regions were identified. The first period corresponds to the intensity of  $\text{Si}^+$ ,  $\text{SiOCs}^+$  and  $\text{Cs}_2\text{O}^+$  ions. This part of the profile corresponds to the plasma coating itself. Above 320 s of sputtering (2nd period), the  $\text{Si}^+$ ,  $\text{SiOCs}^+$  and  $\text{Cs}_2\text{O}^+$  signals start to decrease, while the  $\text{CsFe}^+$  and  $\text{CsCr}^+$  signals strongly increase, showing the transition from the plasma-deposited film to the steel surface oxide layer.

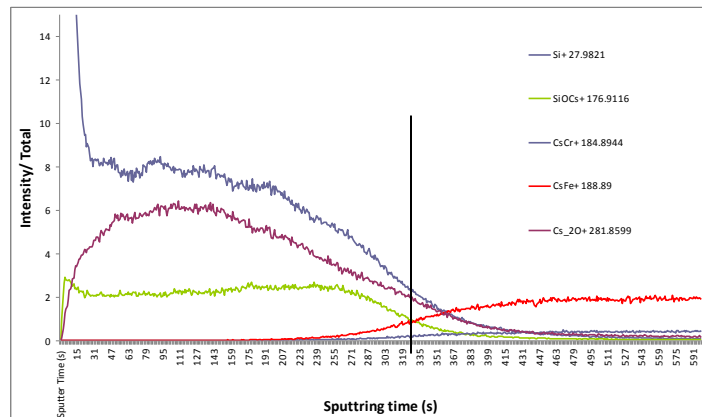


Figure 4.9: ToF-SIMS sputtering depths profiles of the HMDSO coating.

## 3. XPS

XPS was used to determine the elemental composition of the HMDSO coatings (Table 4.3).

Table 4.3: The XPS elemental analysis of the HMDSO coating.

Quantification				
Element	binding energy (eV)	RSF	FWHM (eV)	%Atomic
C 1s	285,0	0,278	1,9	23,3
Si 2p	103,7	0,328	2,3	26,6
O 1s	533,2	0,78	2,0	50,0

The survey spectrum recorded for HMDSO coatings is presented in Figure (4.6). It reveals the presence of three elements: Si, O and C.

Analyses were performed by looking at the chemical environment of Si2p and C1s detected in the coatings. Figure (4.10) shows the XPS spectra of C1s and Si2p for the HMDSO coating. By decomposing these peaks, we found that the C1s signal, reported in Figure 4.10a, included the contributions of C-C bonds (285.0 eV) resulting from plasma decomposition/polymerization of the HMDSO precursor and probably from CH<sub>3</sub> initially present in HMDSO. The broad O1s signal contained contributions of organic silicon compounds (533.2 eV) and/or probably metal oxide (Figure 4.10c). The Si2p spectra for HMDSO coatings presented a signal at 103.7 eV (Figure 4.10b).

HMDSO silicon atoms has 2 to 6 atoms and 1 oxygen, and the atomic ratios are respectively measured by XPS  $C / Si = 0.9$  and  $O / Si = 1.9$ .

The binding energies of Si2p peak (103.7 eV) and O1s (533.2 eV) and the  $O / Si = 1.9$ , It is observed that only contribution to the O1s, Si2p and C1s spectra. We can conclude from these results that we have the presence of a layer of SiO<sub>2</sub> and that the coatings are mainly organosilicon-like, with a combination of organic R<sub>2</sub>SiO<sub>2</sub> compound.

The iron is not detected, indicating that the SiO<sub>2</sub> layer is thick enough (> 10 nm) to cover the stainless steel surface.

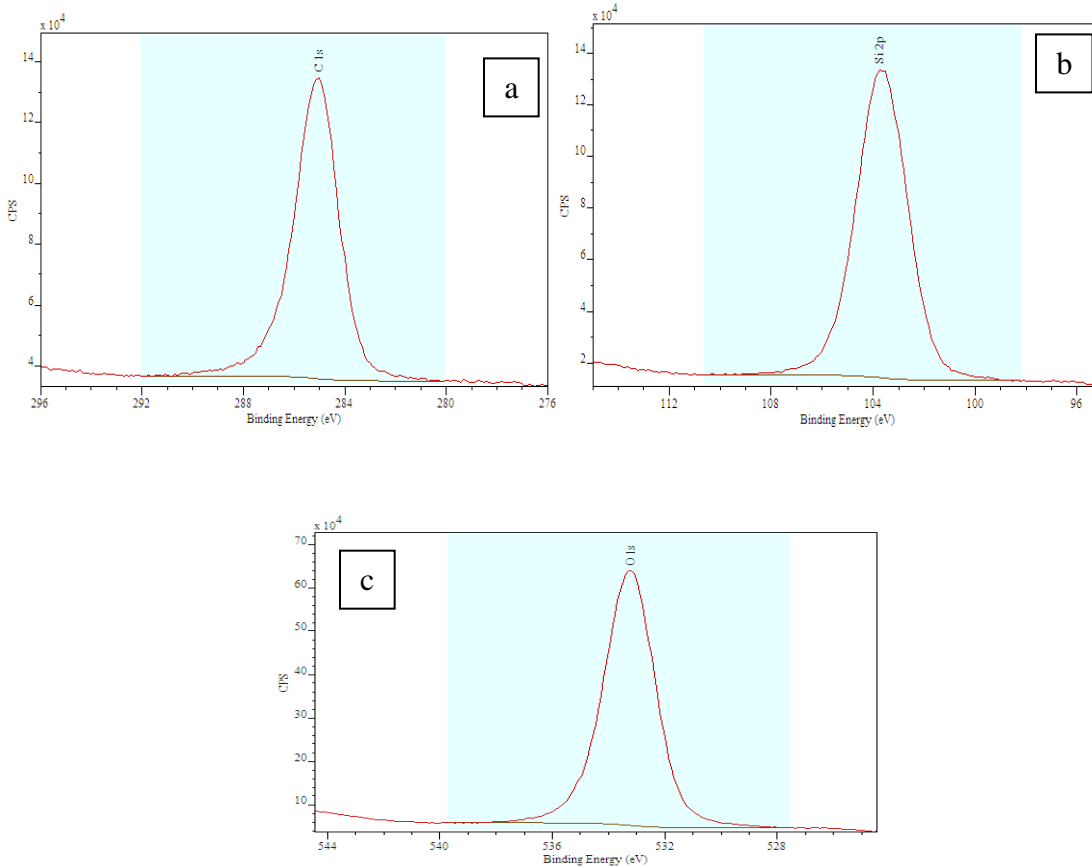


Figure 4.10: XPS (a). C1s, (b). Si 2p and (c) O1s spectra from HMDSO plasma coating.

### 3.1.3.2 Small Scale Fouling Test

Before carrying the pilot plant fouling test, fouling tests using the home made lab scale test (in static conditions) were carried out. The results of this quantitative fouling test are given in Figure (4.11). As demonstrated in this figure there was a significant reduction of fouling with HMDSO coated surfaces compared to the uncoated stainless steel. The best reduction is obtained for the NNN treatment (-95 %).

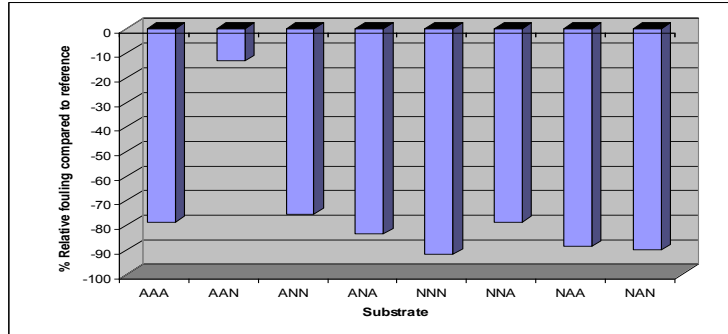


Figure 4.11: Small scale fouling test results.



Figure 4.12: The HMDSO coating substrates after Laboratory fouling test.

These deposits could not be washed off from the stainless steel plates by simple rinsing with water, but they could be removed rather easily by mechanical means after being dried and leaving the adhering initial fouling layer on the substrate (Figure 4.12).

### ***3.1.3.3. Pilot-Plant Test with Fouling Model Fluid***

In order to better simulate the industrial conditions, experiments were then carried out in the pilot-plant. Figure (4.13) show the results of this fouling test.

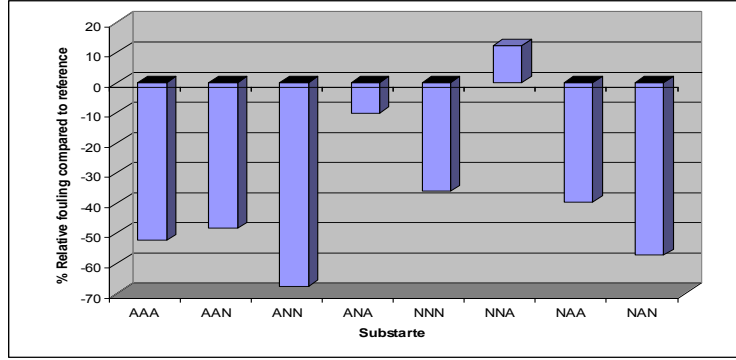


Figure 4.13: Pilot-plant fouling test for HMDSO coatings.

We can see that the two tests do not correlate, the amount of fouling obtained are not the same than those obtained before. Indeed, the two tests are not the same; one is in static condition and the other in dynamic condition. Thus, it can induce different in the deposition behaviors of the fouling. However, in both cases, the amount of fouling is reduced. In this test, the ANN experiment gives the less fouling (-65%).

Figure (4.14) shows the fouling layer on the surface of HMDSO coated stainless steel, the corresponding microanalyses images show a peak of Si, which prove the presence of the coating layer. The Figure (4.15) shows the coated surface after fouling cleaned with NaOH solution. After cleaning, only areas with a remaining HMDSO layer can be found with surface microanalysis on the stainless steel surface.

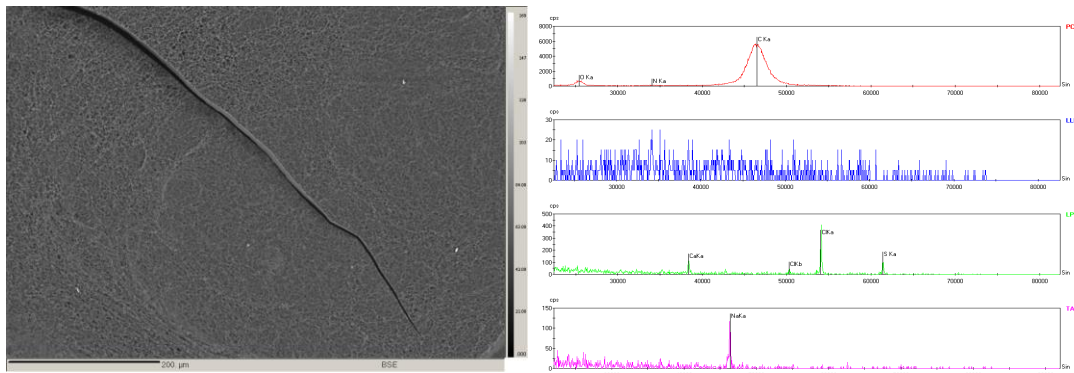


Figure 4.14: EPMA image and chart analyses of fouling on the uncoated stainless steel.

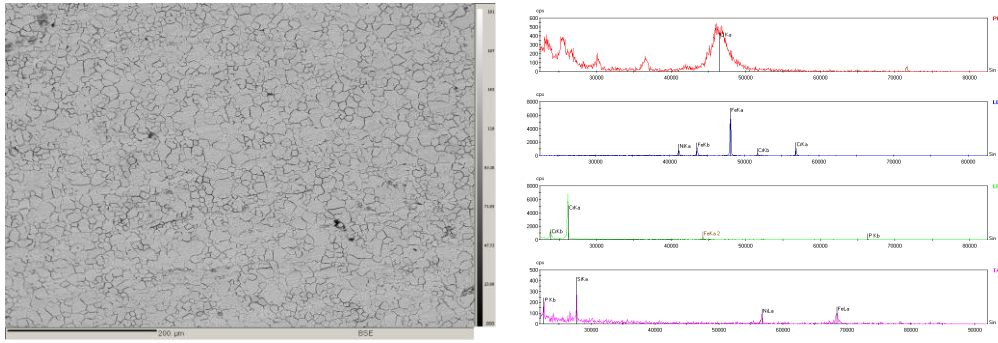


Figure 4.15: EPMA image and chart analyses of fouling on the HMDSO coated stainless steel.

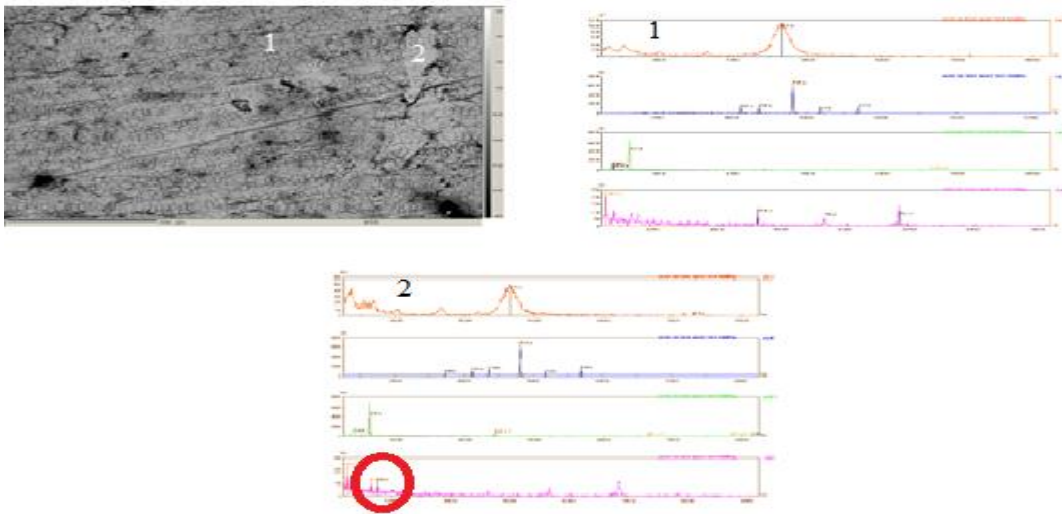


Figure 4.16: EPMA image and chart analyses of HMDSO coated stainless steel after cleaning with NaOH solution.

This results show that unfortunately the coating layer is mostly removed after having washed the plates with the cleaning solution. It indicates that the interactions between the surface of stainless steel and the coating layer were not strong enough to overcome the standard industrial cleaning process. For this reason, we used an oxalation pretreatment on the surface of stainless steel before the plasma atmospheric pressure or sol-gel coatings.

#### 4. Roughness Effect

The average values of surface roughness for the unmodified (Reference sample) and modified surfaces are presented in Table (4.5).

The morphology of the coatings was examined using a profilometer. The average roughness ( $R_a$ ) and root-mean square roughness ( $R_q$ ) values were obtained from 3 scans of the coated and uncoated surfaces. The unmodified surface (Reference) had a surface roughness of ( $R_a= 97.13$  nm) which was almost in the similar value to the modified surfaces ( $\pm 15.5$ ) and suggested that none of the surface coatings significantly modified the surface roughness of the substrate.

Table 4.5: The morphology of the modified surfaces.

Samples	$R_a$ (nm)	$R_q$ (nm)
Reference	97.13	126.05
HMDSO	91.18	114.18
TMDSO	91.44	114.37
HMDS	108.12	138.37
TEOS	123.20	153.93
MTES	129.04	174.4
PS	62.79	77.48
TC	51.3	64.94
PS/TC	91.22	109.59
PS/HM	88.98	108.71
PS/TE	85.63	107.02
TC/HM	73.89	92.10
TC/TE	73.15	89.35
PS/TC/HM	76.69	97.10
PS/TC/HM/TE	69.55	78.74

## 5. Surface Energy Effect

Table (4.7) presents the average values of water contact angle and calculated surface energy components. Most of the coatings exhibited high water contact angles. In particular, PS/HM, TC/HM and PS/TC/HM exhibit superhydrophobic properties (water contact angles above 124°).

The surface energy values showed a noticeable difference among the modified and reference surfaces. All the modified surfaces showed a lower total surface energy than the reference surface, indicating the hydrophobic nature of the coatings.

Table 4.7: The water contact angle of the different coatings.

Samples	WCA	Surface energy (mN/m <sup>2</sup> )
Reference	56.4	48.7
HMDSO	92.4	31.1
TMDSO	98.1	24.7
HMDS	101.9	27.6
PS	78.7	33
TC	89.4	29.9
PS/TC	93.0	48.4
PS/HM	124.9	24.9
PS/TE	60.7	45.1
TC/HM	130.0	41.9
TC/TE	59.5	46.6
PS/TC/HM	133.4	37.5
PS/TC/HM/TE	94.2	25.4

The percentages of the fouling deposits for some coated surfaces were lower than uncoated stainless steel surfaces (figure 4.4 and 4.5; table 4.7).

The lower average mass of the fouling deposits for the modified surfaces could be due to the lower surface energy of the coatings compared with the stainless steel surfaces.

From figures (4.4 and 4.5) and compared with table (4.7) we can see that the average mass of the fouling deposits was not related with the energy surface. The results are in contrast to the literature which reported a huge benefit in reduction of the fouling deposition with a variety of fouling solutions ([Augustin et al., 2007](#); [Rosmaninho and Melo, 2006](#); [Santos et al., 2003, 2006a](#)).

It is worth noticing that, though the drying of the deposit is not followed in the industry, the peeling off behaviour of the fouling layer for the HMDSO modified surfaces suggests that the adhesion of the fouling is weak to HMDSO modified surface. This observation could not be clearly correlated with any of the measured surface properties, since such peeling off behaviour was not observed for the other modified surfaces. This peeling off behaviour suggests that the fouling deposits for the HMDSO modified surface might be easier to clean than for the unmodified stainless steel surface. If this is the case it would represent a significant advantage in the dairy industry.

This phenomenon indicated also that there was weaker adhesion of the fouling deposits with the HMDSO modified surface in comparison to the stainless steel surface. It was speculated that this may enhance the cleaning efficiency and potentially reduce cleaning time and chemical usage. This was in accordance with the study carried out by [Britten et al. \(1988\)](#) who suggested that surface coatings do not reduce fouling deposition, but may offer weaker adhesion of the initial depositing fouling layer that would ease its removal during cleaning. Similarly [de Jong \(1997\)](#) suggested that the

effect of surface modification may be more prominent in the removal of the fouling deposits rather than in their build-up.

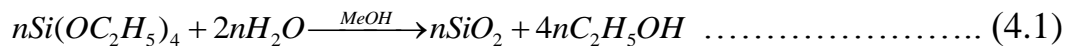
This phenomenon was in accordance with the findings reported by [Bansal et al. \(2010\)](#). Thus, the effect of the HMDSO modified surfaces on fouling reduction was not conclusive. This is in line with the results reported by [Beuf et al. 2003](#); [Patel et al., \(2013\)](#) who investigated the fouling behaviour of a fouling on diamond like carbon (DLC) modified surfaces at pilot-scale and found no significant benefit in fouling mitigation for the modified surfaces studied, but reported easier cleaning of the deposits for low energy surfaces.

➤ *Chemical method by Sol-Gel technics*

**6. Sol-Gel Based Coating**

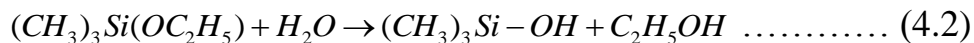
Sol-gel processes in general are known to involve both, hydrolysis and polycondensation reactions leading up to the formation of network structures in liquid solution with varying degrees of cross-linking. The nature of these structures depends on a number of reaction parameters, which are easy to describe phenomenologically but rather cumbersome to understand in detail. Various types of precursor compounds are available for the synthesis of metal oxides such as silica. The choice of precursor and solvent are perhaps the central pillars of any particular sol-gel system. Alkoxides are undoubtedly the most common and well-established precursors used for the synthesis of various morphologies of silica via sol-gel chemistry.

During the sol-gel process, in the mixture of TEOS and TMES alkoxides, TEOS is preferentially hydrolyzed in the early stages of the reaction leading to the condensation reactions and the formation of silica clusters as per the following chemical reaction:

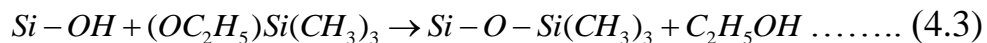


At latter stages of the above reaction (2.4), the MTES monomers get hydrolyzed and condensed in the following manner:

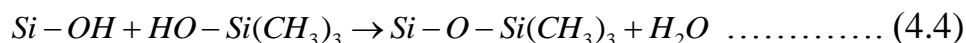
Hydrolysis:



Alcohol condensation:



Water condensation:



Thus, the  $\text{Si}(\text{CH}_3)_3$  groups are attached to the silica clusters through oxygen bonds leading to the formation of a hydrophobic silica film surface.

## 7. Sol-Gel Results

### 7.1. Effect of the Deposition Time

The optimized deposition protocol was elaborated starting from a “standard” deposition solution with a molar ratio of TME /TEOS: EtOH:  $\text{H}_2\text{O}$  was kept constant at 1:38.6:8.68, respectively. Starting from the time of the basic addition, the dip coating process was carried out at different times from 4, 8 and 12 minutes. When the substrates were pulled out from the solution early on (up to 4 minutes time), the observed films were non-uniform and of poor quality, mostly due to incomplete hydrolysis and condensation reactions. The coating was found uniform at a deposition time of 10 minutes. The Figure (4.17) shows that the value of contact angle increases with the increase of the dipping time.

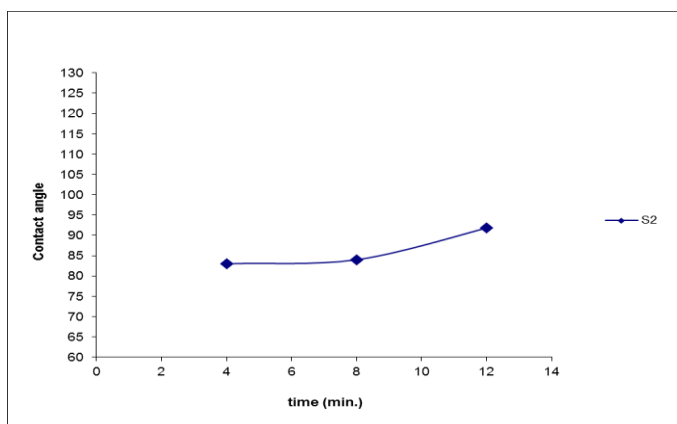


Figure 4.17: Effect of the dipping time on the contact angle.

## 7.2. Water Contact Angle

In order to improve adhesion of the sol-gel coatings (S1, S2, S3 and S4) on the stainless steel plate, an oxalation was carried out on some of the SS plates before coating. Figure (4.18) shows the water contact angles of the different substrates prepared: S, means sol-gel coating on stainless steel surface. In all cases, the four sol-gel (S1, S2, S3 and S4) were tested.

A superhydrophobic surface is obtained with oxalated stainless steel as oxalation increases the roughness and thus the contact angle. It is known that surface hydrophobic properties are enhanced by increasing surface roughness and superhydrophobic surfaces require both appropriate surface roughness and low surface energy ([Wanzel, 1963](#); [Cassie and Baxter, 1944](#)).

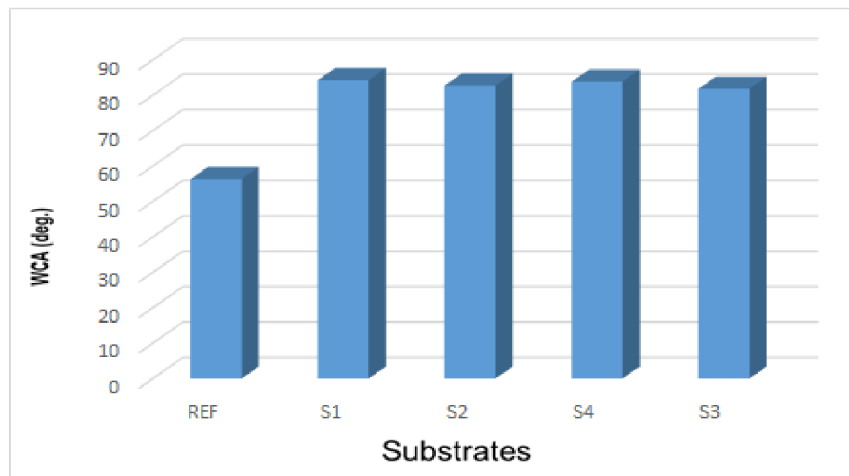


Figure 4.18: The water contact angle of different substrates.

Figure (4.19) show EPMA image of sol-gel coatings with elements analysis charts. The sol gel coating is transparent and too thin to be observed by EPMA.

A peak of Si characteristic of the sol-gel coating only appears on some part of the sample, which means that the sol-gel layer doesn't cover all the surface of samples or is too thin to be detected.

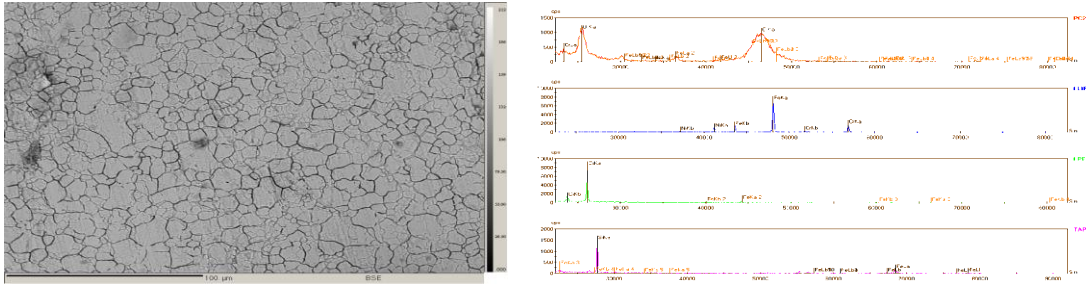


Figure 4.19: Sol-gel (S2) coated on stainless steel with chemical analysis chart.

The only difference that could be observed among the various plates was that the probability to have “cracks” (as observed under the microscope after drying) in the initial coherent layer was greater in most of the coated/treated stainless steel surfaces than in uncoated ones.

### 7.3. Antifouling Effect of Sol-Gel Coatings

The antifouling performance of the four sol-gel coatings was evaluated by the pilot-plant tests. Results show that S1, S2, S3 and S4 surfaces decrease the fouling formation. S4 surfaces promote the formation of more fouling than the unmodified stainless steel.

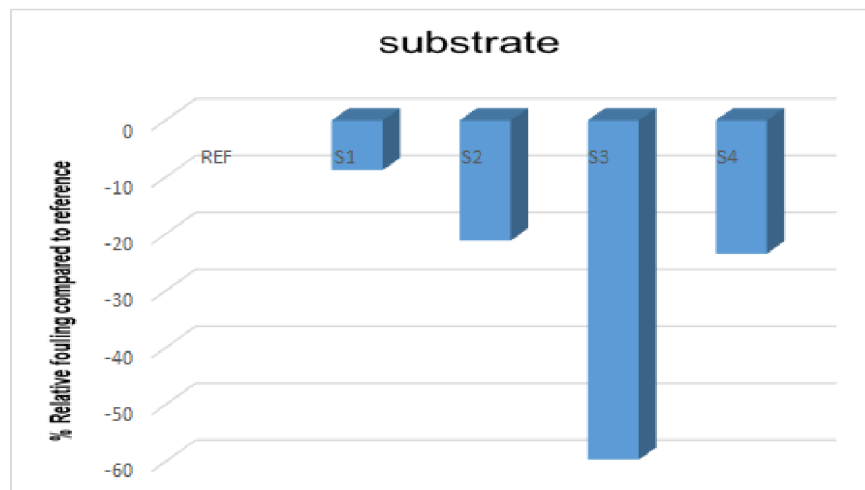


Figure 4.20: Pilot-plant test with fouling model fluid

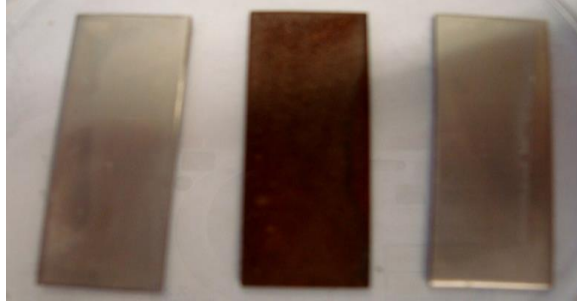


Figure 4.21: The sol-gel coating substrates after cleaning with NaOH.

These deposits could not be washed off from the stainless steel coupons by simple rinsing with water, but they could be removed rather easily by mechanical means after being dried, leaving the adhering initial layer on the substrate. After cleaning with NaOH no sol-gel coating layer remained (Figure 4.21).

## ***Conclusion***

The 316L 2B stainless steel was surface modified using atmospheric pressure plasma. The surface water contact angle was improved to target hydrophilic surface after plasma treatment and the following optimized plasma treatment conditions were obtained: distance between the plasma source and substrate of 2 cm, aging time in air of 60 minutes, and 5 or 4 passes for air or nitrogen respectively.

In the atmospheric pressure treatment we have two types of precursors: silicon and fluorosilane based precursors. For silicon based precursor, all the coatings are hydrophobic with water contact angles above 90°. The HMDSO, HMDS, MTES, DMP/HM, Phos./HM and the TTMSP/HM surfaces showed less fouling formation, while the other surfaces promoted the formation of more fouling than the reference stainless steel.

While for Fluorosilane based precursor, all coatings are hydrophobic with water contact angles above 90°. The TC, PS/HM, TC/HM and the PS/TC/HM/TE surfaces showed less fouling formation, while the other surfaces promoted the formation of more fouling than on the reference stainless steel.

From all the precursor, the HMDSO was the best to decrease the fouling effect on the stainless steel surface and was the more repeatable. ToF-SIMS and XPS were used to characterize the HMDSO coated layer on the stainless steel surface. The results of ToF-SIMS analyses demonstrated that the coating formed and oxidized layer covering the entire stainless steel surface. The XPS analyses show that the deposition of HMDSO creates a thick layer

of SiO<sub>2</sub> on the stainless steel (greater than 10 nm thick). The fouling layer is easier to remove when the steel is coated with HMDSO than when it is not. The other surface treatment technique sol-gel coatings have a water contact angle value under (91.8°). The fouling mass on the sol-gel coating plates did not differ appreciably from that on unmodified stainless steel plates, but the initial layer did not adhere as strongly as on the untreated metal surfaces. The surface coatings analysis and fouling percentage are show in appendix 4.

## ***GENERAL CONCLUSION***

Dairy fouling results from the accumulation of unwanted material on heated surfaces. In general terms, fouling of milk products can mainly be divided into two groups: organic fouling and mineral fouling. The calcium phosphate and whey proteins are the main components of milk deposits, and the  $\beta$ -lg plays a dominant role in the fouling heat exchangers. The factors affecting on milk fouling in heat exchangers can be classified into three major categories: milk composition, operating conditions in heat exchanger and surface state of heat exchanger.

Cleaning in the dairy industry is done every 5-10 hours depending on fouling severity and this operation is expensive and causes great losses in time and energy, for this reason the phenomena occurring at the interface steel-milk must be understood and surface modifications of stainless steel to reduce fouling must be extensively investigated. Cleaning can result from either or both adhesive and cohesive failure depending on the part of the respective strengths. In removing a deposit during cleaning, both cohesive (deposit-deposit) and interfacial adhesive (surface-deposits) forces must be overcome. In this context, surface modification for reduction of fouling, either by inhibiting attachment of depositing species or by increasing the ease of the removal during cleaning has received more and more attention in the food sector.

In this study, many surface characterization techniques were used to investigate the growth mechanisms of fouling and then the antifouling properties and adhesion strength of the coating thin film deposit on a stainless steel surface. These include ToF-SIMS uses mass spectrometry to

determine the type and quantity of ionizable chemical groups of a surface's top nanometer, XPS to determine the atomic composition of a solid's top several nanometers, AFM is widely used to generate topographic maps of surfaces. SEM used to image the topography of the sample surface.

Other microscopy techniques and methods sensitive to surface properties (contact angle, roughness, and surface free energy analysis) were used in association with the above mentioned techniques.

To understand the interfacial behavior and the role of calcium in the growth mechanism of fouling, two fouling solutions were used: one containing a low amount of calcium (30 ppm), the second one containing 120 ppm calcium.

In the first case, the fouling solution is not saturated in calcium, the calcium mostly chelated or trapped in the protein layer, without creating a particular roughness effect. The fouling growth mechanism in this configuration is quite simple: particles (size 60 nm) of denatured and unfolded proteins (mainly  $\beta$ -Lg) deposit on the steel plate and inside the grain boundaries in the first fouling seconds and accumulate in these places during fouling. After 2 hours some grain boundaries are totally filled in with the protein and the surface is completely covered with a homogeneous protein layer.

In the second case, with calcium, the fouling layer is thick, white and rough. After 2 hours the fouling is present both on the surface and inside the grain boundaries and creates strong anchorage points which explain why it is so difficult to remove the fouling layer by cleaning. In this fouling configuration the calcium plays a major role. We evidenced by ToF-SIMS that the fouling was initiated by the unfolded protein (size of 60 nm) in the first seconds of exposition to the fouling solution. The unstable amorphous calcium carbonate nuclei (size 150-400 nm) formed in the tapwater at 90°C

are stabilized and dredged by the unfolded proteins. They then precipitate preferentially in the steel cavities and grain boundaries, in which they are mechanically trapped. Then, the unfolded protein covers again these calcium particles, etc. This leads to a final thick arborescent growth structure.

By preparing different grade of surface roughness of stainless steel surface, it has been established in this part that the decrease of surface roughness decrease the amount of fouling. However, it has also been noticed that with equivalent roughness surface energy has to be taken into account to reduce the fouling.

After the comprehension of the growth mechanism, antifouling coatings were researched through with different technique. The 316L 2B stainless steel was surface pre-modified using atmospheric pressure plasma to improve coating adherence. The surface water contact angle was improved to target hydrophilic surface (to create a high degree of adhesion property between the surface of material and the coating film) after plasma treatment and the following optimized plasma treatment conditions were obtained: distance between the plasma source and substrate of 2 cm, aging time in air of 60 minutes, and 5 or 4 passes for air or nitrogen respectively.

In the atmospheric pressure treatment we have two types of precursors: silicon and Fluorosilane based precursors, from the two type of precursor, the HMDSO was the best coating deposited on the stainless steel surface too obtain repeatable antifouling properties. Moreover, the fouling layer was easier to remove when the steel was coated with HMDSO than when uncoated.

To improve the adhesion of the coating, we have oxalated the surface of stainless steel, however, unfortunately this technique increases the surface

roughness of stainless steel and have the tendency to increase the fouling phenomenon.

Finally, the sol-gel coatings fouling behavior did not differ appreciably from that of unmodified stainless steel surface, but the initial layer of fouling did not adhere as strongly as on the untreated metal surfaces.

## ***RECOMMENDATIONS FOR FUTURE RESEARCH***

Several improvements can still be carried out on this subject. For example, the study of the calcium phosphate and protein fouling behavior on the developed coatings was not carried out. Thus, the next step will be to study the fouling mechanism of the coatings. . Moreover, in order to better understand the fouling behavior, kinetic modelling studies or computer modellings would be a great advance to access the fouling simulation of coatings.

To finish with, some work were initiate in this study to obtained nanostructure surfaces by Femto laser in order to create a nanostructured hydrophobic surface, however, the antifouling effect was not studied yet and more work are still needed.

## ***References***

- Alexandrov, S.E., Hitchman, M.L., 2009. Plasma enhanced chemical vapour deposition processes. In: Jones, A.C., Hitchman, M.L. (Eds.), *Chemical Vapour Deposition: Precursors, Processes and Applications*. Royal Society of Chemistry, Cambridge, UK.
- Augustin, W., Geddert, T., Scholl, S., 2007. Surface treatment for the mitigation of whey protein fouling. In: *Proceedings of 7th International Conference on Heat Exchanger Fouling and Cleaning—Challenges and Opportunities*. The Berkeley Electronic Press, Berkeley, Tomar, Portugal.
- Bhagat D., Kim Y., Ahn Y. (2006). Room temperature synthesis of water repellent silica coatings by the dip coat technique, *Applied Surface Science*, 253, 2217–2221.
- Bansal, B., Habib, B., Patel, J., 2010. Effect of milk composition on dairy fouling in plate heat exchanger. In: *Fouling and Cleaning in Food Processing 2010*, Jesus College, University of Cambridge, Cambridge, UK, Department of Chemical Engineering and Biotechnology.
- Belmar-Beiny, M.T., Fryer, P.J., 1993. Preliminary stages of fouling from whey protein solutions. *J. Dairy Res.* 60, 467–483.
- Beuf M, Rizzo G, Leuliet JC, Müller-Steinhagen H, Yiantsios S, Karabelas A, Benezech T. (2003). Potency of stainless steel modifications in reducing fouling and in improving cleaning of plate heat exchangers processing dairy products. In: *Proceedings of heat exchanger fouling and cleaning—fundamentals and applications*. Santa Fe, N.M, U.S.A. May 18-22: Engineering Conferences International, New York, U.S.A.
- Bradley, S.E., Fryer, P.J., 1992. A comparison of two fouling resistant heat exchangers. *Biofouling* 5, 295–314.

- Britten, M., Green, M.L., Boulet, M., Paquin, P., 1988. Deposit formation on heated surfaces: effect of interface energetics. *J. Dairy Res.* 55, 551–562.
- Cassie, A. B. D.; Baxter, S. (1944). Wettability of porous surfaces. *Trans. Faraday Soc.*, 40, 546-551.
- Chen, X.D., Li, D.X.Y., Lin, S.X.Q., Ozkan, N., 2004. On-line fouling/cleaning detection by measuring electric resistance-equipment development and application to milk fouling detection and chemical cleaning monitoring. *J. Food Eng.* 61 (2), 181–189.
- Cheong W.C., Gaskell P.H., Neville A. (2013). Substrate effect on surface adhesion/crystallization of calcium carbonate. *Journal of Crystal Growth*, 363 7–21.
- Choi S.-B., Jepperson J., Jarabek L., Thomas J., Chisholm B., Boudjouk P. (2007). Novel Approach to Anti-Fouling and Fouling-Release Marine Coatings Based on Dual-Functional Siloxanes. *Macromol. Symp.* 249–250, 660.
- de Jong, P., 1997. Impact and control of fouling in milk processing. *Trends Food Sci. Technol.* 8 (12), 401–405.
- Delplace, F., Leuliet, J.C., Tissier, J.P., 1994. Fouling experiments of a plate heat exchanger by whey proteins solutions. *Food Bioprod. Process.:* *Trans. Inst. Chem. Eng., Part C* 72 (C3), 163–169.
- Delplace, F., Leuliet, J.C., Leviex, D., 1997. A reaction engineering approach to the analysis of fouling by whey proteins of a six-channels-per-pass plate heat exchanger. *J. Food Eng.* 34 (1), 91–108.
- De Menezes J.V. and Des Barros F. (1978). On the mössbauer spectrum of  $\text{FeC}_2\text{O}_4 \cdot 2\text{H}_2\text{O}$ . *Phys. Status Solidi*, (a) 45, K139.

- Dowling D. P., Ramamurthy A., Rahman M., Mooney D. A., MacElroy J. M. D. (2009). Influence of Atmospheric Plasma Source and Gas Composition on the Properties of Deposited Siloxane Coatings. *Plasma process polym.* 6, S483.
- Elofsson, U.M., Paulsson, M.A., Arnebrant, T., 1997. Adsorption of b-lactoglobulin A and B: effects of ionic strength and phosphate ions. *Colloids Surf., B* 8 (3), 163–169.
- Jimenez M., Hamze H., Allion A., Ronse G., Delaplace G., Traisnel M. (2012). Antifouling stainless steel surface: Competition between roughness and surface energy., *Materials Science Forum* 706-709, 2523-2528.
- Jeurnink, T.J.M., Verheul, M., Stuart, M.C., de Kruif, C.G., 1996. Deposition of heated whey proteins on a chromium oxide surface. *Colloids Surf., B* 6 (4–5), 291.
- Hamdy A.S. and Butt D.P. (2006). Environmentally compliant silica conversion coatings prepared by sol–gel method for aluminum alloys, *Surface & Coatings Technology* 201, 401–407.
- Kim Y., Choi Y., Kim J., Park J., Ju W., Paek K, Hwang Y. (2003). Characterisations of atmospheric pressure ejected plasma sources. *Surface and Coatings Technology*, 174 – 175. 535–540.
- Krishnan S., Weinman C., Ober C. (2008). Advances in Polymers for Anti-Biofouling Surfaces. *J. Mater. Chem.* 18, 3405.
- Latthe S. S. et al (2009). Superhydrophobic silica films by sol–gel coprecursor method, *Applied Surface Science*, 256, 217–222.
- Malayeri M.R., Al-Janabi A., Müller-Steinhagen H. (2009). Application of nano-modified surfaces for fouling mitigation. *Int. J. Energy Res.* 33, 1101.

- Müller-Steinhagen, H., 1998. Mitigation of process heat exchanger fouling: an integral approach. *Chem. Eng. Res. Des.* 76 (2), 97–107.
- Nomura K. and Ujihira Y. (1983). Analysis of oxalate coating on steels by conversion electron Mossbauer spectrometry. *Journal Of Materials Science*, 18, 1751-1757
- Mutushima Y. and Matsumura T. (1972). Oxalate conversing method of stainless steel, United States Patent, 858, 139.
- Nwankire C E, Favaro G, Duong Q-H and Dowling D P. (2010). Enhancing the mechanical properties of superhydrophobic atmospheric pressure plasma coatings, Submitted to *J. Plasma Processes and polymers*
- Nwankire C.E., Ardhaoui M., Dowling D.P. (2009). The effect of plasma-polymerised silicon hydride-rich polyhydrogenmethylsiloxane on the adhesion of silicone elastomers. *Polym. Int.* 58, 996.
- Patel S.J., Bansal B., Jones M. I. (2013). Margaret Hyland a. Fouling behaviour of milk and whey protein isolate solution on doped diamond-like carbon modified surfaces. *Journal of Food Engineering.* 116, 413–421.
- Rosmaninho, R., Melo, L.F., 2006. Calcium phosphate deposition from simulated milk ultrafiltrate on different stainless steel-based surfaces. *Int. Dairy J.* 16 (1), 81–87.
- Santos O, Nylander T, Rizzo G, Müller-Steinhagen H, Trägårdh C, Paulsson M. (2003). Study of whey protein adsorption under turbulent flow rate. In: *Proceedings of heat exchanger fouling and cleaning—fundamentals and applications*; Santa Fe, New Mexico, U.S.A.; May 18-22. New York, U.S.A.: Engineering Conferences International.

- Santos, O., Nylander, T., Paulsson, M., Trägårdh, C., 2006a. Whey protein adsorption onto steel surfaces-effect of temperature, flow rate, residence time and aggregation. *J. Food Eng.* 74 (4), 468–483.
- Santos, O., Nylander, T., Schillen, K., Paulsson, M., Trägårdh, C., 2006b. Effect of surface and bulk solution properties on the adsorption of whey protein onto steel surfaces at high temperature. *J. Food Eng.* 73 (2), 174–189.
- Sheir L.L., Jarman R.A. and Burstein G.T. (1994). *Corrosion*. vol. 2, Butterworths–Heinemann, Oxford.
- Stein J., Truby K., Wood C.D., Stein J., Gardner M., Swain G., Kavanagh C., Kovach B., Schultz M., Wiebe D., Holm E., Montemarano J., Wendt D., Smith C., Meyer A. (2003). Silicone Foul Release Coatings: Effect of the Interaction of Oil and Coating Functionalities on the Magnitude of Macrofouling Attachment Strengths. *Biofouling J. Bioadhesion Biofilm Res.* 19, 71.
- Visser, J., Jeurnink, T.J.M., 1997. Fouling of heat exchangers in the dairy industry. *Exp. Thermal Fluid Sci.* 14 (4), 407–424.
- Wenzel, R. N. (1936). RESISTANCE OF SOLID SURFACES TO WETTING BY WATER. *Ind. Eng. Chem.*, 28, 988-994

**APPENDIX 1: Roughness terms and its definition, calculations and uses.**

Term	Definition	Calculation	Use
$R_a$	Roughness average is the main height as calculated over the entire measured length or area. It is quoted in micrometers or micro-inches.	<p>Two-dimensional <math>R_a</math></p> $R_a = \frac{1}{n} \sum_{i=1}^n  Z_i - \bar{Z} $ <p>Three-dimensional <math>R_a</math></p> $R_a = \frac{1}{MN} \sum_{j=1}^N \sum_{i=1}^M  Z_{ij} $ <p>Where M and N = number of data points in X and Y, and Z is the surface height relative to the mean plane.</p>	$R_a$ is typically used to describe the roughness of machined surfaces. It is useful for detecting general variations in overall profile height characteristics and for monitoring an established manufacturing process.
$R_q$	The Root means square (rms) average between the height deviations and the mean line/surface, taken over the evaluation length/area. The parameters "RMS" and " $R_q$ " are equivalent in and are computed using the same equation.	<p>Two-dimensional <math>R_q</math></p> $R_q = \sqrt{\frac{1}{n} \sum_{i=1}^n (Z_i - \bar{Z})^2}$ <p>Three-dimensional <math>R_q</math></p> $R_q = \sqrt{\frac{1}{MN} \sum_{j=1}^N \sum_{i=1}^M Z^2(x_i, y)}$	RMS roughness describes the finish of optical surfaces. It represents the standard deviation of the profile heights and is used in computations of skew and kurtosis.

$R_p, R_v$	Maximum profile peak height and Maximum profile valley depth are the distances from the mean line/surface to the highest/lowest point in the evaluation length/area.	Measured	Peak height provides information about friction and wear on a part. Valley depth provides information about how a part might retain a lubricant.
$R_t$	Maximum height is the vertical distance between the highest and lowest points in the evaluation length/area.	$R_t = R_p + R_v$	Maximum height describes the overall roughness of a surface.
$R_z$	The Average maximum profile of the ten greatest peak-to-valley separations in the evaluation area. Vision excludes an 11 x 11 region around each high (H) or low (L) point such that all peak or valley points won't emanate from one spike or hole.	$R_z = \frac{1}{10} \left[ \sum_{i=1}^{10} H_i - \sum_{j=1}^{10} L_j \right]$	$R_z$ is useful for evaluating surface texture on limited-access surfaces such as small valve seats and the floors and walls of grooves, particularly where the presence of high peaks or deep valleys is of functional significance.
$R_{sk}$	Skewness is a measure of the asymmetry of the profile about the mean line. Negative skew indicates a predominance of valleys, while positive skew is seen on surfaces with peaks.	$R_{sk} = \frac{1}{nR_q^3} \sum_{i=1}^n (Z_i - \bar{Z})^3$	$R_{sk}$ illustrates load carrying capacity, porosity, and characteristics of non-conventional machining processes. Negative skew is a criterion for a good bearing surface.

$R_{ku}$	<p>Kurtosis is a measure of the distribution of spikes above and below the mean line.  For spiky surfaces, <math>R_{ku} &gt; 3</math>; for bumpy surfaces, <math>R_{ku} &lt; 3</math>; perfectly random surfaces have kurtosis 3.</p>	$R_{ku} = \frac{1}{nR_q^4} \sum_{i=1}^n (Z_i - \bar{Z})^4$	<p>Kurtosis describes machined surfaces and is rarely used for optical surfaces. It is sometimes specified for the control of stress fracture.</p>
----------	---	--	--

## APPENDIX 2: Surface characterization techniques

N	Technique	Type of Analysis	Information provides
1	ToF-SIMS	Physical and chemical	Elemental, isotopic, molecular, interface chemistry
2	XPS	Physical and chemical	Quantify percent Atomic composition and stoichiometry ratios
3	AFM	Physical	Surface morphology on an atomic scale
4	SEM	Physical	surface topography information
5	EPMA	chemical	Chemical composition of small volumes of solids materials
6	Optical Microscopy	Physical	Surface images, morphology
7	Contact angle	Physical-chemistry	Wettability, surface tension, surface energy
8	Roughness	Physical	quantify the quality of a surface topography
9	Weighting	Physical	Fouling mass

**APPENDIX 3:** The physical tests and chemical analysis carried up on each sample

Fouling Solution	Stainless Steel	Solution1: with 30 ppm of calcium		Solution 2: with 120 ppm of calcium	
Fouling duration	0	1 minute	2 hours	1 minute	2 hours
Physical analysis	AFM Optical microscopy Contact angle	AFM (4x4, 2x2, $\mu\text{m}^2$ ) Zoom (500x500 $\text{nm}^2$ ) 3D image	AFM (2x2 $\mu\text{m}^2$ ) Optical microscopy (200x200 $\mu\text{m}^2$ ) SEM (X300, X1000, X7000)	AFM (4x4, 2x2, $\mu\text{m}^2$ ) Zoom (500x500 $\text{nm}^2$ ) 3D images	SEM BSE cross-section X-Ray cross-section
Chemical analysis	ToF-SIMS          XPS	ToF-SIMS (100x100 $\mu\text{m}^2$ ) $\text{Ca}^{2+}$ , $\text{CsCN}^{2+}$ 3D image EPMA ( $\text{Ca}^{2+}$ , S (protein), Steel (Cr, $\text{Fe}^{\circ}$ )) X-ray mapping ( $\text{Ca}^{2+}$ / crystals)	-----	ToF-SIMS (100x100 $\mu\text{m}^2$ ) $\text{Ca}^{2+}$ , $\text{CsCN}^{2+}$ 2D and 3D images EPMA ( $\text{Ca}^{2+}$ , S (protein), Steel (Cr, $\text{Fe}^{\circ}$ )) X-ray mapping ( $\text{Ca}^{2+}$ / crystals)	-----
Fouling results	-----	-----	Thin, Homogeneous, blue reflects, low Roughness, Cluster 60<dp<120nm Unfolded protein	-----	Thick 200 $\mu\text{m}$ (2h), white, rough Ca is entrapped into protein. Arborescences growth (sponges structure). Mineral particle 300/400 nm (supersaturating)

**APPENDIX 4: The surface coatings analysis and fouling percentage**

Treatment			Analysis				Fouling %				
			R <sub>a</sub>	R <sub>q</sub>	WCA	AFM	ToF-SIMS	XPS	Lab	Pilot	Cleaning
Ref 316L-2B			97.13	126.05	56.4	✓	✓			0	
Plasma	Fluorosilane	PS	62.79	77.48	78.7				19.3	0	
		TC	51.3	64.94	89.4				-22.5	0	
		PS/TC	91.22	109.59	93.0				29.12	0	
		PS/TE	88.98	108.71	124.9				38.7	0	
		PS/HM	85.63	107.02	60.7				-37.2	0	
		TC/HM	73.89	92.10	130.0				9.1	0	
		TC/TE	73.15	89.35	59.5				-39.8	0	
		PS/TC/HM	76.69	97.10	133.4				58.3	0	
		PS/TC/HM/TE	69.55	78.74	94.2				-12.9	0	
		Silicone	TMDSO	HMDS	91.44	114.37	98.1				23
TEOS	108.12			138.37	101.9				-27	-96	0
MTES	123.20			153.93	10.5				28	4	0
HMDSO	129.04			174.4	27.5				6	-93	0
AAA	28.6			37.7	102.7	✓	✓	✓	-52	-78	0
AAN	394.4			481.8	97.1				-48	-13	0
ANN	91.1			114.1	116.2				-67	-75	0
ANA	354.3			433.9	99.7				-10	-83	0
NNN	84.2			108.8	119.5				-36	-91	0
NNA	61.8			81.3	94.7				-12	-78	0
Sol-Gel	S1	NAA	84.08	107.1	96.3				-39	-88	0
		NAN	80.3	102.4	97.5				-57	-90	0
		S2	81.89	111	84.3				-4.21	0	
		S3	92.6	118	82.8				-23.7	0	
Sol-Gel	S4	S3	90.5	108	81.9				-59.6	0	
		S4	74.6	123	83.9				-23.4	0	

## ***Résumé***

Le présent travail porte sur un problème crucial de l'industrie laitière : l'encrassement causé par le lait pendant un traitement thermique. L'objectif de ce travail était de comprendre le mécanisme de dépôt et de croissance de l'encrassement laitier à la surface de conduites en acier inoxydable afin de pouvoir élaborer une surface qui permette de limiter, voire d'empêcher cet encrassement.

La morphologie et composition de la couche d'encrassement dépendent fortement de la solution d'encrassement. Quand de l'eau avec une dureté nulle est utilisée, la couche d'encrassement est fine, lisse et homogène. Inversement, avec de l'eau du robinet fortement concentrée en calcium, la couche d'encrassement est très épaisse, rugueuse et montre un mécanisme de croissance en arborescence. Afin de mieux comprendre l'initiation des mécanismes d'encrassement, des échantillons ont été soumis à un processus d'encrassement limité à une minute pour les deux solutions, ce qui entraîne la formation de couches d'encrassement d'épaisseur nanométrique. Les interactions entre les protéines du lait et le calcium à la surface de l'acier ont pu être étudiées par des techniques d'analyse d'extrême surface (XPS, ToF-SIMS et AFM), ce qui a permis d'améliorer la compréhension des mécanismes d'encrassement. L'étude s'est ensuite portée sur la réduction de l'encrassement par l'intermédiaire de revêtements sur acier inoxydable, soit par voie plasma atmosphérique soit par voie sol-gel. Parmi les différents revêtements étudiés, un revêtement déposé par voie plasma atmosphérique (utilisant l'hexaméthylsiloxane HMDSO comme précurseur) conduit à une réduction importante de l'encrassement laitier.

## ***Abstract***

This work presents an important problem in the dairy industry: the fouling caused by milk during heat treatment. The objective of this study was to understand the mechanism of deposition and growth of dairy fouling on the surface of stainless steel pipes in order to develop a surface that limited or even prevent this contamination.

The morphology and composition of the fouling layer strongly depends on the solution of fouling. When water with Total Hardness zero is used, the fouling layer is thin, smooth and homogeneous. Conversely, with tap water in highly concentrated calcium, the fouling layer is very thick, rough and shows a mechanism for tree growth. To better understand the mechanisms of fouling initiation, samples were subjected to a process of fouling than one minute for both solutions, resulting in the formation of layers of fouling thickness interactions nanométrique. Les between milk proteins and calcium on the surface of the steel could be studied by techniques of extreme surface (XPS, ToF-SIMS and AFM) analysis, which has improved the understanding of the mechanisms fouling. The study is then focused on the reduction of fouling by means of coatings on stainless steel, either by atmospheric plasma or by sol-gel. Among the different coatings studied, a coating deposited by atmospheric plasma (using hexamethyldisiloxane HMDSO as precursor) leads to a significant reduction in milk fouling